Development of a Multi-Objective Optimisation Model for Mitigating Frequency Instability in a Renewable Energy-Sourced Power System

by

Ayamolowo Oladimeji Joseph

Thesis submitted in fulfilment of the requirements for the degree

Doctor of Engineering in Electrical Engineering

In the Department of Electrical, Electronic and Computer Engineering

Faculty of Engineering, Built Environment and Information Technology

Central University of Technology, Free State

Promoter: Dr Patrick Manditereza

Co-Promoter: Prof. K. Kusakana

August 2023

DECLARATION

I, Ayamolowo Oladimeji Joseph, student number #########, hereby declare that this research project, which has been submitted to the Central University of Technology, Free State, for the degree Doctor of Engineering in Electrical Engineering, is my own independent work and complies with the Code of Academic Integrity, as well as other relevant policies, procedures, rules, and regulations of the Central University of Technology, Free State. This project has not been submitted before by any person in fulfilment (or partial fulfilment) of the requirements for the attainment of any qualification.

_____ _____

O.J. Ayamolowo Date: 24/08/23

DEDICATION

Firstly, I would like to dedicate this thesis to God Almighty for his great love and care shown towards me. Also, to my lovely wife, Opeyemi Ayamolowo, for your love, support, patience, and understanding during the trying period of my doctoral study. Finally, to my parents and siblings for their continued prayers, comfort, and support.

ACKNOWLEDGMENTS

I would like to express my sincere appreciation to my supervisors, Dr Patrick Manditereza and Prof. Kanzumba Kusakana, for their guidance, financial support, advice, and mentorship throughout my doctoral study.

Furthermore, I would like to thank the Central University of Technology, Free State, for providing the much-needed financial assistance to me through the M&D grant award.

Special thanks to my wife, Opeyemi Ayamolowo, for your support, assistance, prayers, and comfort during my PhD journey. I also appreciate my parents (Mr Adeleke Ayamolowo and Mrs Yemisi Ayamolowo) and my siblings (Tope Ajibola, Ibukun Ayamolowo, Kemi Ayamolowo, and Bankole Ayamolowo) for their great show of love and affection.

Lastly, I would like to appreciate my senior lecturers, friends, and colleagues, Prof. Markus Elijah, Prof. Saheed Oke, Dr Michelle Erasmus, Mrs Ifedolapo Oke, Mr Oladele Daniel, Dr Elutunji Buraimoh, Dr Senbore Samson, Mr Fredrick Mulinge, and Mr Izuchukwu Emmanuel, for their inspiration and support during my doctoral study.

ABSTRACT

The power grid is changing in order to reduce the negative effect of greenhouse gas emissions from thermal generators while meeting the global net zero emission goal by 2050. Conversely, as the drive towards a renewable energy-dominant grid is propelled, the overall system inertia of the power grid declines, which causes frequency instability in the modern power grid.

This study aimed to develop a multi-objective optimisation model for mitigating frequency instability in a renewable energy-sourced power system. This was achieved by firstly reviewing the various types of virtual inertia control strategies and topology in the power system while highlighting the inertia requirement of the modern power system. The review revealed that adequate system inertia is required for the modern renewable energy-dominant grid to ensure stability; it should therefore be considered in power system operational and planning optimisation models.

A new mathematical model was formulated to maximise the overall system inertia of the grid, while minimising system cost and carbon dioxide (CO_2) emissions. The model was developed as a mixed-integer quadratic constrained programming (MIQCP) problem and solved using CPLEX solver in the General Algebraic Modeling System (GAMS). The model was validated using a modified Institute of Electrical and Electronics Engineers (IEEE) 9-bus test system. The results revealed that the developed model achieved higher system inertia than the conventional model, which does not consider the inertia requirement of the grid in planning.

Furthermore, the model was extended to consider possible expansion in the transmission network as more renewable energy generators (REGs) are integrated into the grid, while considering the inertia requirement of the grid. A new mathematical model was formulated as an MIQCP problem and solved using CPLEX solver in GAMS. To combat declining inertia and mitigate frequency instability in the modern grid, appropriate inertia constraint was introduced into the planning model. Also, an emission reduction initiative (ERI) was introduced in the joint generation and transmission expansion planning (GTEP) model in which power operators were incentivised if they are able to maintain a preset emission limit. The results revealed that the developed model achieved a 24% increase in system inertia and a 9.62% reduction in CO_2 emissions. This shows the effectiveness of ERI constraints in meeting the goal of emission reduction in the power system.

Furthermore, sensitivity analysis of feed-in tariff (FiT) (economic incentive) was considered in the model. A novel FiT and inertia-integrated GTEP optimisation model was developed, which considered the influence of an economic incentive (FiT) in promoting the integration of REGs into the grid while meeting the inertia requirement of the grid. The model was developed as an MIQCP model to minimise the total system cost and CO_2 emissions, while maximising the overall system inertia and FiT incentives. The developed model was implemented on an IEEE 6-bus test system and solved using CPLEX solver in GAMS. Sensitivity analysis of the model revealed that the higher the penetration of renewable energy sources (RESs), the higher the total system cost and total FiT received; however, the fraction of FiT payments received relative to the total investment cost decreased after 50% RES penetration for the same FiT rate.

Finally, the model was extended to consider the uncertainties of renewable energy resources (RERs) and system inertia. The intermittencies of wind speed and solar irradiance were addressed using a scenario-based approach. The variability of RER (solar irradiance and wind speed) in the Mangaung Metropolitan Municipality in the Free State province of South Africa was considered for the year 2019. The model was further developed as an MIQCP model to minimise system cost of energy (CoE) while maximising system inertia. The model was solved using CPLEX solver in GAMS and implemented on an IEEE 6-bus system. The model analysis results revealed that considering both system inertia and renewable energy uncertainties provides appropriate planning results with a notable 9% reduction in the total system cost and a 7.9% reduction in the CoE, while the overall system inertia is enhanced by 7.3%. In addition, January was revealed as the best-performing month for wind resources, while October was revealed as the best-performing month for solar resources at the study location (Mangaung Metropolitan Municipality in the Free State).

These results show the importance of considering system inertia in power system optimisation modelling to ensure the frequency stability of the modern grid with high penetration of renewable generators is not compromised.

Keywords: optimisation; system inertia; renewable energy; renewable energy resources; renewable energy uncertainties; model; mixed-integer quadratic constrained programming model; mixed-integer linear programming model; GAMS; CPLEX solver; power system; CO_2 emissions; economic incentives; feed-in tariff

TABLE OF CONTENTS

LIST OF FIGURES

LIST OF TABLES

LIST OF ABBREVIATIONS

AC	Alternating current
BESS	Battery energy storage system(s)
CAES	Compressed air energy storage
CO_2	Carbon dioxide
CoE	Cost of energy
CPU	Central processing unit
CSP	Concentrated solar power
DC	Direct current
ERI	Emission reduction initiative
ESS	Energy storage system(s)
ESU	Energy storage unit
ETAP	Electrical Transient Analyzer Program
FES	Flywheel energy storage
FiT	Feed-in tariff
GA	Genetic algorithm
GAMS	General Algebraic Modeling System
GB	Gigabyte(s)
GEP	Generation expansion planning
GHG	Greenhouse gas
GTEP	Generation and transmission expansion planning
HES	Hybrid energy storage
IEEE	Institute of Electrical and Electronics Engineers
MILP	Mixed-integer linear programming
MINLP	Mixed-integer non-linear programming
MIQCP	Mixed-integer quadratic constrained programming
N_2O	Nitrous oxide
NSGA-II	Non-dominated sorting genetic algorithm
O&M	Operation and maintenance
PDF	Probability density function
PHES	Pumped hydro energy storage
PMU	Phasor measurement unit
PSO	Particle swarm optimisation
PV	Photovoltaic
RAM	Random access memory

REG	Renewable energy generator
RER	Renewable energy resource
RES	Renewable energy source
RoCoF	Rate of change of frequency
SCES	Supercapacitor energy storage
SMES	Superconducting magnetic energy storage
SoC	State of charge
SPC	Synchronous power controller
TEP	Transmission expansion planning
UK	United Kingdom
USA	United States of America
USD	United States dollar(s)
VI	Virtual inertia
VOC	Virtual oscillator control
VSG	Virtual synchronous generator
VSM	Virtual synchronous machine
VSYNC	Virtual synchronous control

LIST OF UNITS

$	United States dollar(s)
$/hr	Dollars per hour
$/kWh	Dollars per kilowatt-hour
$/MW/yr	Dollars per megawatt per year
$/MW^{2}h	Dollars per square megawatt-hour
$/MWh	Dollars per megawatt-hour
$/t$CO_2$	Dollars per tonne carbon dioxide
$/Wh	Dollars per watt-hour
GHz	Gigahertz
GW	Gigawatt(s)
H(s)	System inertia
Hz	Hertz
Hz/s	Hertz per second
kg/m^2	Kilogram(s) per square metre
kW	Kilowatt(s)
kW/m^2	Kilowatt(s) per square metre

kWh	Kilowatt-hour(s)
M$	Million dollars
m/s	Metre per seconds
m^2	Square metre(s)
ms	Micro seconds
MVA	Megavolt-ampere
MW	Megawatt(s)
MWs	Megawatt-seconds
p.u.	Per unit
rad/s	Radian per second
s	Second(s)
t	Tonne(s)
tCO_2	Tonnes carbon dioxide
tCO_2/kWh	Tonne carbon dioxide per kilowatt-hour
VA	Volt-ampere
W/m^2	Watt per square metre

NOMENCLATURE

Indices and sets

G	Set of thermal generating units indexed by G
P	Set of pumped hydro energy storage (PHES) units indexed by P
V	Set of battery energy storage system (BESS) units indexed by V
W	Set of wind farm units indexed by W
S	Set of solar power plants indexed by S
L	Set of transmission lines indexed by L
I,J	Set of buses indexed by I,J
RL	Set of transmission lines at the receiving bus indexed by RL
SL	Set of transmission lines at the sending bus indexed by SL
CL	Set of candidate transmission lines indexed by CL
HES	Set of hybrid energy storage (HES) indexed by HES
EL	Set of existing transmission lines indexed by EL
k	Blocks considered for piecewise linearisation of the quadratic fuel cost function
T	Set of time intervals in hours indexed by T
i	Set of buses

Parameters

ag,bg,cg	Fuel cost coefficients of thermal generators
B_{ij}	Susceptance of transmission lines connecting bus i to j
$\overline{BU_v}, \overline{BU_p}$	Maximum annualised monetary budget on candidate BESS units and PHES units respectively ($)
$\overline{BU_s}$	Maximum annualised monetary budget on candidate solar plant ($)
$\overline{BU_w}$	Maximum annualised monetary budget on wind turbine ($)
$\overline{BU_{cl}}$	Maximum annualised monetary budget on candidate transmission line ($)

$\overline{BU_T}$	Maximum monetary budget allocation on candidate renewable energy generators (REGs) (solar plant and wind turbine) and energy storage systems (ESS) (BESS and PHES) ($)
$\overline{MB}$	Maximum monetary budget for investment in solar photovoltaic (PV) plants, wind turbines, and BESS
BU_{res}	The available government budget for feed-in tariff (FiT) payment
B_{ij}^{el}	Susceptance of existing transmission lines connecting bus i to j
B_{ij}^{cl}	Susceptance of candidate transmission lines connecting bus i to j
CO_w^{om}	Maintenance cost on wind farm
CF_w, CF_s	Capacity factor of wind turbines and solar PV plants respectively
CO_v^{inv}, CO_p^{inv}	Investment cost in candidate BESS units and PHES units respectively
CO_w^{inv}, CO_s^{inv}	Investment cost on candidate wind turbines and solar plants respectively
CO_{cl}^{inv}	Annualised investment cost of candidate transmission lines
CO_{hes}^{inv}	Annualised investment cost of candidate HES units
CO_w^{cul}	Cost of curtailment of the wind turbine (M$/MWh)
CO_w^{om}	Operation and maintenance cost of wind farms
$\lambda_{man}^{CO_2}$	Carbon penalty tax for CO_2 emissions on humans ($/t$CO_2$)
$\lambda_{eco}^{CO_2}$	Carbon penalty tax for CO_2 emissions on the ecosystem ($/t$CO_2$)
$e_g^{CO_2}$	Emission factor of thermal generators in tCO_2/kWh
$\overline{EM_{\lim}}$	Maximum CO_2 emissions limit permissible from all thermal generators
E^{total}	Total emission from all thermal generators
fl	Flexibility factor used to set different renewable energy source (RES) penetration levels
FiT_s, FiT_w	FiT rates for solar PV plants and wind turbines respectively
f_o	Nominal frequency of the system
$f_r^{\max}, f_r^{\min}$	Maximum and minimum system frequency permissible during contingency

$H^{\max}, H^{\min}$	Maximum and minimum overall system inertia constant permissible respectively
H_{gl}	Inertia constant of lost thermal generator
H_g, H_s	Inertia constant of thermal generators and solar plants respectively (in seconds)
H_w, H_v	Inertia constant of wind farms and battery units respectively (in seconds)
H_p	Inertia constant of PHES units respectively (in seconds)
H_{hes}	Inertia constant of HES units (in seconds)
$IE_{\min}$	Minimum required inertia energy limit
$\lambda_g^{CO_2}$	Carbon tax for CO_2 emissions of thermal generators ($/t$CO_2$)
k	Fraction of the total load demand dedicated as primary frequency reserve
KE_{SG}	Kinetic energy available from all thermal generators (MWs)
KE_{total}	Total available inertia energy available from all thermal generators and storage units (MWs)
$KE_{\min}$	Minimum inertia energy set for system stability (MWs)
KE_{es}	Inertia energy available from all connected ESS
k_{hes}	Power frequency regulation constant
LD_i	Load demand at bus i
LD^{peak}	Peak load demand
$P_g^{\max}$	Maximum active power generation from thermal generators
$P_g^{\min}$	Minimum active power generation from thermal generators
$PXF_{i,j}^{\max}$	Maximum power limit on transmission lines
$P_{th}^{\max}$	Maximum active power generation of thermal generators
$\overline{P_p}, \underline{P_p}$	Maximum and minimum power delivery by PHES respectively
$P_w^{\max}, P_s^{\max}$	Installed capacity of wind turbine and solar plant (in MW) respectively
$\overline{P_{w,t}^{Av}}, \overline{P_{s,t}^{Av}}$	Maximum available power of wind farm and solar PV plant at time t respectively

$P_{hes}^{\min}$, $P_{hes}^{\max}$	Minimum and maximum power delivery by HES respectively
$PR_{\min}$	Minimum primary reserve capacity set
$\Pr_{ss}^{so}$	Probability of occurrence of scenario ss for solar PV plant
$\Pr_{sw}^{wi}$	Probability of occurrence of scenario sw for wind turbine
$PF_{\max}^{ext}, PF_{ij,\max}^{cl}$	Maximum power flow limit of existing and candidate transmission lines respectively
P_w^{cap} , P_s^{cap}	Maximum power capacity of wind turbine, and solar PV plants connected to bus i respectively (MW)
$\overline{P_v^{dis}}, \underline{P_v^{dis}}$	Maximum and minimum discharging power of BESS respectively
$\overline{P_V^{cha}}$, $\underline{P_V^{cha}}$	Maximum and minimum charging power of BESS respectively
$PF_{el}^{\max}$	Maximum power flow limit on existing transmission lines (MVA)
$PF_{cl}^{\max}$	Maximum power flow limit on candidate transmission lines (MVA)
$P_{ij}^{\max}$	Maximum transmission line limit (MVA)
RPU_g	Ramp up limit of thermal unit
RPD_g	Ramp down limit of thermal unit
$\eta_v^{dis}, \eta_v^{cha}$	Charging and discharge efficiency of BESS units respectively
S_{base}	Base apparent power of system (MVA)
S_{hes}	Apparent power of HES units (MVA)
$SC_v^{\max}, SC_v^{\min}$	Maximum and minimum state of charge (SoC) of BESS respectively
$SoC_{bes}^{\max}, SoC_{bes}^{\min}$	Maximum and minimum SoC of BESS units respectively
$SC_{hes}^{\max}$ and $SC_{hes}^{\min}$	Maximum and minimum SoC of HES units respectively
	S_g, S_s Installed apparent power capacity of thermal generators and candidate solar plants respectively (MVA)
S_w, S_v	Installed apparent power capacity of candidate wind farm and battery units respectively (MVA)
S_p	Installed apparent power capacity of candidate PHES units (MVA)
$\chi_{w,t}^{va}$, $\chi_{s,t}^{va}$	Variability of wind turbines and solar PV plants per time respectively (per unit [p.u.])

$Va_{sw}^{wi}, Va_{ss}^{so}$	Variability of wind turbines and solar PV plant for each scenario respectively
ΔPOF	Change in power frequency characteristics of the system following system contingency
ΔP	Magnitude of lost power generation during contingency
$\Delta P^{\max}$	Largest possible loss of power generation
λ_e	Cost of emission of thermal generators ($/tCO$_2$)
σ, β and χ	Non-negative weighting factors of the objective function
α	Duration constant used for annualising the operation and maintenance cost of the generators
θ_i^{sl}	Bus voltage angle at the sending end of the transmission line
θ_j^{rl}	Bus voltage angle at the receiving end of the transmission line
$\theta_{p,i}^{\max}, \theta_{p,i}^{\min}$	Maximum and minimum voltage angle at bus respectively
$TEK_{\min}$	Minimum inertia energy required from all operational generators and storage units
M	Big-M large enough number
n	Number of thermal generators available
$\overline{nw}$	Maximum number of wind farm units that can be built in the planning horizon
$\overline{ns}$	Maximum number of solar plants that can be built in the planning horizon
$\overline{nv}$	Maximum number of BESS units that can be installed in the planning horizon
$\overline{np}$	Maximum number of PHES units that can be installed in the planning horizon
$\overline{ne}$	Maximum unit of ESS (BESS and PHES) that can be installed in the planning horizon
$\overline{nc}$	Maximum number of candidate transmission lines that can be constructed in the planning horizon
$nhes$	Total number of candidate HES that can be installed in the planning horizon

η_v, η_{sces}	Efficiency of BESS and supercapacitor energy storage (SCES) units respectively
η_p	Efficiency of PHES
ς	Proportion of stored kinetic energy from synchronous generators required for system stability
ϑ	Minimum kinetic energy fraction required during system contingency
$RoCoF^{\max}$	Maximum system rate of change of frequency (RoCoF) permissible
$RoCoF^{\min}$	Maximum and minimum system RoCoF permissible
$RS^{\min}$	Minimum reserve limit fraction set
q	Constant for limiting the maximum capacity of an HES unit
x	Power demand safe margin to carter for unanticipated increase in demand
y	Flexibility parameter for setting thermal generator fraction
z	Constant that specifies the fraction of BESS in the HES composite

Variables

f	System frequency
H	Overall inertia constant of the system (in seconds)
$IE_{hes,w,s}$	Total inertia contributed by HES, wind turbines, and solar PV plants
P_g	Active power output generated by thermal generators (MW)
PF_{ij}^{ext-}	Active power flow out of existing transmission line, ext
PF_{ij}^{cl-}	Active power flow out of candidate transmission line, cl
PF_{el}^{ij}	Active power flow into existing transmission lines from branch connecting bus i to j
PF_{cl}^{ij}	Active power flow into candidate transmission lines from branch connecting bus i to j
$P_{w,t}^{Av}, P_{s,t}^{Av}$	Available power of wind farms and solar PV plants at time *t* respectively
P_w, P_s	Active power delivery by wind turbines and solar plants respectively (MW)

P_{hes}, P_v, P_{sces}	Active power delivery by HES, BESS, and SCES units respectively (MW)
$P_{g,t}, P_{g,t-1}$	Active output power generated by thermal generators at time *t* and previous time, *t-1* (MW)
P_p	Power delivery by PHES
$P_{th}^{res}, P_{so}^{res}$	Reserve capacity of connected thermal generators and solar PV plants respectively
P_{wi}^{res}	Reserve capacity of connected wind turbines
P_v^{cha}, P_v^{dis}	Charging and discharging power of BESS respectively
$P_{w,t}^{wc}$	Curtailed power of wind turbine connected to bus i at time t (MW)
$\theta_i^{sl}, \theta_j^{rl}$	Bus voltage angle at the sending and receiving ends of the existing transmission line respectively
$\theta_i^{scl}, \theta_j^{rcl}$	Bus voltage angle at the sending and receiving ends of the candidate transmission line respectively
$SC_{v,t}$	SoC of BESS per time
$SC_{v,t-1}$	SoC of BESS at previous time, *t-1*
$TFiT$	Total FiT received for RES power generation
TEK	Total inertia energy contributed by connected BESS, wind turbines, and solar PV plants
ψ_i	Voltage angle at bus i (radian)

Binary variables

$\mu 1_v$	Binary decision variable that determines investment in BESS; 1 if a BESS is to be installed and 0 if otherwise.
$\mu 1_{hes}$	Binary decision variable that determines investment in candidate HES; 1 if an HES is to be installed and 0 if otherwise.
$\mu 2_p$	Binary decision variable that determines investment in PHES; 1 if a PHES is to be installed and 0 if otherwise.
$\mu 3_w$	Binary decision variable that determines investment in wind turbines; 1 if a wind turbine is to be installed and 0 if otherwise

$\mu 4_s$	Binary decision variable that determines investment in solar PV plants; 1 if a solar PV is to be installed and 0 if otherwise.
$\mu 5_v^{cha}$	Binary variable that determines the charging state of BESS units
$\mu 5_v^{dis}$	Binary variable that determines the discharging state of BESS units
$\mu 6^{cl}$	Binary decision variable that determines investment in candidate transmission lines; 1 if a transmission line is to be constructed and 0 if otherwise

CHAPTER 1: INTRODUCTION

1.1 BACKGROUND

In recent times, there has been a gradual but steady shift away from conventional fossil fuel-driven generators to renewable energy-sourced systems such as photovoltaic (PV), wind, and hydropower systems due to the harmful effect of fossil fuels [1].

Furthermore, the integration of renewable energy sources (RESs), such as PV systems and wind turbines, has led to significant changes in the dynamics of power systems. This is because as synchronous generators are replaced by renewable energy generators (REGs), the overall power system inertia decreases [2], [3]. This often results in frequency instability, a high rate of change of frequency (RoCoF), large frequency nadir, and reduced system reliability, particularly in the case of sudden loss of power generation or a sudden fault in the power system. The dynamic response of the power system during such critical times is very important in ensuring a viable power system [4].

Traditionally, synchronous machines in the form of coal-fired generators [4]–[6], gas-fired generators [2], nuclear generators [1], [7], [8], and synchronous condensers [9]–[12] have played a major role in frequency regulation as the stored kinetic energy in their large rotating masses opposes changes in frequency in the grid [13], [14]. However, although these machines provide higher inertia to the power system, they are limited because they contribute to environmental pollution through greenhouse gas (GHG) emissions. In order to ensure power system stability, REGs and energy storage systems (ESS) are made to provide artificial inertia using a suitable control strategy.

The authors in [7], [12], [15], [16] proposed the use of the deloading technique in RESs such as PV systems and wind turbines to provide additional system inertia. However, although this technique is cheap and can also be used to regulate the active and reactive power output, it is limited by its slow frequency response with a delay of ~50–100 ms, stochastic output, and small virtual inertia (VI) provision [16].

Another approach by authors in [17], [18], [19] includes the use of concentrated solar power (CSP), which is a promising technology to provide synchronous inertia in a renewable energy-sourced grid as it has low carbon emissions and facilitates renewable energy integration into the grid. It is often used in an hybridised form such as CSP-BIO plants or CSP-PV systems in order to provide frequency response in a power system [17]; however, it is limited by its

high cost of installation and slow frequency response. Hydroelectric generators are also used to provide rotating inertia but they are limited because of their high cost of installation and slow response to frequency changes [4], [5].

Other authors have proposed the use of ESS to provide VI with the right control strategy. Battery energy storage systems (BESS) was proposed in [1], [7]–[9], [15], supercapacitor energy storage (SCES) in [20], [21], superconducting magnetic energy storage (SMES) in [7], [15], flywheel energy storage (FES) in [6], [7], [11], [15], [22], pumped hydro energy storage (PHES) in [6], [23], thermal energy storage in [14], and compressed air energy storage (CAES) in [23]. BESS and SCES are the preferred energy storage technologies because of their ability to support fast frequency regulation; however, BESS are limited because of their high cost and shorter life cycles, while SCES has a relatively lower cost [21], [6]. PHES and thermal energy storage are also limited by their high cost, small inertia, and slow frequency response [6], [14]. CAES is a promising technology but it is limited by its complex construction [23]. FES and SMES have a longer life cycle and larger energy storage capacity but are limited by their slow response time [6], [23], [14].

In most cases, since the characteristics of the BESS are complementary to those of SCES, FES, and SMES technologies, a hybrid storage system is often preferred, such as BESS-SCES, BESS-SMES, BESS-FES, FES-BESS, and BESS-SCES-FCES [7], [14]. BESS-SCES is often widely used because it offers faster frequency response and lower cost of energy (CoE) characteristics than the other configurations.

In recent studies, RESs were used together with ESS in order to provide increased VI with an appropriate control strategy. For example, wind turbine-connected ESS [6] provides 45% more inertial power than a wind turbine alone; however, it is limited by its cost and the capacity of the BESS. PV-connected BESS in [7] were used to provide fast frequency response but were also limited by the high cost and the capacity of the BESS. A PV supercapacitors-based microgrid was also investigated in [21]. The authors in [11] proposed a combination of BESS and a synchronous condenser, called synchronous REG, for providing increased system inertia [10], [20], [21]; however, this technique also contributes to environmental pollution (GHG emissions) [11].

On the other hand, the integration of various renewable energy resources (RERs) into the power grid means that the power grid now consists of diverse generation technologies with varying costs of production. The dispatch of these multiple generation sources needs to be done so as to minimise cost and GHG emissions while ensuring that system inertia is maximised.

Only a few authors have considered system inertia in the optimal dispatch of a power system. Power system frequency stability depends on the inertia energy inherent in a power system [24]. High system inertia is considered a frequency stability index for power systems [25], [26], [27].

In the literature, economic, environmental, and technical criteria are very important in order to obtain optimal system configuration. Economic criteria include cost considerations (system cost, CoE, levelised CoE, net present cost, and life-cycle cost), environmental criteria include GHG emissions such as carbon dioxide (CO_2) and nitrous oxide (N_2O), while technical criteria take into account efficiency and reliability [28].

Various algorithms, hybrid algorithms, and tools have been used to obtain optimal system configurations for linear programming, non-linear programming, mixed-integer linear programming (MILP), and mixed-integer non-linear programming (MINLP) models, which include evolutionary algorithms such as genetic algorithms (GAs) [29], Monte Carlo simulation comparison, evolutionary particle swarm optimisation (PSO) [29], non-dominated sorting genetic algorithm (NSGA-II) [30], differential evolution (non-linear) and modified bacteria foraging algorithm [31], PSO [32], feedforward neural network [25], fuzzy optimisation [27], modified rider optimisation algorithm [33], and fmincon solver in MATLAB [34], [35], [31].

The review of the literature revealed that most of the optimisation models used to determine the economic dispatch aim to maximise the consumption of renewable energy at reduced prices, while neglecting the need for adequate inertia that is required for grid stability. The power industry is therefore at a crossroads in making business decisions that will allow the grid to be operated optimally and cost-effectively with less emissions but within acceptable technical constraints [28], [9]. This research therefore proposed a multi-objective optimisation model for a renewable energy-sourced grid considering cost, GHG emissions, and system inertia as the primary objectives.

1.2 PROBLEM STATEMENT

The continued replacement of coal-fired generators with REGs reduces the overall inertia of the power grid, which causes frequency and system instability issues [2], [3]. This is the major drawback of integrating a large amount of RESs into the grid.

While most of the optimisation models used to determine the economic dispatch solely aim to maximise the consumption of renewable energy and to minimise cost and emission, only a few authors have considered the adequacy of system inertia needed to ensure system stability. It is therefore necessary to ensure a balance between grid stability with adequate inertia through minimised investment cost and maximised system inertia with an environmentally friendly power system.

The research questions for the study were as follows:

1) How will adequate system inertia be ensured in a renewable energy-sourced power grid?
2) How can a stable renewable energy-sourced grid with minimal emissions be achieved?
3) How can investors be encouraged to support increased renewable energy penetration into the grid?

1.3 OBJECTIVES

The aim of this project was to develop a multi-objective optimisation model for mitigating frequency instability in a renewable energy-sourced grid with minimised cost and emissions while maximising system inertia.

The objectives of the study were as follows:

1) To develop a new deterministic optimisation model to minimise cost and emission while maximising system inertia in a renewable energy-sourced grid.
2) To develop a new deterministic optimisation model considering hybrid energy storage (HES) and to conduct a sensitivity analysis of the impact of economic incentives (introduced to encourage investors to invest on renewable energy generators thus increasing the renewable energy penetration into the grid) on the optimised model under various level of RES penetration into the grid.
3) To develop a stochastic optimisation model that accounts for uncertainty parameters arising from REGs such as PV plants and wind turbines.

1.4 RESEARCH METHODOLOGY

An MILP model was formulated with three primary objectives: minimise cost (capital, operational, and maintenance), minimise GHG emissions (CO_2), and maximise system inertia subject to inequality, equality constraints, and decision variables. The MILP model was then

optimised using CPLEX solver in the General Algebraic Modeling System (GAMS) and implemented using the Institute of Electrical and Electronics Engineers (IEEE) 9-bus test system to demonstrate the effectiveness of the model. Power generators used for the model design comprised thermal generators, wind turbines, and PV systems. Relevant data on generation capacity were obtained from [36].

A mixed-integer quadratic constrained programming (MIQCP) model considering an HES system (Li-ion batteries and SCES) was developed. The resulting MIQCP model was then optimised using CPLEX solver in GAMS and implemented using the IEEE 6-bus test system to demonstrate the effectiveness of the model.

Furthermore, economic incentives (feed-in tariffs [FiTs]) were incorporated into the developed MIQCP model to investigate the influence of economic incentives on promoting renewable energy integration into the grid. Next, a sensitivity analysis of the optimised model was conducted using four scenarios with different levels of renewable energy penetration – 25%, 50%, 75%, and 100% – while the response of the system to the varying degree of renewable energy penetration was observed.

An MIQCP model was formulated to account for uncertainty parameters such as variation in wind speed and solar irradiance under specific system equality and inequality constraints. The uncertainties were accounted for by using an hourly scenario-based approach, while data for a typical location in Bloemfontein in the Free State province of South Africa were used for the analysis.

Uncertainty data on RERs (wind speed variability and solar irradiance variability) for Mangaung Metropolitan Municipality for the year 2019 were incorporated into the model. Next, the resulting MIQCP model was optimised using CPLEX solver in GAMS and implemented using the IEEE 6-bus test system to demonstrate the effectiveness of the model.

1.5 CONTRIBUTION TO KNOWLEDGE

The key contributions of this research work to the body of knowledge when compared to various studies currently available on power system optimisation model designs and formulations are as follows:

- Most power system optimisation models only consider cost and emissions in their model design and formulation, while neglecting system inertia, which is important to ensure the frequency stability of the grid. This research extended existing models by

incorporating system inertia into the power system optimisation model formulation and design. Hence, a novel deterministic (MILP) optimisation model was developed that maximised overall system inertia while minimising cost and emissions. The overall power design thus helps to provide better frequency stability to the modern grid as adequate system inertia is ensured in the grid at all times.

- This study extended existing power system work to consider both FiT and system inertia in the power system optimisation model. A novel deterministic (MIQCP) model was formulated to maximise both system inertia and economic incentives (FiT) while minimising the overall cost and emissions of the system.
- This study extended existing power system optimisation models to consider the uncertainties of RERs while also considering system inertia. A novel scenario-based deterministic (MIQCP) model was developed to maximise system inertia while minimising cost and emissions in the presence of renewable energy uncertainties.
- This research can also make a social impact:
    - This research provides a model that will guide power system investors and operators as investment decisions are made regarding REGs in a way that minimises cost and still achieves adequate overall system inertia in the modern grid.
    - This research provides guidance to power system operators and investors as the variability of the RERs at a given location is considered using the formulated model before investment decisions are made on REGs. This model formulation therefore helps power system investors and operators to make appropriate investment decisions based on available RERs at a given location and ensures maximum harnessing of RERs at a lower cost.

1.6 HYPOTHESES

The hypotheses of the study are as follows:

- H_1: Achieving high system inertia through power system planning will help to improve the overall frequency stability of the modern grid.
- H_2: Achieving high inertia in the power system will imply a higher cost of investment and increased levelised CoE.
- H_3: Reduced emission levels in the power system will directly affect the power output of thermal generators.

1.7 LIMITATIONS OF THE STUDY

This study was limited by the following:

- The proposed model was validated using a modified IEEE test bus study and not the South African power network.
- In considering the stochastic nature of REGs and load demand, previous data were used and not real-time data.
- In this study, the inertia values of power generators were estimated and not measured using phasor measurement units (PMUs).
- In this study, energy storage units (ESUs) used were limited to BESS, SCES, and PHES. Others types such as SMES and CAES were not considered.

1.8 PUBLICATIONS DURING THE STUDY

Peer-reviewed journal articles that are a direct product of this doctoral research are listed below.

1. **Ayamolowo, O.J**., Manditereza P.T. & Kusakana, K. 2020. Exploring the gaps in renewable energy integration to grid. *Energy Reports*, 6:992-999.
2. **Ayamolowo, O.J**., Manditereza P.T. & Kusakana, K. 2021. Investigating the potential of solar trackers in renewable energy integration to grid. *Journal of Physics*: *Conference Series*, 2022(1):012031.
3. **Ayamolowo, O.J.**, Manditereza P.T. & Kusakana, K. 2022. South Africa power reforms: The path to a dominant renewable energy-sourced grid. *Energy Reports*, 8:1208-1215.
4. **Ayamolowo, O.J.**, Manditereza P.T. & Kusakana, K. 2022. An overview of inertia requirement in modern renewable energy sourced grid: Challenges and way forward. *Journal of Electrical Systems and Information Technology*, 9(1):11.
5. **Ayamolowo, O.J.**, Manditereza, P.T. & Kusakana, K. 2022. Optimal planning of renewable energy generators in modern power grid for enhanced system inertia. *Technology and Economics of Smart Grids and Sustainable Energy*, 7(1):33.
6. **Ayamolowo, O.J**., Manditereza P.T. & Kusakana, K. 2023. Combined generation and transmission expansion planning model for improved modern power system resilience. *Electric Power and Components and Systems*, 51(9):898-914.

7. **Ayamolowo, O.J**., Manditereza, P.T. & Kusakana, K. 2023. Assessing the role of hybrid energy storage in generation expansion planning for enhanced frequency stability. *Energy Reports*, 9(S8):1-10.
8. **Ayamolowo, O.J.**, Manditereza P.T. & Kusakana, K. 2023. Sensitivity analysis of feed-in tariff in joint generation and transmission expansion planning consideration the inertia requirement of the grid. *Energy Systems.* https://doi.org/10.1007/s12667-023-00593-0.
9. **Ayamolowo, O.J.**, Manditereza P.T. & Kusakana, K. Short-term renewable energy uncertainties and inertia consideration in power system generation expansion. Under review by *Australian Journal of Electrical and Electronics Engineering*.

1.9 THESIS LAYOUT

This thesis is divided into seven chapters as outlined below:

Chapter 1 provides an introduction to the research work and highlights the aim, objectives, methodology, contributions to knowledge, hypotheses, delimitations, and structure of the study.

Chapter 2 provides a comprehensive literature review on system inertia requirements in power systems. It further highlights the challenges associated with modern power systems with large share renewable energy generators, and presents a way forward regarding the highlighted challenges.

Chapter 3 presents optimal planning of REGs in modern power grids for enhanced system inertia. This chapter formulates a new mathematical model for planning new generators in the power system, considering the inertia requirement of the grid.

Chapter 4 presents the joint generation and transmission expansion planning model (GTEP) for improved modern power system resilience. In this chapter, the model developed in Chapter 3 is extended to consider transmission line expansion. A new mathematical model that considers system inertia in generation and transmission expansion is developed.

Chapter 5 conducts a sensitivity analysis of FiT in joint GTEP considering the inertia requirement of the grid. In this chapter, a new mathematical model is developed that considers the influence of economic incentives (FiT) on the developed model in Chapter 4. A new model is developed for joint GTEP, considering the influence of FiT while meeting the inertia requirement of the grid.

Chapter 6 presents short-term renewable energy uncertainties and inertia considerations in power system generation expansion. This chapter extends the model presented in Chapter 3 to consider the uncertainties of RERs and system inertia in the generation planning model. Furthermore, the variability of RERs (solar irradiance and wind speed) in the Mangaung Metropolitan Municipality in Bloemfontein in the Free State province of South Africa is considered during the year 2019.

Chapter 7 provides the conclusion of the study and highlights recommended future research work.

CHAPTER 2: LITERATURE REVIEW

2.1 INTRODUCTION

This chapter introduces the changing composition and dynamics of the modern power grid and further explains the concept of frequency stability and system inertia in the new grid. In addition, frequency instability mitigation techniques in the literature are reviewed, while an overview of inertia estimation methods in power systems is provided. Furthermore, a review of VI control topologies and strategies in a renewable energy-sourced grid is presented, while the modelling characteristics of ESS are discussed. Lastly, a review of operational and expansion planning models in power systems with a focus on the objective function and modelling technique is presented.

2.2 COMPOSITION AND DYNAMICS OF THE POWER GRID

The dynamics and structural composition of the power grid are changing due to the increased penetration of REGs into the grid. These changes have led to technical challenges such as high frequency deviations (spike and nadir), unwanted frequency oscillations, high RoCoF, etc. Furthermore, the increasing dominance of these variable REGs in the power grid has led to the reduced overall system inertia of the grid, which causes grid stability challenges such as severe frequency nadir, voltage instability, fast RoCoF, and increased harmonics. For example, countries such as New Zealand, the United States of America (USA), the United Kingdom (UK), Cyprus, and Ireland with high penetration of RESs have already reported cases of power disturbances due to large frequency nadir (47.5 Hz) and fast RoCoF (0.73 Hz/s), which led to power interruptions among a large number of customers [37].

These frequency instabilities are undesirable in power systems as they may lead to cascaded system failures. Figure 2.1 illustrates the transformation in the composition of the grid over the years, from synchronous generators being dominant to REGs being dominant.

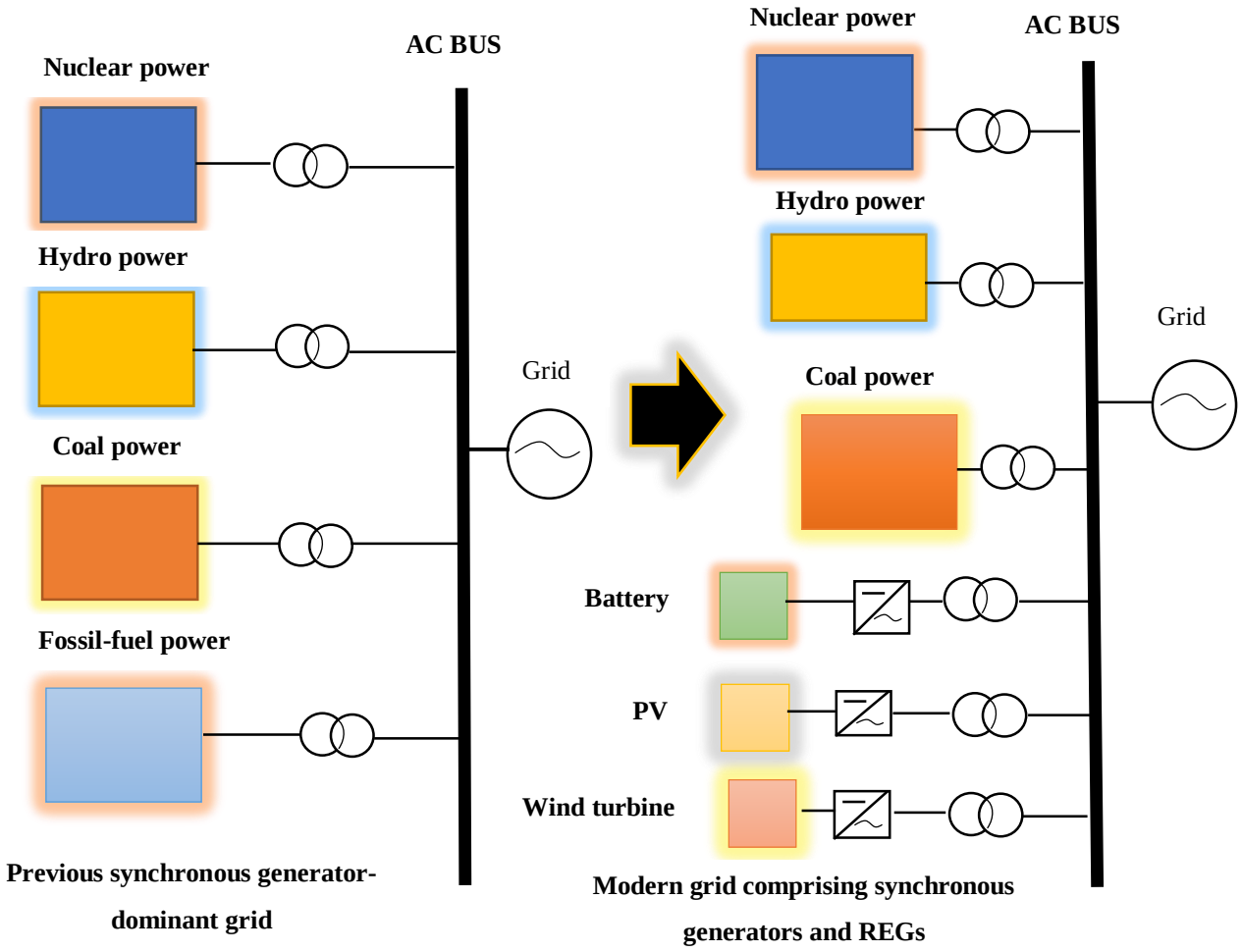

Figure 2.1: Changes in the composition of the power grid

2.3 FREQUENCY STABILITY IN THE POWER GRID

Frequency stability in the grid is important even after contingencies such as sudden loss of generation or load occur. During times of system contingency, the inertia inherent in the grid reacts first by providing instant frequency response within one to 10 seconds after the disturbance, just before the controllers are triggered. Figure 2.2 illustrates the timeline of frequency responses in the power system. It is shown that a system with low inertia will experience larger frequency nadir than a system with high inertia. It is also shown that the primary response takes place between 10 and 30 seconds after using primary frequency controllers, immediately after the inertia response has been provided, while the secondary frequency control or automatic generator control action takes place between 10 and 30 minutes after the contingency has occurred. The tertiary control takes place after 30 minutes using spinning reserves. This research is based on the inertia response of the power system [7].

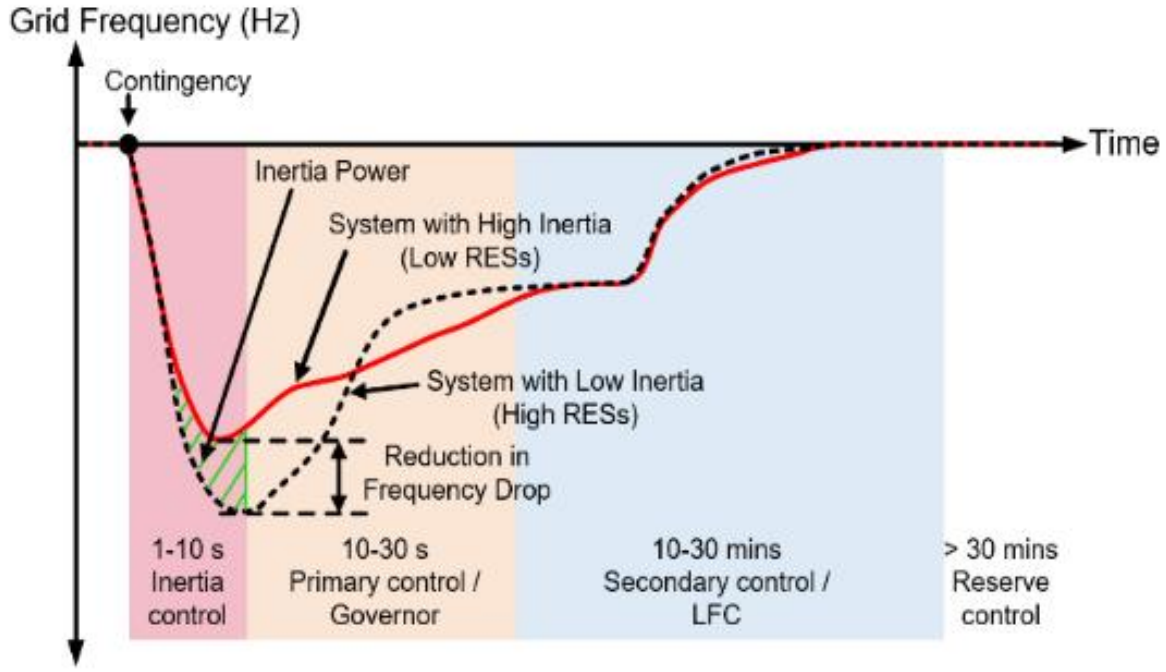

Figure 2.2: Time scale of frequency response during power system contingency [7]

2.3.1 Effects of declining inertia on the power grid: Reports from various countries

Several countries such as New Zealand, the USA, UK, Cyprus, and Ireland that have high penetration of RESs are affected by the declining inertia of the power grid. These countries have in recent times reported cases of power disturbances due to a large frequency nadir (up to 47.5 Hz) and a fast RoCoF (up to 0.73 Hz/s), which led to power interruptions among a large number of customers, tripping frequency relays, and unplanned load shedding [6]. Figure 2.3 illustrates the frequency nadir after a power loss of 2 750 MW at the Electric Reliability Council of Texas power system due to increased RES penetration into the grid.

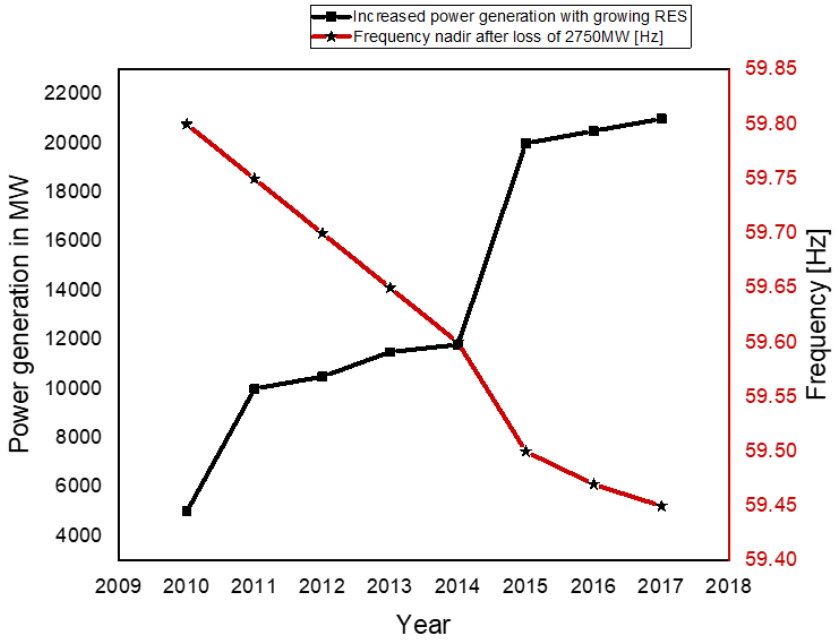

Figure 2.3: Frequency nadir at Electric Reliability Council of Texas power system with a yearly increase in renewable energy power generation

2.4 FREQUENCY-MITIGATING TECHNIQUES IN POWER SYSTEMS

Several methods have been proposed in the literature to mitigate frequency instability primarily by emulating the inertia response of synchronous generators through the use of RESs and ESS with a suitable converter control strategy. This concept is called VI control [38].

The authors in [7], [39] also proposed the use of synchronous generators as spinning reserves, synchronous condensers, and rotating stabilisers to provide inertia to the grid during contingency, while REGs remain the main source of power generation. Although this method provides the needed system inertia, particularly during times of system disturbances, it is, however, limited by its high cost of implementation and high carbon emissions. The authors in [6], [22] proposed the use of ESS together with RESs in a hybrid combination such as PV-BESS, wind turbine-FES, and PV-SCES. The author in [40] proposed a model comprising a hybrid combination of BESS and SCES to mitigate frequency fluctuation at the point of coupling of rooftop solar PV units.

Other methods adopted to provide frequency stability include renewable energy curtailment or deloaded operation of REGs, the use of synchronous condensers to provide synchronous inertia, and load curtailment using incentive-based demand response schemes such as direct load control and time-of-use rates.

In addition, owing to the frequency-related challenges associated with the modern grid, countries such as Ireland and Australia have pegged renewable energy integration into the grid at a certain percentage (70%) to keep the RoCoF below 0.5 Hz/s during contingencies, while others have revised their grid codes in line with the new dynamics of the grid [38].

2.5 CONCEPT AND ANALYTICAL REPRESENTATION OF SYSTEM INERTIA

Inertia can be defined as the amount of kinetic energy stored in the rotor of synchronous generators that tends to resist changes in grid frequency, particularly during times of contingency. The inertia inherent in synchronous machines is called synchronous inertia; the moment of inertia of a synchronous generator can be defined as in Equation (2.1).

$$E = \frac{1}{2} J\omega^2 = S \cdot H \tag{2.1}$$

Where

E defines the kinetic energy of the synchronous generator in (MWs),

J defines the moment of inertia in (kg/m^2),

ω defines the angular frequency in (radian/s),

S defines the base apparent power in VA, and

H is the inertia constant in seconds.

Also, from Equation (2.1), H can be expressed as in Equation (2.2):

$$H = \frac{E}{S} = \frac{J\omega^2}{2S} \tag{2.2}$$

Furthermore, the power imbalance can be represented using the swing equation, as in Equation (2.3):

$$P_m - P_e = P_a = \frac{dE}{dt} = J\omega\frac{d\omega}{dt} \tag{2.3}$$

Equation (2.3) can then be expressed in terms of torque, as in Equation (2.4):

$$\tau_m - \tau_e = \tau_a = J\frac{d\omega}{dt} = J\frac{d^2\theta}{dt^2} \tag{2.4}$$

Where

Pm defines the mechanical power developed in per unit (p.u.),

τ_m defines the mechanical torque developed,

τ_e defines the electrical torque,

Pe defines the electrical power output in p.u.,

Pa defines the acceleration power in p.u.,

θ defines the angular displacement of the rotor in radian,

Equation (2.5) is derived from Equations (2.2) and (2.3):

$$\frac{2H}{\omega} = \frac{J\omega}{S} = \frac{dt}{d\omega}\frac{[P_m - P_e]}{1} \tag{2.5}$$

Rearranging Equation (2.5) gives Equation (2.6):

$$\frac{2H}{\omega}\frac{d\omega}{dt} = \frac{[P_m - P_e]}{S} \tag{2.6}$$

Replacing the angular frequency with the supply frequency and making RoCoF and inertia constant *H* the subject gives Equations (2.6) and (2.7):

$$\frac{df}{dt} = \frac{Pa}{S}\frac{f}{2H} = RoCoF_{p.u} = \frac{Pa_{p.u}}{2H} \tag{2.7}$$

Where

f defines the supply frequency in Hz, and

df/dt is the RoCoF of the system.

Equation (2.7) can be modified to give Equation (2.8), which is used for designing VI controllers:

$$Pa_{p.u} = 2H_{VI}\frac{df_{p.u}}{dt} = K_i\frac{df_{p.u}}{dt} \tag{2.8}$$

Where

H_{VI} is the VI constant,

$Pa_{p.u}$ is the p.u. change in power,

K_i is the VI gain, and

$\frac{df_{p.u}}{dt}$ is the p.u. RoCoF.

Equation (2.7) shows the dependence of RoCoF (df/dt) on the power change P_a and the inertia constant (H). It further reveals that the inertia constant is inversely proportional to the RoCoF, so that the higher the inertia constant, the smaller the RoCoF and vice versa. Also, RoCoF is directly proportional to the acceleration power Pa, so that the greater the power

imbalance, the greater the RoCoF. A reliable and resilient power system can thus be achieved through high system inertia values. Figure 2.4 illustrates the variations of frequency nadir with increasing values of system inertia; it is seen that the higher the system inertia, the lower the frequency nadir. In light of this, frequency instability in the modern power grid can primarily be mitigated by providing adequate inertia in the grid.

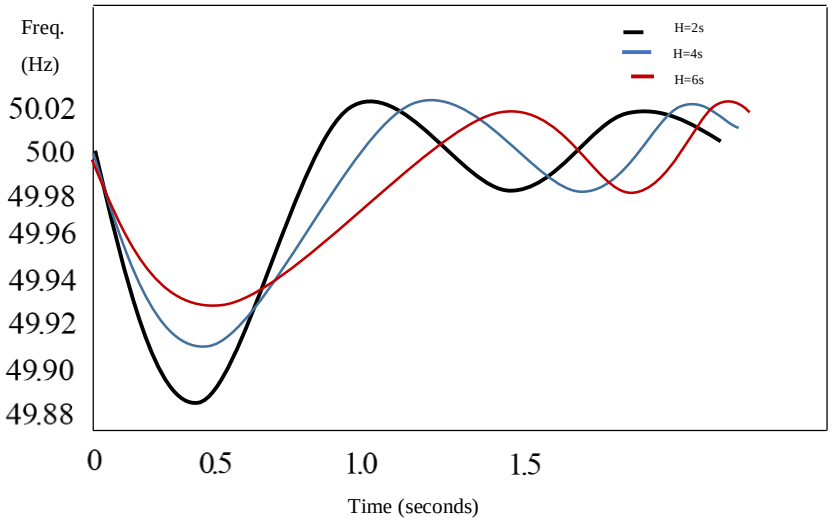

Figure 2.4: Effect of system inertia on frequency nadir

2.5.1 System inertia in a modern power grid

The effective inertia constant in the power system can be represented as the sum of the individual inertia of all connected synchronous generators to the grid, aggregated as a single generator model. It can be expressed as in Equation (2.9):

$$H_{eq} = \frac{\sum_{i=1}^{N} H_i S_{B,i}}{S_B} \tag{2.9}$$

Where

Heq is the aggregated synchronous inertia in the grid,

S_B is the base apparent power,

S_B,*i* is the individual generator apparent power,

N is the total number of connected generators, and

Hi is the inertia constant of each generator.

Similarly, since the modern power system comprises a hybrid combination of synchronous generators, ESS, and REGs, the total inertia in the system will comprise the

synchronous inertia provided by the synchronous generators and the VI obtained from REGs and ESS. The effective inertia *Heq* in a modern power grid can therefore be expressed as in Equation (2.10):

$$H_{eq} = \frac{\sum_{i=1}^{N} H_i S_{B,i} + \sum_{j=1}^{V} H_{VI,j} S_{B,j}}{S_B} \tag{2.10}$$

Where

Hvi,j and S_B,*j* are the VI constant in seconds and the rated apparent power in VA of the jth virtual machine respectively, and

V and *N* define the number of the REGs, and synchronous generators connected in the network respectively.

If *Hvi,j* is very small, then the effective inertia *Heq* in the grid will be substantially reduced; this explains why a renewable energy-dominant power grid is associated with low inertia. Table 2.1 provides the average inertia values of different types of power generators. Table 2.1 shows that the inertia constant from synchronous generators ranges from four to 10 seconds, while the VI constant from ESS ranges from two to four seconds [37]. It can therefore be inferred from Equation (2.10) that the aggregate inertia constant of a modern power system should be four to 10 seconds to ensure the stability of a modern power grid.

Table 2.1: Summary of inertia values of different power generators

Type of generator	Types of inertia	Rated power range (MW)	Inertia constant H(s)
Thermal	Synchronous inertia	10-1 500	2.0-10.0
Hydroelectric	Synchronous inertia	10-200	2.0-4.75
Alternating current (AC) wind turbine	Synchronous inertia	0.016-750	0.5-6.8
Nuclear	Synchronous inertia	1 000-1 200	4.0- 4.8
Biogas fired	Synchronous inertia	200-300	2.0-4.1
Synchronous condensers	Synchronous inertia	50-250	2.0-3.0
CAES	Synchronous inertia	15-600	3.0-4.0
PHES	Synchronous inertia	1-300	2.0-4.0
Open cycle gas turbines	Synchronous inertia	50-150	6.0-6.5

2.6 INERTIA ESTIMATION TECHNIQUES IN POWER SYSTEMS

Inertia estimation in power systems is important to help power operators predict future frequency deviations and make appropriate control decisions. This section provides a review of the various inertia estimation techniques in power systems and highlights their merits and demerits.

The inertia estimation techniques discussed here are classified based on the timing of estimation. Using this criterion, three main approaches are discussed: offline or post-mortem approach, online real-time approach, and forecast or predictive approach. The offline and online techniques are the most used, while the predictive approach is still being advanced.

2.6.1 Offline or post-mortem inertia estimation method

This is a post-mortem disturbance-based inertia estimation method driven by historical data of large disturbance events obtained using PMUs. A PMU is a measuring system installed at generator buses to monitor power system operating conditions such as voltage phasor, current phasor, active power, frequency deviation, harmonics, and power imbalance. The data obtained from the PMU are used to estimate the system's inertia at discrete time instances using an appropriate algorithm. The accuracy of this method depends on the precision of the measuring system and the algorithm used for inertia estimation. This approach is limited by inaccurate frequency measurements due to oscillatory components, as well as distortions and noises in the system. However, its accuracy can be improved by eliminating noise and other distortions in the system [12].

2.6.2 Online inertia estimation approach

Unlike the offline method, the online estimation approach is a dynamic technique that uses real-time measurements from PMUs to provide continuous and discrete inertia values of the power system. Examples of online inertia estimation techniques and models are the dynamic regressor extension technique, autoregressive data-centred models, sliding discrete Fourier transform, and the electro-mechanical oscillation modal extraction method [38].

Challenges of this estimation approach include inaccurate estimation of the total system inertia, extended inertia estimation time, and large computational burdens due to large datasets.

2.6.3 Inertia forecasting or prediction approach

Forecasting techniques are now being used for inertia estimation due to the time-varying nature of inertia from REGs. Several forecasting models have been developed for inertia estimation such as artificial neural network-based models, linear regression models, time series models, and probabilistic inertia forecasting models [12]. However, forecasting techniques are

still being advanced for inertia estimation due to the changing dynamics of the modern power system.

Other unclassified approaches used for inertia estimation are the system identification approach and the zonal inertia estimation technique. The zonal inertia estimation approach sums up the inertia from each contributing zone to provide the total system inertia. The summarised characteristics of different inertia estimation schemes highlighting their merits and demerits are presented in Table 2.2.

Table 2.2: Inertia estimation techniques and their characteristics

Inertia estimation approach	Advantages	Disadvantages
Online	• It is a real-time inertia estimation approach. • Provides higher accuracy as real-time data are used. • Provides continuous as well as discrete inertia estimations. • Well suited for renewable energy-dominant power systems.	• Requires large measurement datasets. • Computation takes a long time. • Associated with a large computation burden.
Offline	• Requires less computation time. • Involves less data. • Has a lesser computation burden.	• Only discrete inertia estimation can be provided. • Not suited for renewable energy-dominant power systems. • Can only estimate inertia after a large disturbance has occurred. • Inaccuracy of inertia estimation exists due to the presence of noise and distortion in the system. • It is not real-time based.
Predictive	• Can be used to predict future frequency response. • Can be used to predict future system inertia so as to take precautionary control measures if needed.	• Accuracy is still low because of the stochastic nature of the RESs. • Technology is still being advanced. • Prediction is limited to short-term prediction.

2.7 VIRTUAL INERTIA (VI) TOPOLOGY AND STRATEGY IN MODERN POWER GRIDS

VI control strategies help to provide artificial inertia to the grid using RESs, ESS, and converters with appropriate control strategies. The control strategies attempt to mimic the characteristics of synchronous generators and induction machines to provide inertia virtually to the grid [41]. Figure 2.5 illustrates the VI control process in the modern grid, while Figure 2.6 provides a broad classification of VI control topologies based on the modelling technique

and solution method. Furthermore, Table 2.2 lists detailed characteristics, merits, and demerits of the different VI control topologies and strategies, while Table 2.3 compares the key parameters among the control strategies.

Several VI control strategies have been adopted in the literature, such as synchronverter, virtual synchronous machine (VSM), synchronous power controller (SPC), virtual synchronous generator (VSG), virtual oscillator control (VOC), virtual synchronous control (VSYNC), and inducverter. These control strategies vary in terms of their characteristics. A further description of the various types of control strategies can be found in [42].

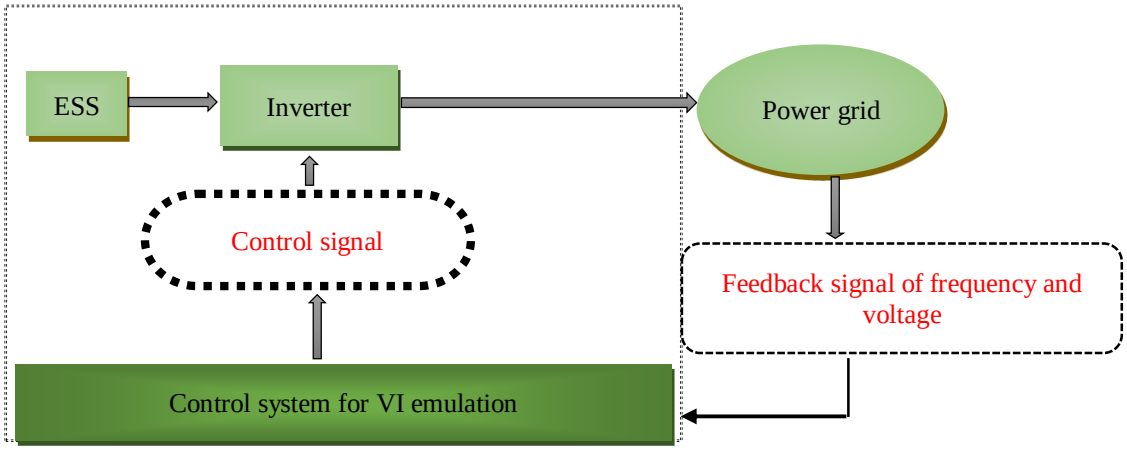

Figure 2.5: Basic configuration of VI control system

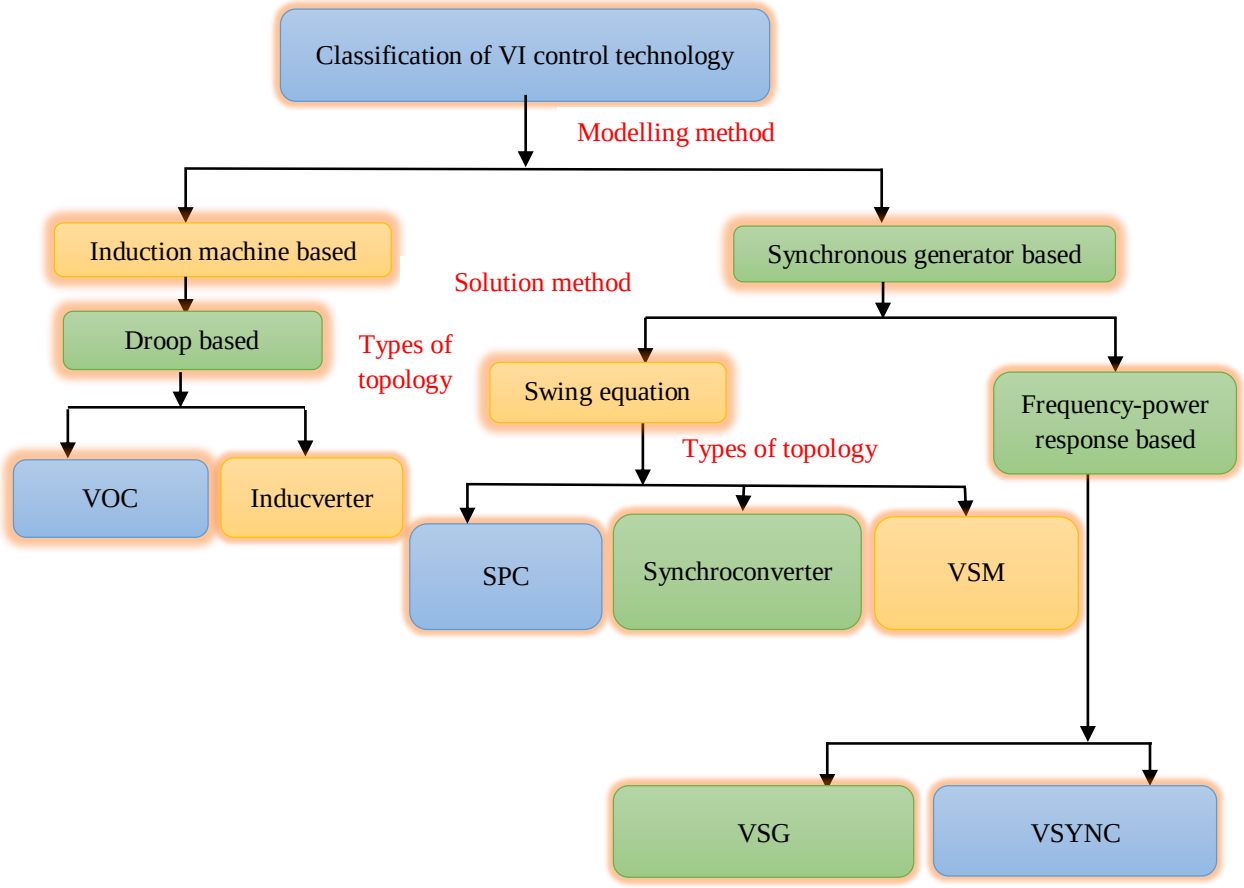

Figure 2.6: VI control classification

2.8 CONTROL EQUATIONS OF VI TOPOLOGY

The various types of inertia emulation topologies and strategies arise from the different mathematical models used to mimic the dynamics of synchronous generators and induction machines. In this section, the mathematical equation that defines the different types of VI topology is provided.

2.8.1 Swing equation-based topology

The swing equation-based topology is governed mathematically by Equation (2.11), which is obtained by considering the damping coefficient in the conventional swing equation [43].

$$P_m - P_e = J\omega\left(\frac{d\omega}{dt}\right) + D_m(\omega - \omega_{ref}) = 2H_{VI}\frac{d\omega_{p.u}}{dt} + D_m(\omega - \omega_{ref}) \tag{2.11}$$

Where

P_m is the input power,

P_e is the output power,

J is the moment of inertia,

ω is the angular frequency,

ω_{ref} is the reference angular frequency, and

D_m is the damping factor.

The control model of the swing equation-based SPC is shown in Figure 2.7, with gain K and time constant T_d.

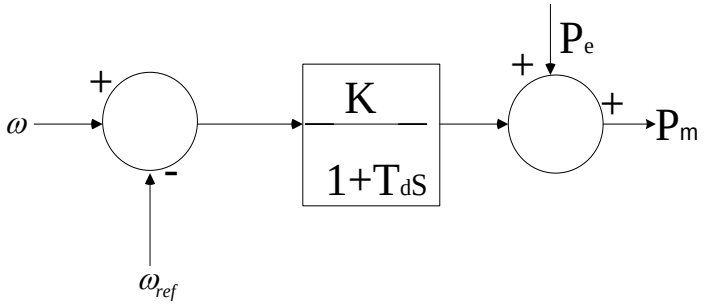

Figure 2.7: Transfer function block diagram of swing equation-based synchronous power controller (SPC) [43]

2.8.2 Frequency-power response topology

The control equation of the frequency-power response-based topologies can be described by Equation (2.12) [43]:

$$P_{out} = K_D \Delta\omega + K_i \frac{d\Delta\omega}{dt} \tag{2.12}$$

Where

$\frac{d\Delta\omega}{dt}$ is the RoCoF,

$\Delta\omega$ is the change in angular frequency,

K_1 is the inertia constant, and

K_D is the damping constant.

Figure 2.8 illustrates the control model of frequency-power response-based VSG.

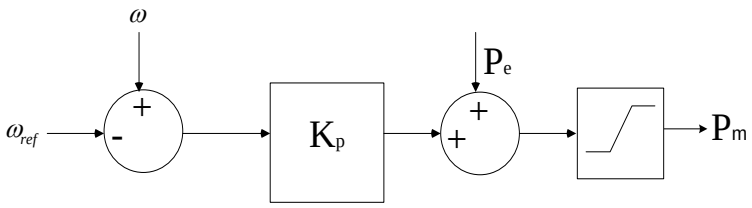

Figure 2.8: Transfer function block diagram of a frequency-power response-based virtual synchronous generator (VSG) [43]

2.8.3 Droop control topology

The droop control-based topology can be represented using Equation (2.13):

$$P_m - P_e = \frac{1}{D_p}(\omega_{ref} - \omega) + \frac{T_f}{D_p}.s.\omega \tag{2.13}$$

Where

ω_{ref} is the reference angular frequency,

ω is the grid frequency,

D_p is the active power droop,

P_m is the reference active input power,

P_e is the active output power, and

T_f is the time constant of the low pass filter.

Figure 2.9 shows the transfer functions block diagram of the droop control-based topology:

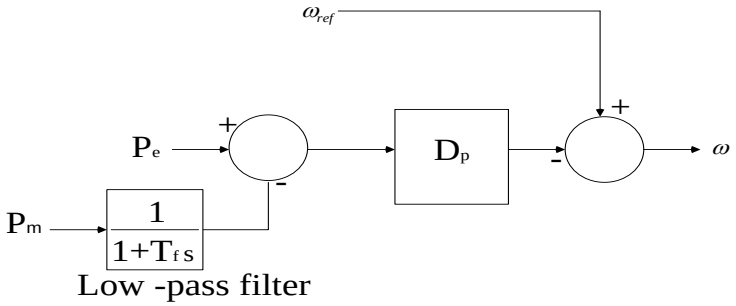

Figure 2.9: Transfer function block diagram of droop control-based topology [43]

Table 2.3: Overview of the characteristics of VI control strategy

Classification based on solution method	Types of control strategy/topology	Merits	Demerits	Ref.
Frequency-power response-based topology	VSG and VSYNC	• Can provide fast frequency response in a steady state. • It has inherent overcurrent protection. • Simplified strategy for reducing frequency nadir in the modern power grid. • Achieves better stability in a weak power grid compared to the droop control method.	• Frequency response is not as fast as synchronous generators. • Inaccurate frequency derivative data from phase-locked loop. • Can be used only in grid-connected mode. • Prone to instability as a result of noise.	[38]
Swing equation-based topology	Synchronverter and VSM	• Has a small damping ratio with lower distortions. • It can operate in both off-grid and on-grid mode. • Provides frequency and voltage regulation. • Phase-locked loop is not required.	• Complex algorithms used may result in numerical instability. • No inherent overcurrent protection; external protection devices are thus required during transient conditions. • Difficult to implement in real life. • Lacks fault ride-through capability. • Presence of high-frequency noise due to converter switching.	[44]
	SPC	• Simple to implement. • Can operate in island as well as grid-connected mode. • Has inherent overcurrent protection.	• Prone to numerical instabilities. • Difficulty of obtaining accurate control parameters may lead to unwanted oscillation.	[44]
Droop control	VOC and inducverter	• Phase-locked loop is not required. • Less prone to grid faults.	• Responds slowly to transients. • Can operate in grid-connected mode only. • Prone to instability in a weak grid. • Associated with high-frequency noise and vibrations.	[45]

Table 2.4: Comparative analysis of VI control parameters

Types of topology	Protection scheme	Grid connectivity	Off-grid connectivity	Stability level	Model order	Model complexity
VSG	Internal	✓	×	High	1st	Simplified
VSYNC	Internal	✓	×	High	1st	Simplified
Synchronverter	External	✓	✓	Medium	2nd	Complex
VSM	External	✓	✓	Medium	5th, 7th	Complex
SPC	Internal	✓	✓	Medium	Low order	Simplified
Inducverter	External	✓	×	Low	High order	Complex

2.9 OPERATIONAL AND EXPANSION PLANNING OPTIMISATION IN POWER SYSTEMS

2.9.1 An overview of power system optimisation methods and techniques

The increasing complexity, changing dynamics, and the need to ensure grid stability have necessitated power system researchers to focus on advanced optimisation techniques that have capabilities of handling new grid peculiarities.

Power system optimisation problems can be solved using several methods. These methods can be classified as exact and approximate approaches. Exact approaches are also called mathematical or classical methods, while approximate methods use heuristics or meta-heuristics algorithms [37]. These modelling approaches are the best suited to capture the dynamics and address the specific challenges of the power grid with clearly defined objective functions, decision variables, and constraints.

Mathematical optimisation models can be defined by the nature of the constraints, which can be linear or non-linear. Linear optimisation problems are solved using linear programming and MILP techniques, while non-linear programming, MINLP, and MIQCP are used to solve non-linear mathematical models [46].

Furthermore, complex mathematical optimisation models are now being solved using algebraic modelling languages such as GAMS, the Advanced Interactive Multidimensional Modeling System, Grid Reliability and Adequacy Risk Evaluator software package, Python, PLEXOS, and Multi-Area Reliability Simulation [37].

On the other hand, heuristic and meta-heuristics optimisation techniques are formulated based on the social behaviours of living organisms. They have shorter processing times and achieve faster convergence; however, they do not guarantee optimal solutions, unlike mathematical techniques. Examples are GA, Benders decomposition, simulated annealing,

tabu search algorithm, differential evolution, binary fireworks algorithm, PSO, nodal ant colony optimisation, evolutionary programming, etc. [37]. These algorithms can also be used in hybridised forms such as GA-PSO [45].

Several optimisation models and expansion planning models have also been proposed to address the peculiarities of the modern renewable energy-dominant grid as seen in Tables 2.4 and 2.5. Furthermore, to account for uncertainties arising from RESs as well as variations in load demand, robust optimisation models were developed in [47], [48], while stochastic optimisation models and risk assessment methods were adopted in [48], [49]. Table 2.5 provides an overview of operational optimisation models and techniques used to address related power system problems.

Table 2.5: Review of operational optimisation models in power systems

Objective function	Model description	Software and solvers	System specification	Ref.
Minimise hydropower curtailment and water spillage	Robust MINLP optimisation	BARON solver in GAMS 24.7.1	Not given	[50]
Maximise energy production	MILP	Xpress solver in Python	Intel Core i5 processor, 8 GB RAM	[51]
Minimise cost and peak load regulation	Robust unit commitment model	Not given	Not given	[52]
Minimise load changes	MILP	Not given	3.3 GHz processor and 8 GB RAM	[53]
Minimise operational cost and maximise the utilisation of ESS	Scenario-based stochastic model	BARONS solver and SCENRED2 tool in GAMS	Intel 2.4 GHz computer	[54]
Minimise total operating cost	Robust optimisation and MILP model	Gurobi solver in MATLAB	Not given	[55]
Minimise the operating cost of the power system	Mixed-integer second-order cone programming model	CVX toolbox and GUROBI 7.52 solver in Python	2.6 GHz CPU Intel Core 2 Duo, and 4 GB RAM	[56]

2.10 EXPANSION PLANNING OPTIMISATION MODEL IN POWER SYSTEMS

Expansion planning optimisation models are gaining prominence in modern power system analysis due to the expected dominance of RESs in power grids and increasing energy demand. Expansion planning models are formulated as optimisation problems with well-defined objectives and constraints. Power system expansion planning models are mainly of three types: generation expansion planning (GEP), transmission expansion planning (TEP), and distribution expansion planning [37].

GEP determines the type of generators to be installed, the optimal capacity and location of generators, the construction time of prospective generating units, and the cost implications of new generators' installations. Similarly, TEP determines the best choice for the installation of new transmission lines, which aids power transfer within a planning horizon.

The planning period for expansion can be static or dynamic (multi-period). In static expansion planning models, the decisions are made within a given target year, while distribution expansion planning involves making decisions in different phases of the planning horizon; thus making use of a yearly representation of the investment decisions. Table 2.5 provides a summarised overview of various optimisation techniques, methods, and solvers used in expansion planning models. Furthermore, it can be observed that most optimisation techniques and models only consider the economic objective, such as the operational cost of generators, and technical objectives, such as power flow, ramping limits, voltage limits, etc., but do not consider the inertia requirement of the grid, which is important to ensure grid stability in renewable energy-sourced power systems.

Table 2.6: Overview of expansion planning models in power systems

Objectives	Types of uncertainties	Model framework	Solver/software/ system configuration	Inertia consideration	Ref.
Minimise cost comprising operating, investment, and environmental costs	Not considered	Deterministic MILP	CPLEX 12.9.0.0. solver. 2.67 GHz processor and 64 GB RAM	No	[57]
Minimise emission and maximise profit	Varying capacity of wind turbines	Linear programming	CPLEX solver in GAMS. Core i5, 3 GHz processor, and 16 GB of RAM	No	[58]
Minimise cost, energy losses, and voltage violation	Not considered	MILP	CPLEX solver in GAMS. Intel Core i7-4770 processor	No	[59]
Minimise investment costs	Not considered	MILP	LINPROG function in MATLAB and CPLEX solver in GAMS. 2.5 GHz CPU, Core i5, and 4 GB RAM	No	[60]
Minimise investment, maintenance, and CO_2 emission cost	Load demand and RES variations	MINLP	Accelerated Benders dual decomposition algorithm	No	[61]
Minimise cost and energy not served	Not considered	MILP	Benders decomposition algorithm	No	[62]

Objectives	Types of uncertainties	Model framework	Solver/software/ system configuration	Inertia consideration	Ref.
Minimise cost and CO_2 emission	Load demand variation	Deterministic MILP	Branch-and-bound method and weighted sum bisection method	No	[63]
Minimise cost	Not considered	Multi-level game theory model	Game theory and bi-level modelling in MATLAB, 8 GB RAM	No	[64]
Minimise cost and CO_2 emission	Load demand and generation variations	MINLP	CPLEX solver using the branch-and-bound algorithm	No	[65]
Minimise the investment costs while considering system uncertainties	Not considered	MILP	Gurobi solver in Python, eight cores and 32 GB of RAM	No	[66]

2.11 DESCRIPTION OF UNCERTAINTIES ASSOCIATED WITH RENEWABLE ENERGY SOURCES (RESs)

The output power of REGs is uncertain and easily affected by environmental factors such as wind speed, solar irradiance, temperature, air density, snow mass, cloud cover, humidity, air pressure, etc. Statistical analysis can therefore be used to describe the uncertain behaviour of solar irradiance and wind speed, as well as to compute the respective output power of the REGs [67]. Uncertainty parameters can be represented using probability distribution functions such as Weibull, lognormal, beta distribution, etc. [68].

In this section, wind speed variability is described using the Weibull distribution, while solar irradiance variability is represented using the beta distribution.

2.11.1 Modelling wind power uncertainty

In this sub-section, the Weibull probability density function (PDF) is used to describe the uncertainty of wind power. The output power for a wind turbine can be estimated as a function of its wind speed, as in Equation (2.14) [69]. Figure 2.10 indicates that a wind turbine's output power can also be estimated according to a power curve graph and provides the relationship between wind turbine output power and wind speed. It is shown that the wind turbine will begin to generate active power above the cut-in speed (between 2.5 m/s and 4 m/s), which is determined by the manufacturers. Furthermore, as the wind speed increases above the cut-in wind speed, the output power will continue to increase until it reaches the rated power output obtained at a rated wind speed (between 10 m/s and 20 m/s). At the rated wind speed, the wind

turbine is expected to maintain a constant power output using an appropriate blade pitch control technique. The wind turbine will shut down if the wind speed is above the cut-out speed (above 25 m/s) for safety reasons [70], [54].

$$P_{wd}(v)=\begin{cases}0 & v<v_{cui}\\ P_{wdr}\cdot\left[\dfrac{v-v_{cui}}{v_{wr}-v_{cui}}\right] & v_{cui}<v<v_{wr}\\ P_{wdr} & v_{wr}<v<v_{cuo}\\ 0 & v>v_{cuo}\end{cases} \tag{2.14}$$

Where

$P_{wd}(w)$ is the wind power output (kW or MW),

P_{wdr} is the rated wind power (kW or MW),

v_{cui} is the cut-in wind speed (m/s),

v_{wr} is the rated wind speed (miles per hour),

v_{cuo} is the cut-out wind speed, and

v is the actual wind speed.

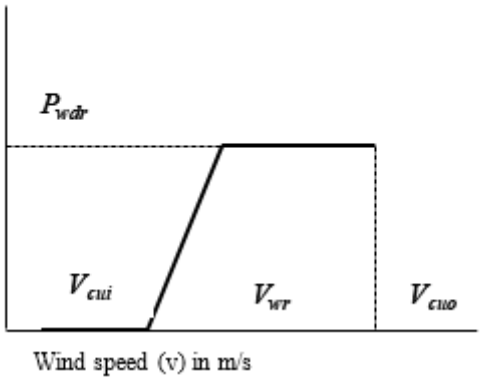

Figure 2.10: Ideal power curve of a wind turbine

Furthermore, the Weibull PDF is used to model wind speed distribution $f(w)$ as expressed in Equation (2.15) [54]. Equations (2.16) and (2.17) provide the mathematical expression of the shape and scale parameter of the PDF respectively [71].

$$f(w)=\left(\frac{\varphi}{\alpha}\right)\left(\frac{v}{\alpha}\right)^{\varphi-1}e^{-\left(\frac{v}{\alpha}\right)^{\varphi}} \tag{2.15}$$

$$\alpha=\left(\frac{\sigma_w}{v_{me}}\right)^{-1.086} \tag{2.16}$$

$$\varphi = \frac{v_{me}}{\Gamma\left(1+\frac{1}{\alpha}\right)} \tag{2.17}$$

Where v is the wind speed (m/s), α and φ are the shape and scale parameters of PDF respectively. The estimated values of the shape factors are calculated based on the mean v_{me} and standard deviation σ_w of the wind speed [72].

2.11.2 Modelling solar power uncertainty

The output power of an ideal solar PV panel is expressed as in Equation (2.18) [73]:

$$P_{pv}(I) = \eta_s^{pv} \cdot I(t) \cdot A_s^{pv} \tag{2.18}$$

Where

A_s^{pv} is the surface area of the PV panel (m^2),

$I(t)$ is the solar irradiance at time t (kW/m^2), and

η_s^{pv} is the efficiency of the PV panel.

Considering solar irradiance uncertainties, the output power of solar PV plants can be expressed as in Equation (2.19) [74], [68]:

$$P_{pv}(I) = \begin{cases} P_{pv}^{rated} \cdot \left[\frac{I^2}{I_{std} \cdot I_c}\right] & 0 < I < I_c \\ P_{pv}^{rated} \cdot \left[\frac{I}{I_{std}}\right] & I \geq I_c \end{cases} \tag{2.19}$$

Where

$P_{pv}(I)$ is the output power from the solar PV plant,

I is the solar irradiance,

P_{pv}^{rated} is the rated output power from solar PV plant,

I_c is the certain set irradiance point, and,

I_{std} is the solar irradiance in a standard environment.

Furthermore, the beta PDF of solar irradiance can be expressed as in Equation (2.20). Beta PDF follows the Jacobi method [75], [76]. Equations (2.20) to (2.22) provide the mathematical expression of the shape and scale parameter of the beta PDF respectively [77].

$$PDF(I) = \frac{\Gamma(\alpha+\beta)}{\Gamma(\alpha)\Gamma(\beta)} \cdot I^{\alpha-1} \cdot (1-I)^{\beta-1} \tag{2.20}$$

$$\alpha = \frac{\mu_I \cdot \beta}{1-\mu_I} \tag{2.21}$$

$$\beta = (1-\mu_I) \cdot \left(\frac{\mu_I(1-\mu_I)}{\sigma_I^2} - 1 \right) \tag{2.22}$$

Where α and β are the shape parameters of the beta PDF, which can be obtained using the mean μ_I and standard deviation σ_I of the measured solar irradiance.

2.12 CONCLUSION

This chapter highlighted the challenges associated with the modern power grid and explained the role of inertia in ensuring frequency stability in the power grid. A concise review of the modelling characteristics of different ESS used to provide inertia support to the grid was provided. The chapter also provided a mathematical formulation of system inertia in the power system. The chapter presented an overview of inertia estimation methods in a power system, and reviewed different VI control topologies and strategies and highlighted their merits and demerits. A review of optimisation planning methods, techniques, and tools was also provided.

Furthermore, after careful review of available related literature on power system optimisation models, the following research gaps were identified:

- Most power system optimisation models do not consider the inertia requirement of the grid in their model formulation but focus more on emissions (environmental) and cost (economic) considerations. However, adequate system inertia is important to mitigate frequency instability and to ensure stability in the modern renewable energy-dominant grid.
- Most power system optimisation models do not consider the uncertainties of RERs, while also neglecting the inertia requirement of the grid in their model formulation.
- Most power system optimisation models do not consider the role of economic incentives such as FiT to promote REGs' integration into the grid while simultaneously considering the inertia requirement of the grid.

The following challenges were also identified:

- As more REGs are added to the grid, the overall inertia of the grid reduces, which makes the grid vulnerable to frequency stability challenges such as high RoCoF and large frequency nadir.
- Neglecting system inertia in power system planning and optimisation models could lead to frequency instability in the modern grid.
- Neglecting system inertia in power system planning could lead to inappropriate investment decisions regarding new REGs, which make the modern grid vulnerable to frequency stability challenges.

To address the identified challenges, this research formulated novel mathematical models (operational and expansion planning models) that consider system inertia in the model formulation, while simultaneously considering cost, RER uncertainties, and emissions.

CHAPTER 3: OPTIMAL PLANNING OF RENEWABLE ENERGY GENERATORS (REGs) IN MODERN POWER GRIDS FOR ENHANCED SYSTEM INERTIA

3.1 INTRODUCTION

As more non-inertia REGs are being integrated into the power grid, the overall system inertia of the power grid is reduced, which makes the new grid less resistant to system contingencies such as sudden loss of load [78], [79]. This makes the modern grid prone to frequency instabilities such as fast RoCoF and large frequency nadir. The use of ESS was investigated in [79] to mitigate grid frequency instability due to increasing RES penetration into the grid. The optimal operation and placement of ESS in the modern grid were also investigated in [80] using GA, and in [81] using an improved binary PSO algorithm.

Several studies have been conducted on the optimal scheduling and planning of new power system generators into the power grid using heuristic algorithms, metaheuristic algorithms, and mathematical methods. The authors in [82] developed a dynamic multi-objective model for power system planning to minimise system cost and emissions. The model was solved using the binary PSO algorithm. The authors, however, did not consider the need for REGs and ESUs in their model formulation. Furthermore, the authors in [83] developed an economical-environmental-technical dispatch model to minimise the total system cost, system emission, voltage deviation, and power loss. The model was solved using three metaheuristic optimisation algorithms: coronavirus herd immunity optimiser, salp swarm algorithm, and ant lion optimiser. The key findings of the study were that the coronavirus herd immunity optimiser technique outperformed the other optimisation approaches. However, the authors did not consider the inertia requirement of the grid in the model formulation. Similarly, the authors in [84] developed an economic-environmental dispatch model to minimise the total system cost and emissions. The model was implemented on a 30-bus IEEE test system and solved using the Harris hawks optimisation algorithm and flower pollination algorithm. The key findings of the study were that the Harris hawks optimisation technique outperformed the flower pollination technique in achieving the model objectives; however, the model also did not consider the inertia requirement of the grid, nor the need for ESUs in the model formulation. A multi-objective optimal power flow model was developed in [85] to minimise cost, emissions, and power loss using a decomposition-based multi-objective PSO algorithm. The model was implemented on a modified IEEE 30-bus and IEEE 57-bus test power systems.

The findings of the study revealed that the developed model algorithm performed better than other metaheuristic optimisation algorithms. However, the model also did not consider the inertia requirement of the grid, nor the need for ESUs to combat frequency instabilities in their model formulation framework. The authors in [86] developed an optimal power flow optimisation model to minimise cost and emissions. The model was solved using a hybrid optimisation algorithm comprising the salp swarm optimisation and PSO algorithms. The key findings of their study were that the hybrid optimisation model performed better than other metaheuristic optimisation algorithms used in the analysis. However, the model also did not consider the inertia requirement of the grid in their model formulation, nor the need for ESUs.

Few studies have considered the inertia requirement of the grid in operation and expansion planning models. The authors in [37] explained the importance of VI as a solution to the declining inertia of the power grid, while the authors in [1] explained the importance of adequate inertia in an AC power system network in order to ensure frequency stability. The authors further proposed a minimum effective inertia constant of 3.6s required in the conventional grid to ensure frequency stability of the grid. However, the authors did not consider the capacity of the grid in their research. The authors in [87] highlighted the various types of ESS that can be used to provide VI to the grid. The various characteristics of the ESS were also explained. The authors in [88] conducted a comparative analysis of the stability of the grid using different VI control techniques. Their findings revealed that VI control techniques can be used to improve the stability of the modern power grid; however, GEP in the presence of ESUs was not considered in their model analysis. The authors in [89] investigated the effect of decreasing system inertia on the frequency stability of the modern grid. The key findings of their study were that a low-inertia grid will be associated with frequency instabilities; however, these instabilities can be mitigated using fast frequency responding devices. The authors in [90] investigated the system inertia of Rwanda's power system under varying RES penetrations. Their research findings indicated that the overall system inertia in Rwanda's power system decreased with an increase in RES penetration; thus causing the system frequency to deviate above the acceptable limit during system contingency. However, the impact of the study in [90] on other system parameters such as cost and emissions was not investigated. In [91], the impact of increasing renewable energy penetration on the rotational inertia of the European power system was investigated. The findings of the study revealed that setting a minimum inertia limit in the grid may truncate the net zero carbon goals by 2050. However, this study did not consider the need for ESUs in the model formulation.

For expansion planning models, the authors in [92] highlighted the importance of inertia considerations in GEP. The authors in [93] presented an analytical framework for frequency constraint formulation in an economic dispatch problem. The authors in [94] developed an MILP model using simplified system frequency constraints to plan for expansion in the power system. Their results showed the importance of enhancing system inertia in order to combat frequency instability in the expanding grid. However, the expansion model was developed for an integrated power and natural gas system, while the need to minimise the resulting emissions from the model was not considered. The authors in [5] conducted a curtailment analysis of the Nordic power system by setting a minimum inertia limit of 113 GWs in the grid. The findings of their study revealed that considering the inertia requirement of the grid in planning will not lead to significant energy curtailment in the grid. However, the study did not consider the need to minimise emissions from thermal generators in their model formulation. A GEP model was developed in [95] to accommodate new REGs in the grid. The model was solved using a differential evolution algorithm to minimise system cost and emissions. The findings revealed that as RES penetration into the grid increases, the overall system cost increases and the system efficiency decreases. However, the model did not consider the inertia requirement of the grid, nor the need for ESS in the model analysis. Similarly, the authors in [65] developed a GEP model to minimise cost and CO_2 emissions. The model also considered investment in REGs. The key findings of their study were that investment in wind turbines reduced the total CO_2 emissions in the system; however, the total system cost increased. The study also did not consider system inertia and the need for ESUs in the model analysis. The authors in [96] incorporated BESS into their GEP model. The model was developed as an MILP model and solved using an agglomerative hierarchical clustering decomposition algorithm; however, the influence of system inertia was not considered in the model formulation and analysis.

A summarised review of related literature is presented in Table 3.1, in which the novelty of this study can be seen in relation to related studies. To the best of the student's knowledge, as seen in the reviewed literature and in Table 3.1, no study was found that carried out GEP considering the inertia requirement of the grid, cost and emissions in the presence of ESS and REGs. To this end, this research aimed to develop a new deterministic optimisation model that maximises the overall system inertia in the grid while minimising the cost of operation, emissions from thermal generators, and investment in new REGs and ESS. The model was developed as an MILP optimisation problem and solved using CPLEX solver in GAMS. The resulting model was validated using the modified IEEE 9-bus system to test the robustness of

the system, while optimal scheduling of the generators was obtained. The main contributions of the proposed model are as follows:

- Formulation of a new deterministic GEP model of new REGs and ESS for enhanced system inertia.
- Conducting performance evaluation of the developed model in terms of cost and system inertia.
- Conducting sensitivity analyses of the developed model under different RES penetration levels.

Table 3.1: Summarised highlights of related literature versus this study

Reference	GEP	Inertia consideration	Cost consideration	Emissions consideration	RES presence	ESS presence
[83]	✓	×	✓	✓	✓	×
[84]	✓	×	✓	✓	✓	×
[85]	✓	×	✓	✓	✓	×
[97]	×	✓	×	×	×	×
[98]	×	×	✓	✓	✓	✓
[99]	×	×	×	×	×	✓
[90]	×	✓	×	×	✓	×
[5]	×	✓	✓	×	✓	×
[91]	×	✓	✓	✓	✓	×
[100]	✓	×	✓	✓	✓	×
[95]	✓	×	✓	✓	✓	×
[65]	✓	×	✓	✓	✓	×
[101]	✓	×	✓	✓	✓	✓
This study	✓	✓	✓	✓	✓	✓

The remaining part of this chapter is structured as follows: Sections 3.2 and 3.3 provide the mathematical formulation of the new deterministic optimisation model and its implementation on a modified IEEE 9-bus system, Section 3.4 presents the model simulation results and discussion, and Section 3.5 concludes the chapter.

3.2 MODEL FORMULATION

The proposed GEP model formulated to maximise overall system inertia while minimising the total cost and CO_2 emissions of the system is described in this section.

3.2.1 Objective function formulation

This model sought the optimal planning of new ESS and REGs in such a way as to minimise the total cost and CO_2 emissions while maximising system inertia. The total cost comprises the operational cost of thermal generators and the investment cost of new REGs and ESS. In order to minimise the total cost and maximise system inertia simultaneously, a multi-objective optimisation model was formulated, as presented in Equation (3.1). PV systems and wind turbines are considered candidate REGs, while BESS and PHES are considered candidate ESUs. The multi-objective optimisation problem was converted into a single objective function in order to obtain a Pareto optimal solution using the weighted sum approach. The model assumed that the inertia from the synchronous generators and the VI from REGs and ESS can be aggregated.

$$\min\left\{\begin{array}{l}\alpha\left[\begin{array}{l}\sigma\left[\sum_{g}^{n} a_g (P_g)^2 + b_g (P_g) + c_g + \sum_{g}^{n} \lambda_e e_g (P_g) + \sum_{w}^{nw} CO_w^{cul} (P_w)\right] \\ + \sum_{v}^{nv} CO_v^{inv} \cdot \mu 1_v + \sum_{p}^{np} CO_p^{inv} \cdot \mu 2_p + \sum_{w}^{nw} CO_w^{inv} \cdot \mu 3_w + \sum_{s}^{ns} CO_s^{inv} \cdot \mu 4_s\end{array}\right] \\ -\beta\left[\dfrac{\sum_{g=1}^{n} H_g \cdot S_g + \sum_{s=1}^{ns} H_s \cdot S_s + \sum_{w=1}^{nw} H_w \cdot S_w + \sum_{v=1}^{nv} H_v \cdot S_v + \sum_{p}^{np} H_p \cdot S_p}{S_{base}}\right]\end{array}\right\} \tag{3.1}$$

The non-negative weighting factors in Equation (3.2) were used to transform the economic and technical objective into a single objective function:

$$\alpha + \beta = 1 \tag{3.2}$$

The total operating cost is given as the sum of the quadratic fuel cost of the thermal generators, curtailment cost of wind turbines, and the cost of emissions from thermal generators. The quadratic fuel cost in Equation (3.3) was linearised by approximating it by a set of piecewise segments *k*, as presented in Figure 3.1 [80]. The resulting linear equation could then be solved easily and faster using a linear programming solver.

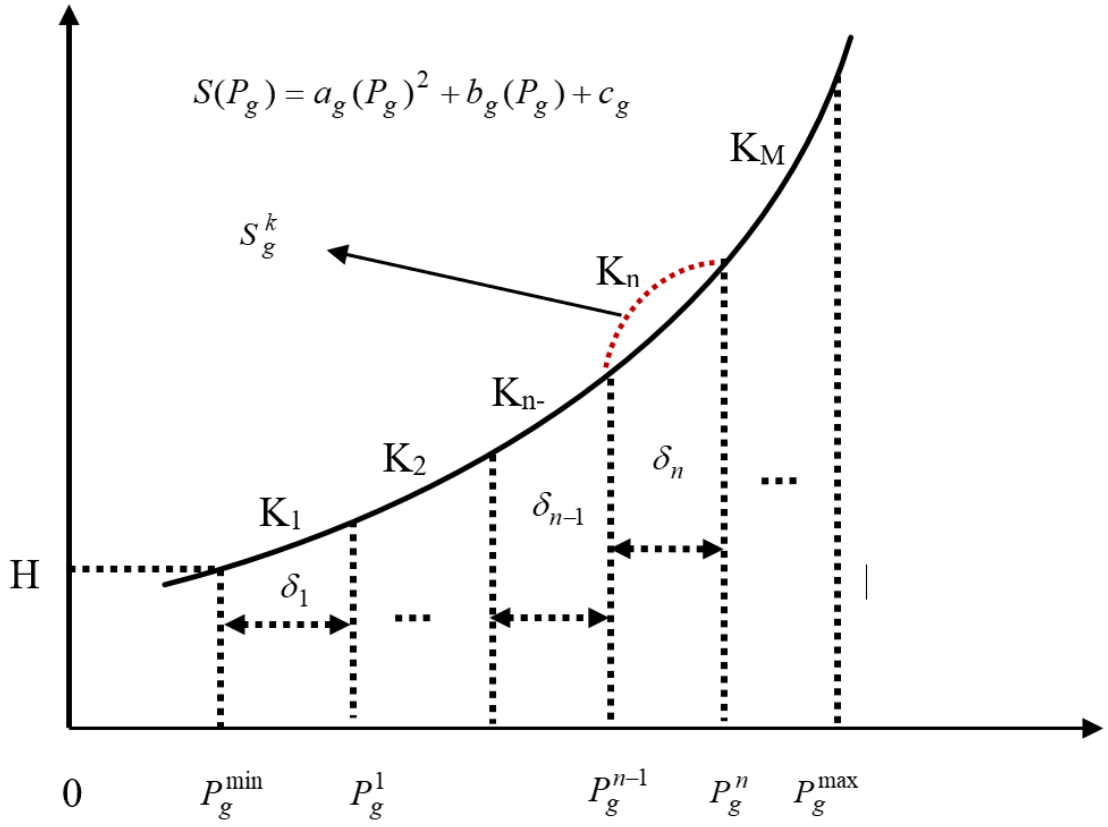

Figure 3.1: Piecewise linear fuel cost

The linear version of the fuel cost calculation is expressed in Equation (3.4), while the mathematical formulation used for the linearisation is given in Equations (3.4) to (3.9).

$$\sum_g^n a_g(P_g)^2 + b_g(P_g) + c_g = S(P_g) \tag{3.3}$$

$$S(P_g) = a(P_g^{\min})^2 + b(P_g^{\min}) + cu_{g,t} + \sum_k S_g^k P_g^k \tag{3.4}$$

Where

$$S_g^k = \frac{C_{g,fin}^k - C_{g,ini}^k}{\Delta P_g^k} \tag{3.5}$$

$$C_{g,ini}^k = a(P_{g,ini}^k)^2 + b(P_{g,ini}^k) + c \tag{3.6}$$

$$C_{g,fin}^k = a(P_{g,fin}^k)^2 + b(P_{g,fin}^k) + c \tag{3.7}$$

$$0 \le P_{g,t}^k \le \Delta P_g^k \qquad \forall k = 1:n \tag{3.8}$$

$$\Delta P_g^k = \frac{P_g^{\max} - P_g^{\min}}{n} \tag{3.9}$$

3.2.2 Model constraints

The proposed MILP model was subjected to investment, power generation, power balance, inertia, direct current (DC) optimal power flow, ramp rate, emission, budgetary, energy storage, and renewable energy flexibility constraints.

3.2.2.1 Investment constraints

Equations (3.10) to (3.14) set an upper bound on number of investments in BESS, PHES, wind farm, and solar PV technology respectively. Equation (3.14) defines the binary investment variables used for selecting investment in BESS, PHES, wind turbine, and solar PV systems respectively. The variable is equal to 1 if a particular technology is to be built, and 0 if otherwise.

$$\sum_{v} \mu 1_{v} \leq \overline{nv} \qquad \forall v = 1,2,\ldots nv \tag{3.10}$$

$$\sum_{p} \mu 2_{p} \leq \overline{np} \qquad \forall p = 1,2,\ldots np \tag{3.11}$$

$$\sum_{w} \mu 3_{w} \leq \overline{nw} \qquad \forall w = 1,2\ldots nw \tag{3.12}$$

$$\sum_{s} \mu 4_{s} \leq \overline{ns} \qquad \forall s = 1,2\ldots ns \tag{3.13}$$

$$\mu 1_{v}, \mu 2_{p}, \mu 3_{w}, \mu 4_{s} \in \{0,1\} \tag{3.14}$$

3.2.2.2 Power generation constraints

The power output of each generating unit is limited by the following constraints:

$$\underline{P_{g}} \leq P_{g} \leq \overline{P_{g}} \tag{3.15}$$

$$0 \leq P_{s,t} \leq \mu 4_{s} \cdot \overline{P_{s,t}^{Av}} \tag{3.16}$$

$$0 \leq P_{w,t} \leq \mu 3_{w} \cdot \overline{P_{w,t}^{Av}} \tag{3.17}$$

$$P_{w,t}^{wc} = P_{w,t}^{Av} - P_{w,t} \tag{3.18}$$

$$P_{w,t}^{Av} = P_{w,t}^{cap} \cdot \chi_{w,t}^{va} \tag{3.19}$$

Equation (3.15) sets the minimum and maximum operating limits for the thermal generators. Equations (3.16) and (3.17) set the operating limits of the solar PV system and wind farm respectively. Equation (3.18) specifies the power curtailment for the wind farm, while Equation (3.19) specifies the wind farm available power per time.

3.2.2.3 *Power balance constraints*

Equation (3.20) states that the sum of power from all online thermal units, wind farms, solar PV systems, PHES, discharge power from BESS, charging power from BESS, and the power flowing in and out of the transmission lines should be greater than or equal to the total load demand. A power demand safe margin *x* was introduced to cater for an unanticipated increase in demand. The power demand safe margin was taken as 105% of the peak load demand in this study.

$$\sum_{g}^{n} P_g + \sum_{w}^{nw} P_w + \sum_{s}^{ns} P_s + \sum_{p}^{np} P_p + \sum_{v}^{nv} P_v^{dis} - \sum_{v}^{nv} P_v^{cha} + \sum_{l \in rl} P_{ij}^{+} - \sum_{l \in sl} P_{ij}^{-} \geq x \cdot \sum_{i} D_i \tag{3.20}$$

3.2.2.4 *Direct current (DC) optimal power flow constraints*

Equation (3.21) sets the voltage angle at bus within a specified limit to ensure that the power flow in the transmission line is below the static stability limit. Equation (3.22) states that the transmission line limit is a function of the voltage angle at bus and line susceptance. Equation (3.23) specifies the transmission line flow limit.

$$-\frac{\pi}{2} \leq \psi_i \leq \frac{\pi}{2} \tag{3.21}$$

$$P_{ij} = B_{ij}(\psi_i - \psi_j) \tag{3.22}$$

$$-p_{ij}^{\max} \leq P_{ij} \leq P_{ij}^{\max} \tag{3.23}$$

3.2.2.5 *Emission constraints*

Equation (3.24) limits the total emissions from thermal generators to a maximum permissible value:

$$\sum_{g} e_g(P_g) \leq E_{\lim} \tag{3.24}$$

3.2.2.6 *Inertia constraints*

Equation (3.25) sets the permissive overall inertia constant in the power system model within a specified range:

$$H_{\min} \leq H_{eq} \leq H_{\max} \tag{3.25}$$

3.2.2.7 *Ramp rate constraints*

Equations (3.26) and (3.27) constrain the active power of the thermal power plants by their ramp rate limits. Equation (3.26) provides the ramp down limit, while Equation (3.27) provides the ramp up limit:

$$P_{g,t-1} - P_{g,t} \leq RPD_g \tag{3.26}$$

$$P_{g,t} - P_{g,t-1} \leq RPU_g \tag{3.27}$$

3.2.2.8 *Energy storage constraints*

ESS are used to increase the flexibility of power system operation as they discharge their stored energy in times of energy deficiency and charge during times of excessive energy [85], [102]. In addition, they are used to provide VI to the grid through VI control schemes. Investment decisions regarding ESS should be based on the inertia requirement of the grid, as well as the individual characteristics of the ESS.

Equation (3.28) describes the state of charge (SoC) of the BESS. Equation (3.29) provides the SoC capacity limit of prospective BESS. Equations (3.30) and (3.31) provide the charging and discharging power limits of BESS respectively. Equations (3.32) and (3.33) describe the binary variable used to prevent charging and discharging of the BESS at the same time. Equation (3.34) sets the maximum number of ESS comprising BESS and PHES that can be installed during the planning horizon.

$$SC_{v,t} = SC_{v,t-1} + (P_{cha} \cdot \eta_v^{cha} - P_{dis} / \eta_v^{dis}) \tag{3.28}$$

$$SC_{v,t}^{\min} \cdot u1_v \leq SC_{v,t} \leq SC_{v,t}^{\max} \cdot u1_v \tag{3.29}$$

$$\mu 5_v^{cha} \underline{P_v^{cha}} \leq P_v^{cha} \leq \mu 5_v^{cha} \overline{P_v^{cha}} \tag{3.30}$$

$$\mu 5_v^{dis} \underline{P_v^{dis}} \leq P_v^{dis} \leq \mu 5_v^{dis} \overline{P_v^{dis}} \tag{3.31}$$

$$\mu 5_v^{cha}, \mu 5_v^{dis} \in \{0,1\} \tag{3.32}$$

$$\mu 5_v^{cha} + \mu 5_v^{dis} = 1 \tag{3.33}$$

$$\sum_v \mu 1_v + \sum_p \mu 2_p \leq \overline{ne} \tag{3.34}$$

3.2.2.9 *Budgetary constraints on investment*

Equations (3.35) to (3.39) define budgetary allocation limits on candidate REGs and ESUs:

$$\sum_{v} CO_{v}^{inv} \cdot \mu 1_{v} \leq \overline{BU_{v}} \tag{3.35}$$

$$\sum_{p} CO_{p}^{inv} \cdot \mu 2_{p} \leq \overline{BU_{p}} \tag{3.36}$$

$$\sum_{w} CO_{w}^{inv} \cdot \mu 3_{w} \leq \overline{BU_{w}} \tag{3.37}$$

$$\sum_{s} CO_{s}^{inv} \cdot \mu 4_{s} \leq \overline{BU_{s}} \tag{3.38}$$

$$\sum_{v} CO_{v}^{inv} \cdot \mu 1_{v} + \sum_{p} CO_{p}^{inv} \cdot \mu 2_{p} + \sum_{w} CO_{w}^{inv} \cdot \mu 3_{w} + \sum_{s} CO_{s}^{inv} \cdot \mu 4_{s} \leq \overline{BU_{T}} \tag{3.39}$$

Equations (3.35) to (3.39) provide the budgetary constraints that also guide investment in BESS, PHES, wind farm, and solar PV technology respectively. They subject the total investment per technology to be less than or equal to its budgetary allocation. Equation (3.39) constrains the total investment in candidate REGs and ESS to a maximum monetary budget.

3.2.2.10 *Renewable energy flexibility constraints*

Equations (3.40) to (3.42) constrain RES penetration into the grid within a specified limit in order to conduct sensitivity analysis on the model. RES penetration target levels are set to 33%, 66%, and 100%, using a flexible parameter *fl*. Equation (3.40) constrains the total power generation from RES using the flexible parameter *fl*, which is given as a fraction of the total load demand. Equation (3.41) limits the total power generation from thermal generators to at most *(1- fl)* percent of the total load demand [103]. Equation (3.42) defines the range of values of the flexible parameter *fl*, which is used to confine the RES penetration level to between 33% and 100% of the total load demand.

$$\left[\sum_{s=1}^{ns} P_{s} \cdot \mu 4_{s} + \sum_{w=1}^{nw} P_{w} \cdot \mu 3_{w}\right] \leq fl \cdot \left[\sum_{i} D_{i}\right] \tag{3.40}$$

$$\left[\sum_{g=1}^{n} P_{g}\right] \leq (1 - fl) \cdot \left[\sum_{i} D_{i}\right] \tag{3.41}$$

$$fl \in [0.33, 0.66, 1.0] \tag{3.42}$$

3.3 MODEL DESIGN

The proposed MILP model was analysed for a time horizon of one year. Tables 3.2 and 3.3 provide the data for the thermal generators and candidate REGs and ESUs used in the model formulation. Transmission line parameters, load demand data at buses, and model parameters were obtained from [104], [105], [106], [107].

In order to make provision for expansion in the power network, the load demand at buses is assumed as increased by 50%. Candidate REG units are then placed at buses with the least load demand (buses 5, 6, 8, and 9) because of the intermittency of REGs, while ESUs are placed at buses with the highest load demand (buses 1, 4, 5, and 6) to provide support during times of peak load demand. Figure 3.2 illustrates the flowchart of the model design.

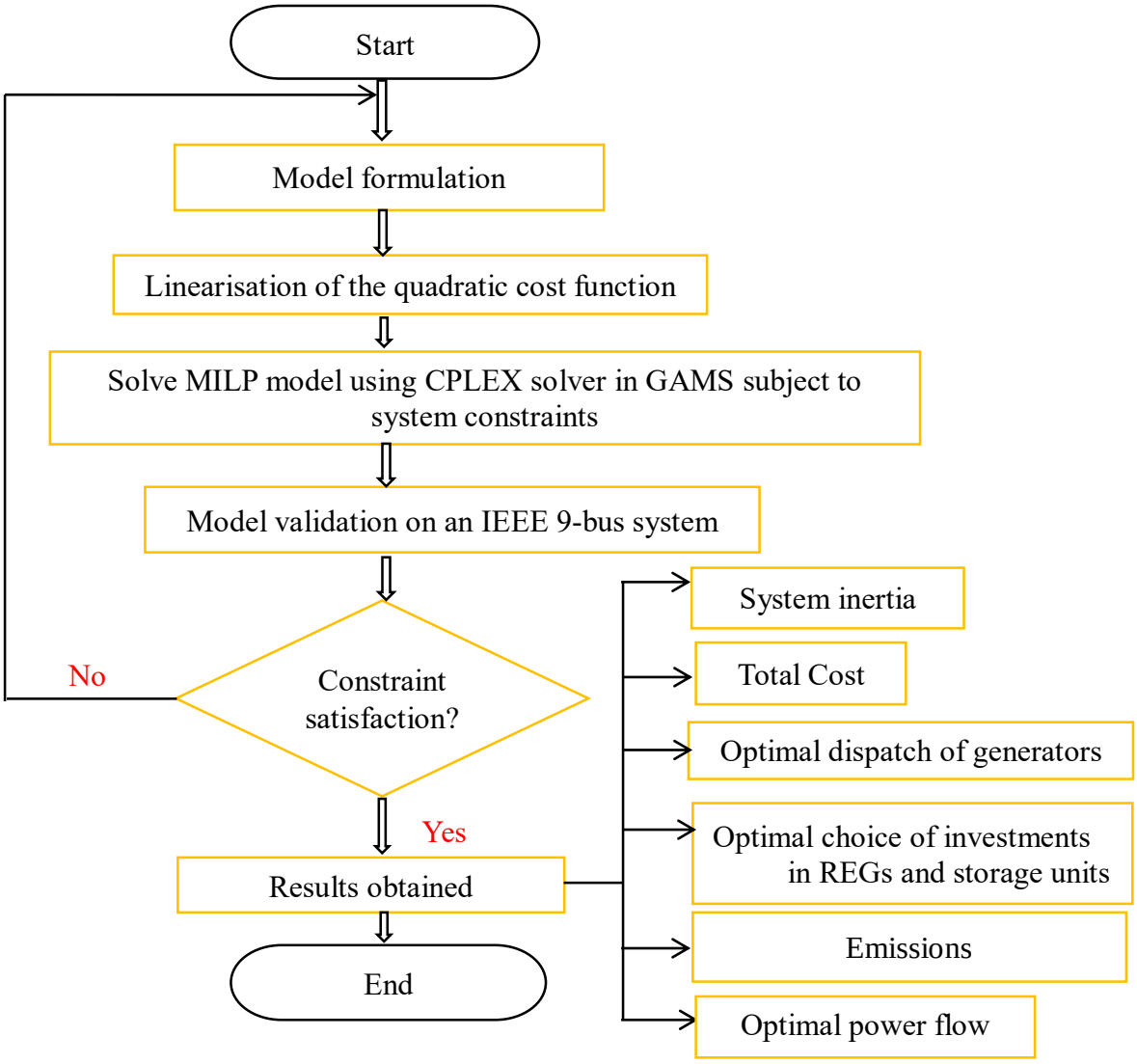

Figure 3.2: Flowchart of the proposed model design

Table 3.2: Generation data on thermal generators [104]

Gen. unit	Bus no.	Ag ($/MW^{2}h)	Bg ($/MWh)	Cg ($)	Capacity (MVA)	Pmax (MW)	Pmin (MW)	Inertia (s)
G1	1	0.00043	16.6	900	250	203.1	81.2	6.0
G2	2	0.00073	15.5	800	240	194.4	77.8	6.0
G3	3	0.00059	14.8	700	625	500.0	100.0	4.0
G4	4	0.00075	15.9	470	500	400.0	40.0	2.5
G5	6	0.00079	16.6	200	550	441.8	44.2	2.5

Ag, Bg, and Cg = Quadratic cost coefficient of the thermal generator; Pmax = Maximum power delivery of the thermal generator, Pmin = Minimum power delivery of the thermal generator.

Table 3.3: Data on candidate REGs and energy storage systems (ESS)

REG type	Bus	Pmax (MW)	MaxInvest $\mu_{v,p,w,s}$	InvestCost ($/MW/yr) $CO^{inv}_{v,p,w,s}$	Inertia (s)
Wind + VI (W_1, W_2)	5, 9	200	2	80 000.0	4
Wind (W_3, W_4)	5, 9	200	2	72 641.8	2
Solar (S_1, S_2)	6, 8	200	2	84 467.2	0
Solar + VI (S_3, S_4)	6, 8	200	2	84 467.2	4
BESS + VI	1, 4, 5, 6	100	4	16 000	10
PHES	1, 4, 5, 6	400	4	17 500	2

Table 3.4 lists the system parameters used for modelling, while the time variability data of the wind and solar resources are provided in Table 3.5.

Table 3.4: System parameters used for modelling [107]

Parameter	Values
Cost of emission ($/t$CO_2$)	75
System base power (MVA)	100
Base frequency (Hz)	50
Minimum required inertia (s)	4.0
Maximum required inertia (s)	10
Minimum SoC of BESS SC_{min} (MW)	20
Maximum SoC of BESS SC_{max} (MW)	100
Maximum charging /discharge power (MW)	20
Minimum charging/discharge power (MW)	0
Maximum permissible CO_2 emission (tonnes [t])	10 000
Power demand safe margin (x)	1.2
Budget for new REGs and ESS ($)	5.0E + 05
Annualised time duration (s)	8 760
BESS charging efficiency (%)	95
BESS discharging efficiency (%)	95

Table 3.5: Time variability of wind and solar resources

Time	Wind1	Wind2	PV1	PV2
t1	0.35	0.35	0.00	0.00
t2	0.38	0.38	0.00	0.00
t3	0.41	0.41	0.00	0.00
t4	0.47	0.47	0.00	0.00
t5	0.53	0.53	0.00	0.00
t6	0.59	0.59	0.00	0.00
t7	0.65	0.65	0.00	0.00
t8	0.71	0.71	0.00	0.00
t9	0.77	0.77	0.06	0.06
t10	0.79	0.79	0.13	0.13
t11	0.81	0.81	0.20	0.20
t12	0.84	0.84	0.22	0.22
t13	0.86	0.86	0.22	0.22
t14	0.87	0.87	0.18	0.18
t15	0.89	0.89	0.12	0.12
t16	0.92	0.92	0.05	0.05
t17	0.95	0.95	0.01	0.01
t18	0.96	0.96	0.00	0.00
t19	0.97	0.97	0.00	0.00
t20	0.97	0.97	0.00	0.00
t21	0.96	0.96	0.00	0.00
t22	0.94	0.94	0.00	0.00
t23	0.90	0.90	0.00	0.00
t24	0.84	0.84	0.00	0.00

3.3.1 Case study and model validation

The proposed MILP model was implemented on an IEEE 9-bus test system with prospective investment in new REGs and ESS to reduce emissions and enhance system inertia. The configuration of the IEEE 9-bus test system is shown in Figure 3.3. The model comprises 13 existing transmission lines, eight candidate ESS (four BESS and four PHES), eight candidate REG units (four wind farms and four solar PV systems), nine load centres, five thermal generators, and an average load of 3 414 MW. The developed model was solved using the CPLEX solver in GAMS with an Intel(R) core i3 (TM) CPU and 2.53 GHz personal computer.

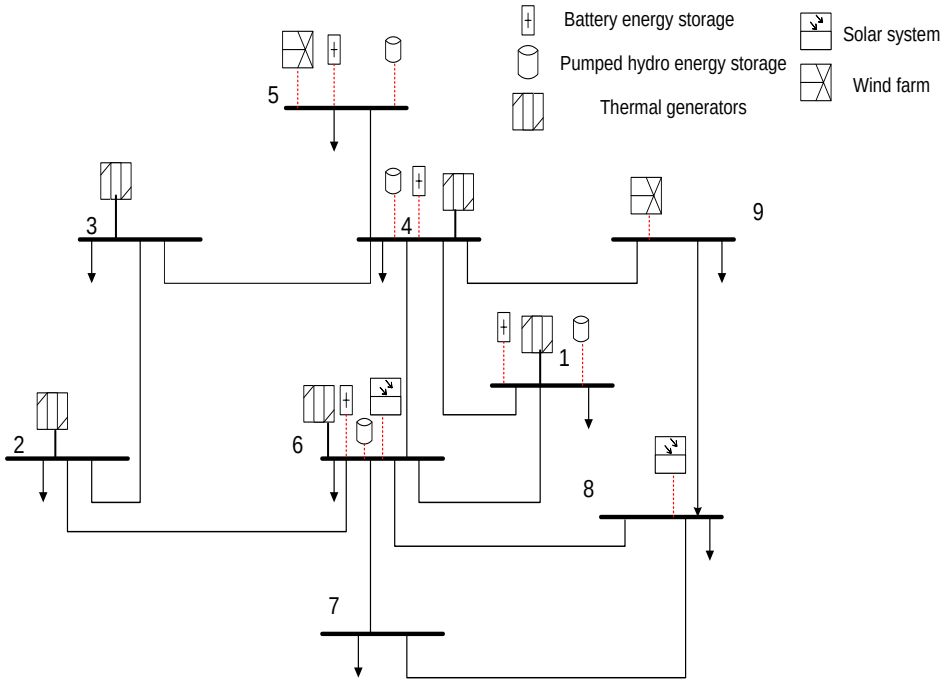

Red dash lines represent candidate generating and ESUs, while thick lines represent existing generating units.

Figure 3.3: Institute of Electrical and Electronics Engineers (IEEE) 9-bus network with existing thermal and candidate generating and storage units

3.4 RESULTS AND DISCUSSION

The developed model was evaluated under three scenarios:

- Scenario 1: Model without REGs and ESS.
- Scenario 2: Inertia is not considered in the GEP model with available REGs and ESS.
- Scenario 3: Inertia is considered in the GEP model with available REGs and ESS.

3.4.1 Model results

A comparison of the results obtained under all three scenarios is presented in Table 3.6. The results are discussed in terms of the economic (cost) and technical (system inertia) implications of the design.

Table 3.6: Results of the generation expansion planning (GEP) model under three scenarios

Scenario	Inertia constant (s)	Emissions (t)	Total cost (10^6)	Operational cost (10^6)	Cost of emission (10^6)	Cost of investment in ESS and REGs (10^6)	Fuel cost (10^6)
Scenario 1	7.204	414.562	1 808.432	1 808.432	3.6316	-	1 804.8
Scenario 2	5.067	389.532	1 795.57	1 795.22	3.4123	0.38422	1 784.8
Scenario 3	8.776	389.532	1 806.125	1 805.7	3.4123	0.39293	1 784.8

Scenario 1: In this case, there was no provision for REGs and ESS; hence the overall system inertia was provided only by the thermal unit. It can be observed that the system inertia was high in this scenario compared to Scenario 2; however, the emission from the thermal generators was the highest among the three scenarios. Furthermore, the fuel, operational, and total costs were the highest in this scenario compared to Scenarios 2 and 3.

Scenarios 2: In this case, there was provision for REGs and ESS, but no consideration was made for system inertia in the GEP model design; hence the overall system inertia was the lowest among all three scenarios because of inappropriate investment decisions. Furthermore, the emission from the thermal generators was lower than in Scenario 1 because of the presence of REGs and ESS. Also, the cost of investment in new REGs and ESS was lower than in Scenario 3. Sub-optimal investment decisions were made in this case, which favoured the installation of solar PV systems S_1 and S_2, wind farms W_3 and W_4, and PHES P_1, P_2, P_3, and P_4.

Scenario 3: This case is the most preferred among the three scenarios, as the inertia requirement of the grid was considered in the GEP model in the presence of REGs and ESS. This scenario achieved the highest overall system inertia among the three scenarios because appropriate investment decisions for candidate REGs and ESS were made. In addition, the emissions from the thermal generators were lower in Scenario 3 (389.532 tons) than in Scenario 1 (414.562 tons), with just a slight increase in the cost of investment in REGs and ESS compared to Scenario 2. Overall, this scenario achieved the highest system inertia at the lowest possible cost; thus validating the importance of this research, which aimed to enhance the system inertia of the modern power grid comprising REGs and ESS. The investment decisions in this scenario favoured the installation of solar PV systems S_3 and S_4, wind farms W_1 and W_2, and BESS B_1, B_2, B_3, and B_4 with VI capabilities.

It can also be observed that this scenario preferred investment in BESS compared to PHES units because BESS offered higher VI than the PHES. Furthermore, the results obtained in this scenario revealed that by considering the inertia requirement of the grid in planning, higher system inertia can be achieved in the grid compared to Scenarios 1 and 2, where inertia was not considered in the planning model.

In addition, a slight increase in investment cost in candidate REGs and ESS was observed, as seen in Table 3.6, because of the extra cost incurred to equip the REGs and BESS with VI capabilities. With higher system inertia, the new model is thus more stable than the

conventional model without inertia consideration. Figure 3.4 illustrates the generating capacity of candidate REGs in Scenarios 2 and 3.

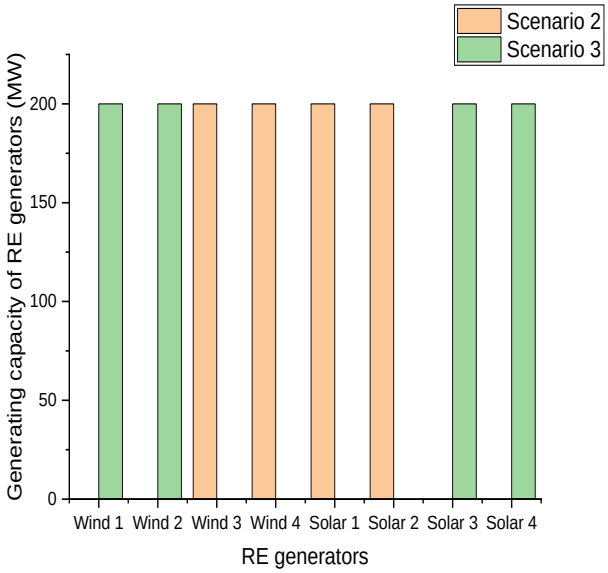

Figure 3.4: Generating capacity of REGs in Scenarios 2 and 3

Furthermore, the optimal power flow across the transmission lines in the network is shown in Table 3.7. It can be observed from Table 3.7 that the power flow across the transmission lines is well below its maximum power flow limit with no congested lines. Figure 3.5 shows the voltage angle across the buses in the network at various times. It can also be observed that the bus voltage angle is maintained within standard limit. The observed spike in voltage angle at buses 2 and 5 between 3:00 and 14:00 is as a result of increase power demand at buses.

Table 3.7: Optimal power flow on transmission line

Transmission line connecting bus	Power flow (MW)	Transmission line connecting bus	Power flow (MW)
1-6	150.7	4-9	156.8
2-6	87.2	5-4	294.1
3-2	131.8	6-7	186.3
3-6	66.9	6-8	1.543
4-1	99.6	8-7	0.867
4-3	39.7	9-8	0.914
4-6	75.0		

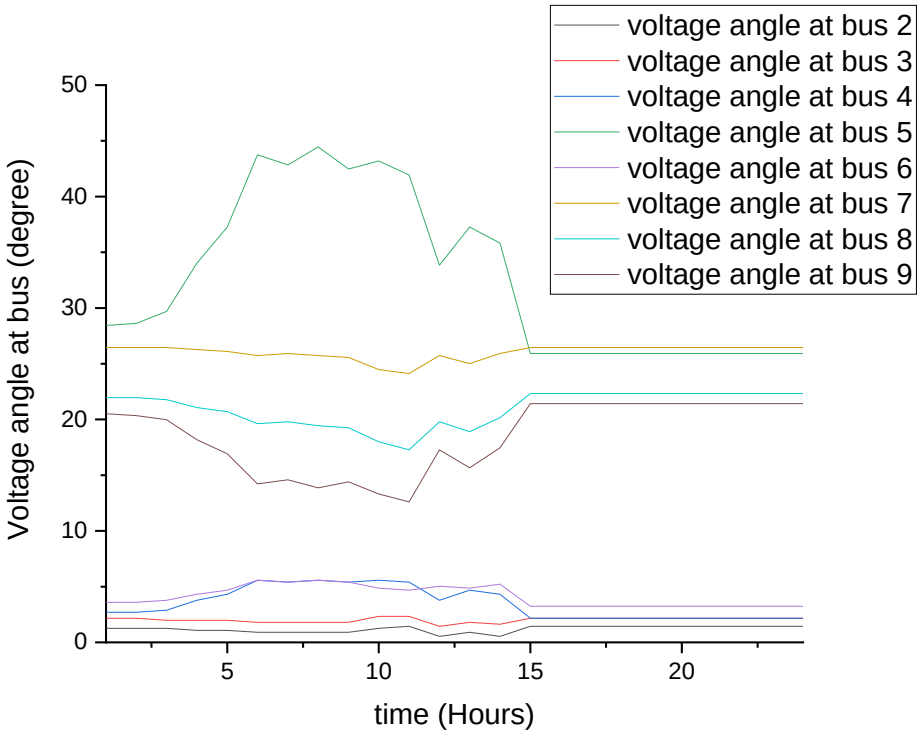

Figure 3.5: Voltage angle at bus at various times

3.4.2 Sensitivity analysis of system inertia with increasing renewable energy penetration

This sub-section evaluates the effect of increasing renewable energy generation on the overall system inertia of the developed model. The sensitivity analysis was conducted under different levels of renewable energy penetration, as follows: 33% RES penetration, 66% RES penetration, and 100% RES penetration. The REGs and ESS selected for the analysis were assumed to be equipped with VI capability. Table 3.8 and Figure 3.6 show the variation of system inertia under the different RES penetration levels. It can be seen from Table 3.8 that the overall system inertia constant decreased at a rate of 4.4% with an increase in RES penetration. It can also be observed that the total synchronous inertia energy decreased as RES penetration increased.

It is important to note that at 100% RES penetration level, the total synchronous inertia energy in the power system was zero, even though the overall system inertia constant was still above the permissible range, because of the provision of system inertia by the VI-providing REGs and ESS. The stability of the grid at 100% RES penetration level will be researched in the future because of the obvious decline in the amount of synchronous inertia available in the model.

Table 3.8: Capacity mix for different RES penetration levels

Generator installed capacity per technology (MW)	Generator type	RES penetration level (%)		
		33%	66%	100%
	Thermal	2 165	1 365	-
	Wind	800	1 600	1 600
	Solar	200	400	1 600
	BESS	200	200	100
System inertia constant (s)		6.45267	6.265985	6.167873
Synchronous inertia energy		7 565	5 190	0

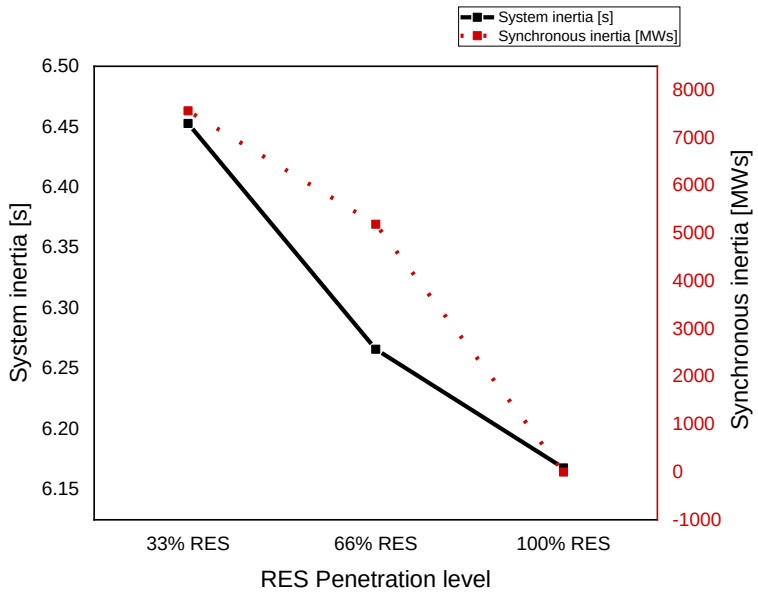

Figure 3.6: System inertia variation for different RES penetration levels

3.4.3 Discussion of results

The simulation results from the three scenarios show that considering system inertia in the GEP model (Scenario 3) led to a significant increase in the overall system inertia and a decrease in total system cost and CO_2 emissions.

It is observed that in Scenario 3, where system inertia was considered in the planning model in the presence of wind turbines and solar PV plants, the overall system inertia constant increased from 7.204s in Scenario 1 to 8.776s in Scenario 3 (21.8% increase), and from 5.067s in Scenario 2 to 8.776s in Scenario 3 (73.2% increase). This shows that considering system inertia in the GEP model helps to improve the overall system inertia constant by making appropriate investment decisions.

In addition, the introduction of REGs and ESS into the model reduced the total CO_2 emissions in the model. This can be observed as the total CO_2 emissions reduced from 414.562 tCO_2 in Scenario 1 to 389.532 tCO_2 in Scenario 3 (6% decrease).

Also, the overall system cost was reduced due to the incorporation of REGs and ESS into the model, which resulted in reduced emissions and fuel costs. The total cost reduced from $1 808.432 million in Scenario 1 to $1 806.125 million in Scenario 3 (0.13% decrease). These results reveal the importance of the proposed model that incorporated system inertia into the GEP model in the presence of REGs and ESS.

Finally, the sensitivity analysis of system inertia with increasing renewable energy generation shows that as renewable energy penetration into the grid increased from 33% to 100% RES penetration, the total system inertia of the grid decreased from 6.45267s to 6.167873s. It is also noteworthy that the synchronous inertia energy also decreased as the renewable energy penetration into the grid increased. The synchronous inertia of the grid at 100% RES penetration decreased to zero; the stability of the grid at 100% RES penetration level will be investigated in future research work.

3.5 CONCLUSION

The GEP model based on the system inertia requirement of the grid was proposed in this chapter. The proposed model is designed to guide investment in REGs and ESS in such a way as to increase the overall system inertia of the grid and, by implication, improve the resilience of the grid, while minimising the system cost and CO_2 emissions. The model was developed as an MILP problem and solved using CPLEX solver in GAMS. The model was then validated using a modified IEEE 9-bus test system.

The key findings of the research in this chapter revealed the following:

- The developed model, which considered system inertia in the model formulation (Scenario 3), achieved higher system inertia of 8.776s compared to the conventional model in Scenarios 1 (7.204s) and 2 (5.067s) thus the grid will be more stable under scenario 3.
- Sub-optimal investment decisions could be prevented by considering the inertia requirement of the grid in GEP.

- Sensitivity analysis of the model revealed that the overall system inertia constant decreased at a rate of 4.4% with an increase of renewable energy penetration into the grid.
- Investment in VI-equipped REGs and ESS helped to enhance the overall inertia constant of the grid as in Scenario 3, where system inertia was considered in the planning model.
- The developed GEP in Scenario 3 achieved a 0.13% decrease in total cost and 6% decrease in CO_2 emissions due to the incorporation of REGs and ESS into the model design.
- Finally, it should be noted that investment decisions made in this model were based on the IEEE 9-bus test system used for validating the developed model; therefore, in the future, the model will be extended to a larger test system, while TEP will also be incorporated.

CHAPTER 4: JOINT GENERATION AND TRANSMISSION EXPANSION PLANNING (GTEP) MODEL FOR IMPROVED MODERN POWER SYSTEM RESILIENCE AGAINST FREQUENCY INSTABILITY

4.1 INTRODUCTION

In recent times, the world has been challenged with global warming and its effects, such as climate change, which is a threat to the continued sustainability of the ecosystem [108]. This is due to the large-scale combustion of fossil fuels by thermal generators. Efforts are thus now being made through global green energy policies such as the Paris Agreement to increase the share of REGs in the grid while decommissioning more thermal generators. For example, in the USA, onshore wind farm installations are expected to increase by 25% (approximately 110 GW of new installations) by 2026. In Germany, 20 GW of offshore wind installation is expected by 2030, and 40 GW by 2040 [78], [109].

Conversely, the increasing dominance of the grid with REGs has resulted in frequency stability issues such as high RoCoF, large frequency nadir, etc. [110], [111]–[115]. This is because, unlike thermal generators, REGs such as PV systems and variable-speed wind turbines lack rotating mass and are decoupled from the grid through converters; they are thus not able to provide inertia directly to the grid when needed [112], [116]. Power system engineers are therefore now focusing on ways to combat these frequency-related challenges using various frequency control and optimisation techniques such as VI control strategies [13], [112], [117]. A detailed description of the various types of VI control strategies and ESS can be found in [12], [87], [118].

Furthermore, limited studies have attempted to address the inertia concern associated with the modern power system using expansion planning models. The authors in [5] suggested that a minimum acceptable kinetic energy of 113 GW is required in the Nordic power system for stability. However, the authors did not consider other RESs such as PV systems, nor the presence of ESS in their model. They, however, highlighted the need for expansion in the transmission network in order to limit the curtailment of wind turbine power output. The authors in [119] specified a minimum inertia constant of *3.6s* required in the conventional grid to ensure stability. The authors in [94] highlighted the decline in primary frequency response in a renewable energy-dominant grid, which jeopardises the transient stability of the grid.

The authors further developed a joint GTEP model with simplified frequency constraints; however, their work did not consider the use of ESUs to contribute VI to the grid. Emission concerns were also not considered in their model. The authors in [91] developed a unit commitment model considering a minimum inertia limit for each synchronous area in Europe. The key findings of the work revealed that setting inertia limits is important for a seamless transition to a renewable energy-dominant grid; their work, however, did not consider the place of ESUs and emission limits in ensuring a stable renewable energy-dominant grid. In addition, the need for expansion of the transmission network was not considered. The authors in [92] carried out GEP on a power system considering inertia constraint and BESS. The authors highlighted that the inertia requirement of the grid must be considered for a grid with high penetration of renewable energy. However, the need for expansion of the transmission network to avoid curtailment of RERs and network congestion was not considered in their model.

In this chapter, the model developed in Chapter 3 is extended to consider expansion of transmission lines while also considering the cost, emissions, and inertia requirement of the grid. This chapter thus proposes a new deterministic GTEP model that minimises emissions (environmental objective) and cost (economic objective) while maximising system inertia (technical objective). The GTEP model makes appropriate investment decisions regarding new REGs, transmission lines, and ESS, which will enhance the overall system inertia of the grid.

The novelties of this study are as follows:

- Developing a new deterministic optimisation model for GTEP that considers cost, emission, and the inertia requirement of the modern grid while planning for new REGs, transmission lines, and ESS.
- Introducing novel emission reduction initiative (ERI) constraints in the planning model to reduce CO_2 emissions from thermal generators. This new initiative provides incentives to power producers to maintain emission limits and penalises power operators when the emission limit is violated.
- Investigating the influence of considering inertia on expansion planning investment decisions and its impact on overall system inertia, as well as the frequency stability of the grid during times of contingency.
- Investigating the economic implications of considering inertia in the proposed GTEP model.

The rest of this chapter is organised as follows: Section 4.2 provides the mathematical formulation and description of the proposed GTEP model, Section 4.3 discusses the model

simulation and implementation on an IEEE 9-bus system, Section 4.4 presents the simulation results of three case studies, and Section 4.5 provides the conclusion of the chapter.

4.2 PROPOSED MODEL FORMATION

A new GTEP model was formulated for a one-year planning horizon to determine the best investment decisions that will ensure grid stability. The model sought to minimise the total system cost and CO_2 emissions while maximising system inertia subject to model constraints. The innovation of the model is seen in the (1) inertia estimation in the objective function, (2) limit on annual CO_2 emissions, (3) monetary incentives for maintaining emission limit and penalties for violating the annual emission limit, and (4) budgetary constraints limit for candidate REG units, ESUs, and transmission lines.

The proposed model is deterministic and was formulated as an MIQCP problem to indicate the optimal planning decisions on the type and number of new renewable energy-generating units, ESUs, and transmission lines to be built to achieve the objectives of the model. The flowchart of the proposed model is shown in Figure 4.1.

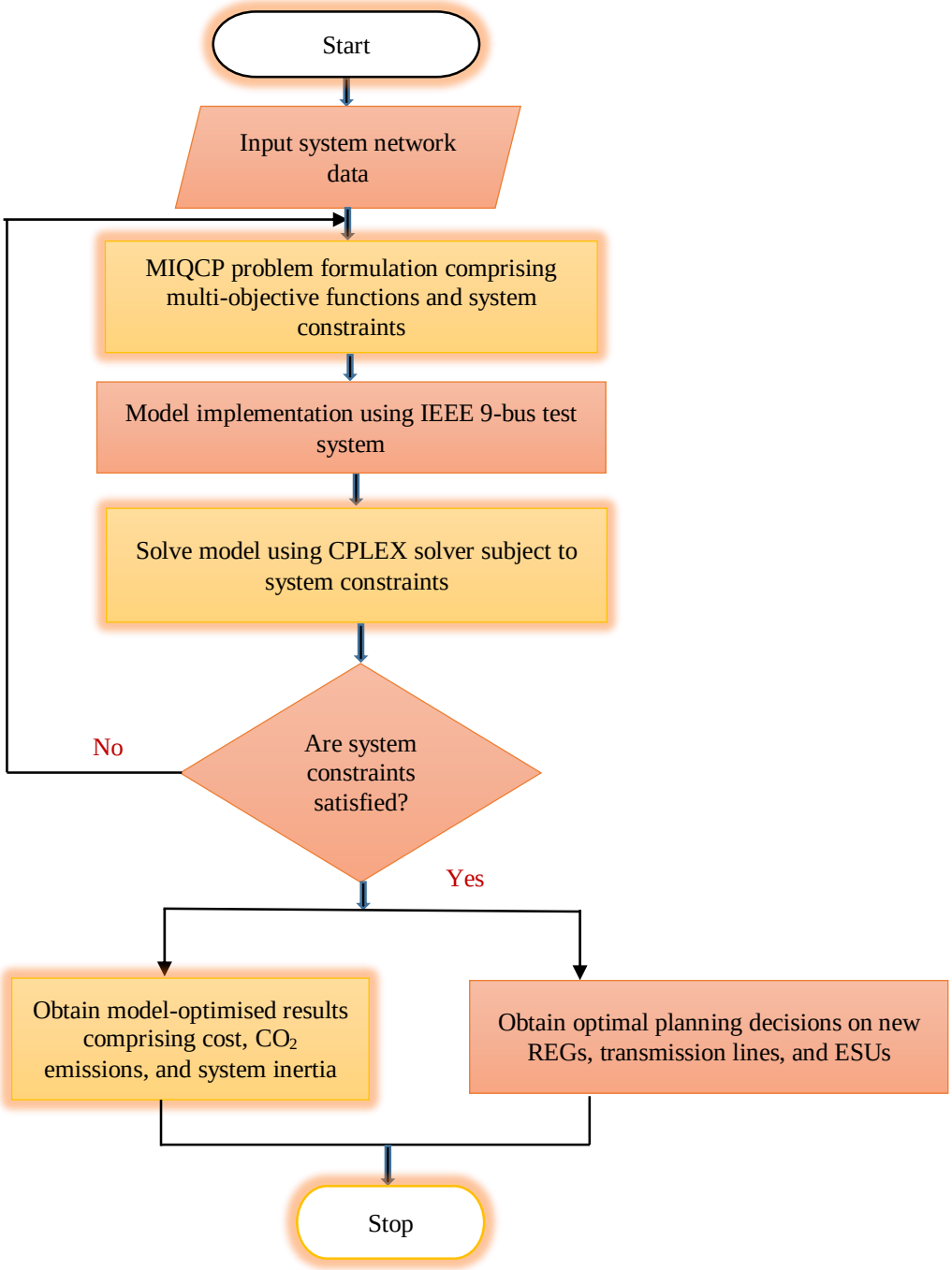

Figure 4.1: Flowchart of proposed GTEP model

4.2.1 Multi-objective function formulation

The multi-objective function in Equations (4.1) to (4.3) sought to (1) minimise the total system cost, (2) minimise CO_2 emissions, and (3) maximise overall system inertia. The total cost comprises the operational cost and investment cost. The operational cost consists of the cost of maintenance of wind farms, CO_2 emissions, and the fuel cost of thermal generators,

while the investment cost comprises the annualised investment cost of new transmission lines, REGs, and ESUs.

$$\min\left\{\alpha\left[\begin{array}{l}\sigma\left[\sum_{g}^{n}\left[a_g(P_g)^2+b_gP_g+c_g\right]+\left[\left[1\pm0.3\right]\sum_{g}^{n}\lambda_g^{CO_2}\cdot e_g^{CO_2}(P_g)\right]+\sum_{w}^{nw}CO_w^{om}(P_w)\cdot\mu3_w\right]\\+\sum_{v}CO_v^{inv}\cdot\mu1_v+\sum_{p}CO_p^{inv}\cdot\mu2_p+\sum_{w}CO_w^{inv}\cdot\mu3_w+\sum_{s}CO_s^{inv}\cdot\mu4_s+\sum_{cl}CO_{cl}^{inv}\cdot\mu6^{cl}\end{array}\right]\right\} \tag{4.1}$$

$$\min\left(\chi\left\{\sigma\sum_{g=1}^{n}e_g^{CO_2}(P_g)\right\}\right) \qquad \forall g\in G \tag{4.2}$$

$$\max\left(\beta\left[\frac{\sum_{g=1}^{n}H_g\cdot S_g+\sum_{s=1}^{ns}H_s\cdot S_s+\sum_{w=1}^{nw}H_w\cdot S_w+\sum_{v=1}^{nv}H_v\cdot S_v+\sum_{p=1}^{np}H_p\cdot S_p}{\sum_{g=1}^{n}S_g+\sum_{s=1}^{ns}S_s+\sum_{w=1}^{nw}S_w+\sum_{v=1}^{nv}S_v+\sum_{p=1}^{np}S_p}\right]\right) \quad \forall g\in G,\forall s\in S,\forall w\in W,\forall p\in P \tag{4.3}$$

The multi-objective functions outlined in Equations (4.1) to (4.3) were converted to a single optimisation function in Equation (4.4) in order to obtain the Pareto optimal solution. Weighting factors with equal preferences were used to convert the multiple objectives into a single objective function.

$$\min\left\{\begin{array}{l}\alpha\left[\begin{array}{l}\sigma\left[\sum_{g}^{n}\left[a_g(P_g)^2+b_gP_g+c_g\right]+\left[\left[1\pm0.3\right]\sum_{g}^{n}\lambda_g^{CO_2}\cdot e_g^{CO_2}\cdot P_g\right]+\sum_{w}^{nw}CO_w^{om}(P_w)\cdot\mu2_w\right]\\+\sum_{v}CO_v^{inv}\cdot\mu1_v+\sum_{p}CO_p^{inv}\cdot\mu2_p+\sum_{w}CO_w^{inv}\cdot\mu3_w+\sum_{s}CO_s^{inv}\cdot\mu4_s+\sum_{cl}CO_{cl}^{inv}\cdot\mu6^{cl}\end{array}\right]\\+\chi\left\{\sigma\sum_{g=1}^{n}e_g^{CO_2}(P_g)\right\}\\-\beta\left[\frac{\sum_{g=1}^{n}H_g\cdot S_g+\sum_{s=1}^{ns}H_s\cdot S_s+\sum_{w=1}^{nw}H_w\cdot S_w+\sum_{v=1}^{nv}H_v\cdot S_v+\sum_{p=1}^{np}H_p\cdot S_p}{\sum_{g=1}^{n}S_g+\sum_{s=1}^{ns}S_s+\sum_{w=1}^{nw}S_w+\sum_{v=1}^{nv}S_v+\sum_{p=1}^{np}S_p}\right]\end{array}\right\} \tag{4.4}$$

The fuel cost of the thermal generators in \$/hr is expressed as a quadratic function of its cost coefficients a_g, b_g, c_g and the generating output power of the generators as seen in Equation (4.4). The emission cost is defined as a function of the carbon tax $\lambda_g^{CO_2}$ (\$/tCO$_2$), emission factor $e_g^{CO_2}$ (tCO$_2$/kWh), and the generating output power of the thermal generators P_g in kWh. The total maintenance cost (\$) of an operational wind turbine is given in terms of the maintenance cost CO_w^{om} (\$/kWh) and the output power P_w of the wind farm. $CO_v^{inv}, CO_p^{inv}, CO_w^{inv}, CO_s^{inv}$, and CO_{cl}^{inv} are the annualised investment costs of BESS, PHES, wind turbines, solar farms, and transmission lines respectively. $\mu1_v, \mu2_p, \mu3_w, \mu4_s, \mu6^{cl}$ are the binary variables that determine investment decisions on BESS, PHES, wind turbines, solar

farms, and transmission lines respectively. The binary decision variable is taken as 1 when a particular technology is selected for installation, and 0 if otherwise. σ is the operating time in hours of the generating units, applied to make the operational and investment costs comparable. H_g, H_v, H_p, H_w, and H_s are the inertia constant of the thermal generators, BESS, PHES, wind turbine, and solar farm respectively. Similarly, S_g, S_v, S_p, S_w, and S_s are the rated apparent power of the thermal generators, BESS, PHES, wind turbine, and solar farm respectively.

The weighting factors are given in Equation (4.5):

$$\alpha + \beta + \chi = 1 \tag{4.5}$$

4.2.2 Model constraints

This sub-section describes the constraints used to capture the essential characteristics of the proposed model. The model was subjected to power balance, generation limit, reserve, emission limit, inertia, transmission line power flow, budgetary, and ESU constraints. The main decision variables are investment decisions on new transmission lines, REGs, and ESUs to be constructed, overall system inertia constant, inertia energy, and total power generated.

4.2.2.1 Power balance constraints

The power balance constraint was formulated using the DC equivalent of Kirchhoff's current law in which the sum of the active power generated, transmitted, and injected at all nodes should be equal to the total load demand at nodes.

$$\sum_{g}^{n} P_g + \sum_{w}^{nw} P_w + \sum_{s}^{ns} P_s + \sum_{p}^{np} P_p + \left[\sum_{v}^{nv} P_v^{dis} - \sum_{v}^{nv} P_v^{cha}\right] + \sum_{l\in rl} PF_{ij}^{el+} - \sum_{l\in sl} PF_{ij}^{el-} + \sum_{l\in rl} PF_{ij}^{cl+} - \sum_{l\in sl} PF_{ij}^{cl-} \geq \sum_{i} LD_i \tag{4.6}$$
$$\forall g \in G, \forall s \in S, \forall w \in W, \forall p \in P, \forall cl \in CL, \forall el \in EL, \forall rl \in RL, \forall rl \in RL, \forall i \in I$$

Equation (4.6) states that the sum of the power generated from the thermal generators, REGs, and ESUs, plus the power injected and transmitted through existing and candidate transmission lines at all nodes, should be equal to or greater than the total load demand at nodes.

4.2.2.2 Generation limit constraints

The generating capacity of all existing and candidate REGs at all nodes is limited according to Equations (4.7) to (4.9). Equation (4.7) provides the generating capacity limit of all thermal generators. Equations (4.8) and (4.9) provide the generating capacity limit of wind

and solar farms respectively, which is a function of their rated power and capacity factor. The capacity factor was introduced due to the variability of REGs.

$$P_g^{\min} \le P_g \le P_g^{\max} \qquad \forall g \in G \tag{4.7}$$

$$0 \le P_w \le P_w^{\max} \cdot cap_w \qquad \forall w \in W \tag{4.8}$$

$$0 \le P_s \le P_s^{\max} \cdot cap_s \qquad \forall s \in S \tag{4.9}$$

4.2.2.3 Reserve constraints

Power reserve is necessary to ensure stability in the power system due to the variability in load demand and power output from REGs.

$$\sum_{g}^{n} P_g^{\max} + \sum_{w}^{nw} P_w^{\max} \cdot \mu 3_w + \sum_{s}^{ns} P_s^{\max} \cdot \mu 4_s \ge (1 + RS^{\min}) \times LD^{peak} \qquad \forall g \in G, \forall w \in W, \forall s \in S \tag{4.10}$$

Equation (4.10) states that the sum of the installed capacity of all existing thermal generators, candidate wind, and solar farms must be greater than or equal to the peak load demand with a minimum reserve limit set (5%). The minimum reserve limit is set to carter for unanticipated spike in load demand. The reserve capacity will also be available for peak shaving during times of peak demand.

4.2.2.4 Emission constraints

In line with global renewable energy policies geared at reducing CO_2 emissions, the total amount of CO_2 emissions was limited by Equations (4.11) and (4.12). Equation (4.11) provides the total amount of CO_2 emission from thermal generators [120]. Equation (4.12) constrains the total CO_2 emissions generated from all thermal generators to be less than a maximum annual emission limit set. A ERI was introduced in the objective function, in which power operators are incentivised with 30% of the total emission cost if they are able to maintain the emission limit set, while a penalty cost of 30% of the total emission cost is introduced in case power operators exceed the maximum permissible emission limit. The penalty cost chosen for this study is strictly the student's novel idea to increase the cost of running fossil-fuel fired generators while encouraging the use of REGs. These novel initiatives were introduced to curb emissions and to discourage overdependence on thermal generators.

$$E^{total} = \sigma \sum_{g}^{n} e_g^{CO_2}(P_g) \qquad \forall g \in G \tag{4.11}$$

$$E^{total} \le \overline{EM}_{\lim} \qquad \forall g \in G \tag{4.12}$$

4.2.2.5 Inertia constraints

As more conventional generators are being replaced with REGs and ESS, it is important to ensure that the equivalent kinetic energy of the decommissioned synchronous generators can be provided by the inertia energy of ESS in order to maintain the system's frequency stability [37], [41]. During times of contingency, the released kinetic energy from synchronous generators and ESUs will help the system to regain stability and significantly reduce the effect of the transient event [91]. To ensure frequency stability in the modern grid, the following constraints were established and enforced:

$$H^{\min} \le H \le H^{\max} \qquad \forall g \in G, \forall s \in S, \forall p \in P, \forall w \in W, \forall v \in V \tag{4.13}$$

$$f^{\min} \le f \le f^{\max} \qquad \forall g \in G, \forall s \in S, \forall p \in P, \forall w \in W, \forall v \in V \tag{4.14}$$

$$\sum_{g=1}^{n} H_g \cdot S_g = KE_{SG} \qquad \forall g \in G \tag{4.15}$$

$$\sum_{v} H_v \cdot S_v + \sum_{p} H_p \cdot S_p = KE_{es} \qquad \forall p \in P, \forall v \in V \tag{4.16}$$

$$KE_{total} = KE_{SG} + KE_{es} \qquad \forall \mathrm{g} \in \mathrm{G}, \forall \mathrm{s} \in \mathrm{S}, \forall \mathrm{p} \in \mathrm{P}, \forall \mathrm{w} \in \mathrm{W}, \forall \mathrm{v} \in \mathrm{V} \tag{4.17}$$

$$KE_{total} \ge (1+\vartheta) KE_{\min} \qquad \forall \mathrm{g} \in \mathrm{G}, \forall \mathrm{s} \in \mathrm{S}, \forall \mathrm{p} \in \mathrm{P}, \forall \mathrm{w} \in \mathrm{W}, \forall \mathrm{v} \in \mathrm{V} \tag{4.18}$$

$$KE_{SG} \ge \varsigma \cdot KE_{total} \qquad \forall \mathrm{g} \in \mathrm{G}, \forall \mathrm{s} \in \mathrm{S}, \forall \mathrm{p} \in \mathrm{P}, \forall \mathrm{w} \in \mathrm{W}, \forall \mathrm{v} \in \mathrm{V} \tag{4.19}$$

Equation (4.13) provides the permissible bounds for system inertia. Equation (4.14) provides the permissible bounds for frequency deviation based on South Africa's grid code. Equation (4.15) states that the total kinetic energy of synchronous generators is given as a function of the individual inertia constant of the generators and their respective apparent power rating. Equation (4.16) states that the total inertia energy of ESUs is given as the function of the individual inertia constant of the storage units and their respective power rating. Equation (4.17) states that the total inertia energy available in the power system is given as the sum of the stored kinetic energy from all synchronous generators and the inertia energy from ESUs. Equation (4.18) ensures stability in the grid during times of system contingency by setting the minimum inertia energy required in the grid for stability with a safe margin; thus constraining the total inertia energy available in the system to be greater than or equal to a minimum inertia energy set. Equation (4.19) states that the sum of the stored kinetic energy from all synchronous

generators should be greater than or equal to a proportion (20%) of the total inertia energy from all generators and storage units.

4.2.2.6 Transmission line power flow constraints

Equations (4.20) to (4.26) define the power flow constraints formulated based on the DC approximation of Kirchhoff's voltage law to regulate power transmission in the existing and candidate transmission lines [121].

$$-PF_{el}^{\max} \le PF_{el}^{ij} \le PF_{el}^{\max} \qquad \forall el \in EL \tag{4.20}$$

$$-\mu 6^{cl} \cdot PF_{cl}^{\max} \le PF_{cl}^{ij} \le \mu 6^{cl} \cdot PF_{cl}^{\max} \qquad \forall cl \in CL \tag{4.21}$$

$$PF_{el}^{ij} = B_{ij}^{el}(\theta_i^{sl} - \theta_j^{rl}) \qquad \forall el \in EL \tag{4.22}$$

$$-(1-\mu 6^{cl})M \le PF_{cl}^{ij} - B_{ij}^{cl}(\theta_i^{sl} - \theta_j^{rl}) \le M(1-\mu 6^{cl}) \qquad \forall i \in I, \forall cl \in CL \tag{4.23}$$

$$\sum_{cl} \mu 6^{cl} \le \overline{nc} \qquad \forall cl \in CL \tag{4.24}$$

$$\mu 6^{cl} \in \{0,1\} \qquad \forall cl \in CL \tag{4.25}$$

$$-\frac{\pi}{4} \le \psi_i \le \frac{\pi}{4} \qquad \forall i \in I \tag{4.26}$$

Equations (4.20) and (4.21) define the power flow limit in existing and candidate transmission lines respectively. Equation (4.22) provides the DC power flow equations for existing transmission lines, which is a function of the bus voltage angle at the sending and receiving ends of the transmission line and line susceptance. Equation (4.23) defines the DC power flow equations for newly constructed transmission lines using the Big-M parameter. M is a large number that can accommodate all possible values of $\mu 6^{cl}$. Equation (4.24) limits the total number of candidate transmission lines that can be constructed in the planning horizon to a maximum. Equation (4.25) defines the binary decision variable that determines if a new transmission line is to be constructed and states that the variable must be 1 if a new transmission line is selected for construction and 0 if otherwise. Equation (4.26) provides the phase angle limit at bus.

4.2.2.7 Budgetary constraints on investment

Equations (4.27) to (4.32) define the budgetary limit on new REG units, transmission lines, and ESUs.

$$\sum_{cl} CO_{cl}^{inv} \cdot \mu 6^{cl} \le \overline{BU_{cl}} \qquad \forall cl \in CL \tag{4.27}$$

$$\sum_{v} CO_{v}^{inv} \cdot \mu 1_{v} \le \overline{BU_{v}} \qquad \forall v \in V \tag{4.28}$$

$$\sum_{p} CO_{p}^{inv} \cdot \mu 2_{p} \le \overline{BU_{p}} \qquad \forall p \in P \tag{4.29}$$

$$\sum_{w} CO_{w}^{inv} \cdot \mu 3_{w} \le \overline{BU_{w}} \qquad \forall w \in W \tag{4.30}$$

$$\sum_{s} CO_{s}^{inv} \cdot \mu 4_{s} \le \overline{BU_{s}} \qquad \forall s \in S \tag{4.31}$$

$$\sum_{v} CO_{v}^{inv} \cdot \mu 1_{v} + \sum_{p} CO_{p}^{inv} \cdot \mu 2_{p} + \sum_{w} CO_{w}^{inv} \cdot \mu 3_{w} + \sum_{s} CO_{s}^{inv} \cdot \mu 4_{s} + \sum_{cl} CO_{cl}^{inv} \cdot \mu 6^{cl} \le \overline{BU_{T}} \qquad \forall g \in G, \forall s \in S, \forall p \in P, \forall w \in W, \forall v \in V \tag{4.32}$$

Equation (4.27) defines the maximum available monetary budget for constructing new transmission lines. Equations (4.28) to (4.31) define the budgetary constraints that regulate investment in BESS, PHES, wind farms, and solar farms respectively. It subjects the total investment per technology to be less than or equal to its budgetary allocation. Equation (4.32) constrains the total investment in candidate REGs and ESUs to a maximum monetary budget.

4.2.2.8 Energy storage unit (ESU) constraints

ESS can be used to provide VI to the grid through VI control schemes [85], [122]. Investment decisions on ESS should be based on the inertia requirement of the grid, as well as the characteristics of the storage units. Equations (4.33) to (4.42) define the constraints for BESS and PHES units.

$$SC_{v,t} = SC_{v,t-1} + \left[P_{v}^{cha} \cdot \eta_{v}^{cha} - P_{v}^{dis} / \eta_{v}^{dis} \right] \qquad \forall \mathrm{v} \in \mathrm{V} \tag{4.33}$$

$$SC_{v,t}^{\min} \times \mu 1_{v} \le SC_{v,t} \le SC_{v,t}^{\max} \times \mu 1_{v} \qquad \forall v \in V \tag{4.34}$$

$$u1_{v} \cdot \underline{P_{v}^{cha}} \le P_{v}^{cha} \cdot \eta_{v}^{cha} \le u1_{v} \cdot \overline{P_{v}^{cha}} \qquad \forall \mathrm{v} \in V \tag{4.35}$$

$$u1_{v} \cdot \underline{P_{v}^{dis}} \le P_{v}^{dis} / \eta_{v}^{dis} \le u1_{v} \cdot \overline{P_{v}^{dis}} \qquad \forall v \in V \tag{4.36}$$

$$\mu 5_{v}^{cha}, \mu 5_{v}^{dis} \in \{0,1\} \qquad \forall v \in V \tag{4.37}$$

$$\mu 5_{v}^{cha} + \mu 5_{v}^{dis} \le 1 \qquad \forall v \in V \tag{4.38}$$

$$\underline{P_{p}} \times \mu 2_{p} \le P_{p} \cdot \eta_{p} \le \overline{P_{p}} \times \mu 2_{p} \qquad \forall p \in P \tag{4.39}$$

$$\sum_{v} \mu 1_{v} \le \overline{nv} \qquad \forall v \in V \tag{4.40}$$

$$\sum_{p} \mu 2_p \leq \overline{np} \qquad \forall p \in P \qquad (4.41)$$

$$\sum_{v} \mu 1_v + \sum_{p} \mu 2_p \leq \overline{ne} \qquad \forall v \in V, \forall p \in P \qquad (4.42)$$

Equation (4.33) defines the hourly SoC of the BESS units. Equation (4.34) limits the SoC of candidate BESS units within minimum and maximum bounds. Equations (4.35) and (4.36) define the charging and discharging power limits of BESS respectively. Equations (4.37) and (4.38) define the binary variable used to prevent charging and discharging of the BESS units at the same time. Equation (4.39) defines the power delivery limits of PHES units within maximum and minimum bounds. Equation (4.40) sets the maximum number of BESS units that can be installed in the planning horizon. Equation (4.41) sets the maximum number of PHES units that can be installed in the planning horizon. Equation (4.42) sets the maximum number of ESUs that can be installed in the planning horizon.

4.3 MODEL SIMULATION

In this section, the proposed GTEP model is applied to an IEEE 9-bus test system. The model network consists of 24 corridors, 11 existing transmission lines, 13 candidate transmission lines, five thermal generators, 10 candidate REGs, 12 candidate ESUs, and nine load buses, as shown in Figure 4.2. The data of the generating units are presented in Table 4.1 with the apparent power capacity of the thermal generators obtained at 0.8 power factor.

Candidate REGs consist of six solar plants and four wind turbines. Two types of wind farms were considered candidate wind farms for installation at buses 5, 7, and 9. Type 1 wind farms are conventional wind farms with inherent inertia, while Type 2 wind farms are variable converter-based wind turbines with VI-provision capabilities. Similarly, two types of solar plants were considered for installation at buses 6 and 8. Type 1 solar plants are without inertia, while Type 2 solar plants are considered to be able to provide VI using a VI control scheme. PHES and BESS are considered candidate storage units to be installed in buses 1, 4, 5, 6, 7, and 8. The placement of REGs and energy storage units at buses were based on the load demand at buses. Table 4.1 presents the capacity, investment cost, capacity factors, and inertia constant of the candidate REGs and ESUs. The candidate solar units are assumed to have no operational cost.

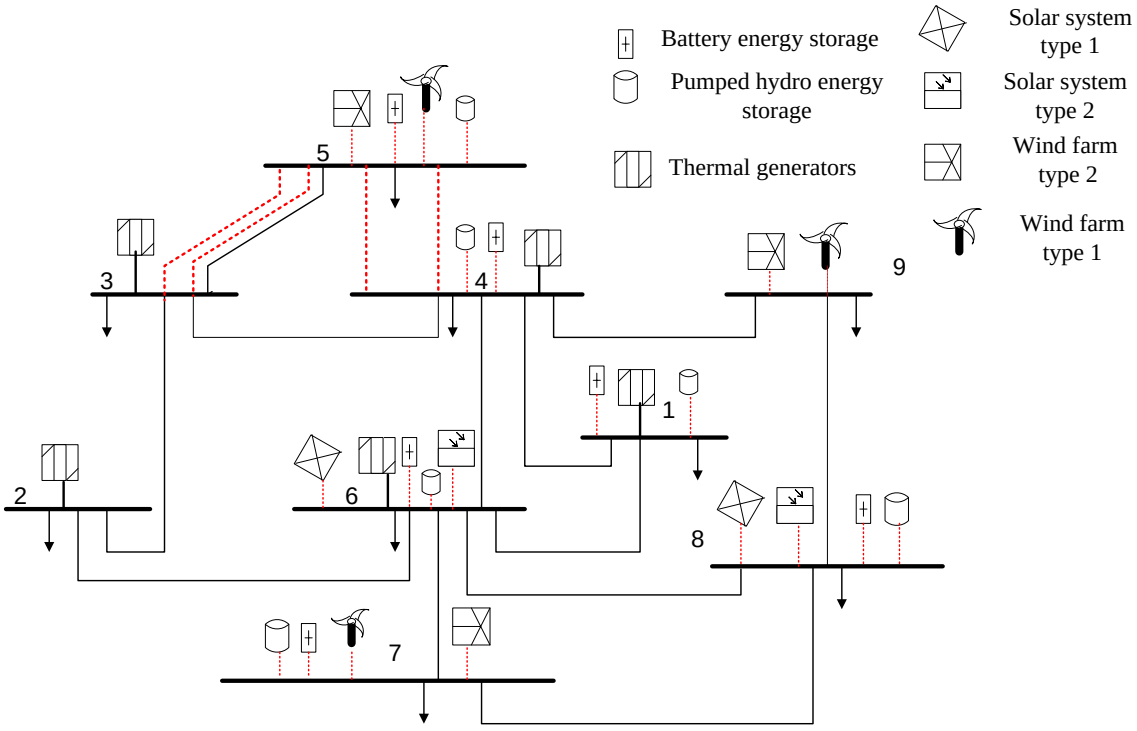

Red dash lines indicate candidate REGs, transmission lines, and ESUs, while solid black lines indicate existing transmission lines and generating units.

Figure 4.2: IEEE 9-bus network with existing thermal generators and candidate REGs and ESUs

Table 4.1: Data on candidate REGs and ESUs

Generation and storage technology	Bus	Capacity (MW)	Capacity factor	Max no. for investment	Investment cost ($/MW/yr)	Inertia (s)
Wind (Type 1)	5, 7, 9	100	0.30	3	72 641.80	2
Wind + VI(Type 2)	5, 7, 9	100	0.30	3	80 000	4
Solar (Type 1)	6, 8	100	0.27	2	84 467.20	0
Solar + VI (Type 2)	6, 8	100	0.27	2	92 654.80	4
BESS + VI	1, 4, 5, 6, 7, 8	100	-	6	3 821	10
PHES	1, 4, 5, 6, 7, 8	300	-	6	4 157	2

Table 4.2 indicates the average load demand at the system buses, while Table 4.3 lists the system parameters used for modelling. Transmission line parameters of existing and candidate transmission lines used in the study were obtained from [93], [104].

Table 4.2: Average load demand at bus

Bus no.	1	2	3	4	5	6	7	8	9
Load demand (MW)	219	106	158	223	151	321	98	109	123
Total load demand (MW)	1508								

Table 4.3: System parameters used for model evaluation [123], [124]

Parameter/Metrics	Values
CO_2 tax on emission ($/t$CO_2$)	20
RoCoF (Hz/s)	1
Maximum permissible frequency (Fmax) (Hz)	51
Minimum permissible frequency (Fmin) (Hz)	49
System base power (MVA)	100
Minimum kinetic energy (MWs)	14 000
Nominal frequency (Hz)	50
Minimum required inertia (s)	4.0
Maximum required inertia (s)	10
Minimum SoC of BESS SC_{min} (MW)	20%
Maximum SoC of BESS SC_{max} (MW)	80%
Maximum charging/discharge power (MW)	20
Minimum charging/discharge power (MW)	0
Maximum permissible CO_2 emission (million tonnes)	500
Minimum reserve limit set (%)	5
Safe margin for minimum inertia energy (%)	10
Budget on new REGs and ESUs ($10^6$$)	900
Annualised planning time duration (hours)	8 760
BESS charging efficiency (%)	95
BESS discharging efficiency (%)	95
Efficiency of PHES	87

4.4 CASE STUDIES AND RESULTS

To assess the performance of the proposed model, three cases were studied.

In Case 1, the GTEP problem was optimised considering only Objective 1 (cost). In Case 2, the GTEP problem was optimised considering Objective 1 (cost) and Objective 2 (emission). In Case 3, the GTEP problem was optimised considering all three objectives (cost, emission, and inertia).

The simulation results obtained from each case study are presented in terms of overall system cost, generation output of thermal generators, overall system inertia, CO_2 emission, frequency nadir under system contingency, and investment decisions on new renewable energy plants, transmission lines, and ESS.

4.4.1 System cost

This sub-section provides a detailed breakdown of the operational and investment costs in each case study. Table 4.4 provides a detailed breakdown of costs for all three cases. It can be observed that the fuel cost was the highest in Case 1 ($10.330 million) and the lowest in Case 2 ($2.6318 million). In addition, the emission cost was the highest in Case 1 ($210.84 million) and the lowest in Case 2 ($32.958 million) due to the ERI introduced in the model. The annualised operational cost was the highest in Case 1, with an operational cost of $221 million and the lowest in Case 2, with an operational cost of $35.7 million, while the annualised investment cost was the highest in Case 3 ($672.504 million) and the lowest in Case 1 ($265 million). The annualised total cost of the system was the highest in Case 3 ($859 million) and the lowest in Case 1 ($486 million).

Table 4.4: Summarised cost analysis of model case study

Case study	Total operational cost ($10^6$$)	Annualised investment cost					Annualised total cost ($10^6$$)
		REG expansion cost ($10^6$$/yr)		Energy storage investment cost ($10^6$$/yr)		Transmission line expansion cost ($10^6$$/yr)	
		Solar plant ($10^6$$/yr)	Wind farm ($10^6$$/yr)	BESS ($10^6$$/yr)	PHES ($10^6$$/yr)		
Case 1	221	16.893	27.93	2.2926	-	224.168	486
Case 2	35.7	-	37.793	2.2926	-	560.42	636
Case 3	141	18.531	24	2.2926	-	672.504	859

4.4.2 Generated power of thermal generators

The generated power from all thermal generators for each case study is presented in Figure 4.3. Case 2 had the lowest power generated (397.2 MW) for all thermal generators, while Case 1 had the highest power generated of all the thermal generators (1 716.4 MW). In Case 3, the power generated by all thermal generators was 1 393.2 MW.

The low generating capacity in Case 2 can be attributed to the ERI constraints introduced to limit the power production of thermal generators as a means of reducing CO_2 emissions during the planning horizon. This situation might not be ideal as the generating capacity of the thermal generators is reduced. However, the operating capacity in Case 3 was ideal as the generated power from the thermal generators was not affected significantly, even as the emission was substantially reduced. This finding supports Hypothesis 3 (H_3) of the study; however, it was achieved with the help of the ERI introduced.

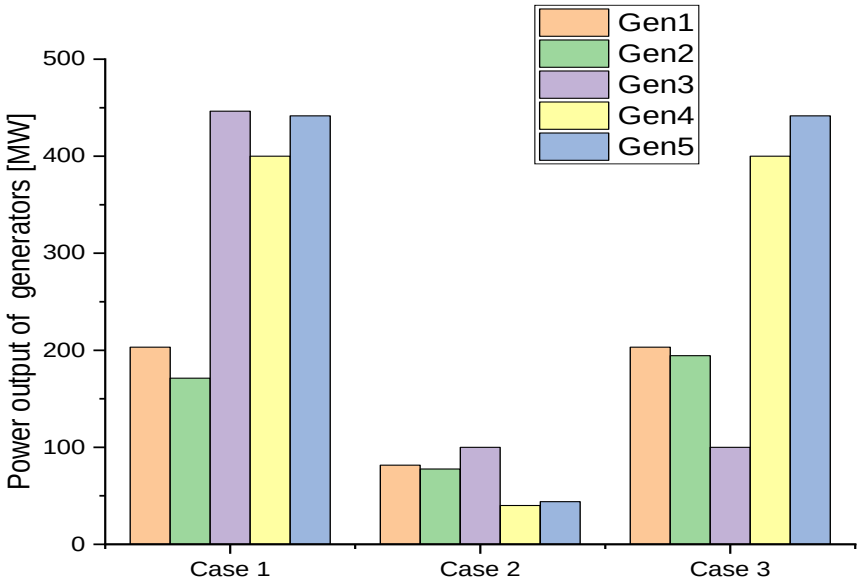

Figure 4.3: Optimal power output of thermal generators for each case study

4.4.3 Carbon dioxide (CO_2) emission

The amount of CO_2 emission and its associated cost are presented in Table 4.5 for all case studies. Table 4.5 provides a detailed breakdown of the annualised emission cost, which comprises the incentives received by power operators for maintaining emission limits in all case studies.

It can be observed from Table 4.5 that the highest CO_2 emission was recorded in Case 1, while the lowest CO_2 emission was seen in Case 2. The low emission recorded in Cases 2 and 3 was as a result of the ERI constraints introduced into the model in which the power operators were incentivised for maintaining emission limits with a rebate of 30% of the total emission cost. Similarly, the cost of CO_2 emission was the highest in Case 1 because ERI constraints were not incorporated in this case.

Table 4.5: Breakdown of CO_2 emission for various case studies

Case study	CO_2 emission in (10^6 tonnes)	Total emission cost (10^6\$)	Emission incentives in (10^6\$)	Net emission cost (10^6\$)
Case 1	10.542	210.84	-	210.84
Case 2	2.3541	47.083	14.125	32.958
Case 3	9.5258	190.52	57.156	133.364

4.4.4 Investment decisions

The investment decisions made in the various case studies are summarised in Tables 4.6 and 4.7. Table 4.6 lists the investment decisions on REGs and ESUs by technology for each case, while Table 4.7 shows the number of transmission lines to be built. Table 4.6 shows that the investment decisions favoured the installation of BESS over PHES in all cases because of its higher inertia constant. In addition, the installed capacity of the REGs and ESUs were the same (1 100 MW) for all cases. However, the generation technology installed differed. In Case 1, two Type 1 solar plants and three Type 1 wind turbines were to be installed in buses 5, 6, 7, 8, and 9. In Case 2, three Type 1 wind turbines and two Type 2 wind turbines were to be installed in buses 5, 7, and 9 with no solar plant. In Case 3, two Type 2 solar plants and three Type 2 wind turbines were to be installed in buses 5, 6, 7, 8, and 9.

In addition, it can be observed that the total number of transmission lines to be constructed was the highest in Case 3 (six) and the lowest (two) in Case 1, which accounted for the high cost of investment ($717 million) in Case 3 and low investment cost ($265 million) in Case 1.

Table 4.6: Generation and energy storage expansion planning investment decisions

Case study	REG investment				Energy storage investment		Total installed energy storage capacity (MW)	Total installed capacity of REGs and storage units (MW)
	Solar plant		Wind farm		PHES	BESS		
	Type 1	Type 2	Type 1	Type 2				
Case 1	2	-	3	-	-	6	600	1 100
Case 2	-	-	3	2	-	6	600	1 100
Case 3	-	2	-	3	-	6	600	1 100

Table 4.7: Transmission expansion planning (TEP) results

Case study	Transmission line expansion decisions	
	New transmission line location	Total number of transmission lines
Case 1	(4-5), (6-7)	2
Case 2	(4-5), (6-7), (6-8), (9-4), (7-8)	5
Case 3	(1-4), (2-3), (3-4), (4-5) (x2), (4-9)	6

4.4.5 System inertia

The overall system inertia constant and energy for each case study are presented in Table 4.8. The overall inertia constant in Cases 1, 2, and 3 is given as 5.133s, 5.671s, and 6.812s respectively. The overall system inertia was the highest in Case 3 (6.812s) due to inertia

considered in the planning model, and the lowest in Case 1 (5.133s), where only cost was considered. Similarly, the inertia energy was the lowest in Case 1 (14 165 MWs) and the highest in Case 3 (15 565 MWs), which further validates the importance of considering inertia in the planning model.

Table 4.8: Overall system inertia constant and energy for the different case studies

Case study	System inertia (s)	Stored inertia energy from thermal generators (MWs)	Available inertia energy from ESUs and REGs (MWs)	Total inertia energy available (MWs)
Case 1	5.133	7 565.000	6 600	14 165.000
Case 2	5.671	7 565.000	7 400	14 965.000
Case 3	6.812	7 565.000	8 000	15 565.000

4.4.6 Frequency deviation under contingency

This sub-section analyses the frequency stability of the model during a loss of the largest generating unit. The frequency nadir value for all three cases when subjected to a 500 MW loss of generation (gen. 3) are presented in Table 4.9. A frequency nadir of 48.5318 Hz, 48.8318 Hz, and 49.0568 Hz was seen for Cases 1, 2, and 3 respectively. Furthermore, it can be observed that Case 3, with the highest overall inertia constant and energy, had the lowest frequency nadir, while Case 1, with the least overall system inertia and energy, had the highest frequency nadir. The minimum frequency deviation permissible was violated in Cases 1 and 2 because inertia was not considered in the planning model, while in Case 3, where inertia was considered in the planning model, the frequency deviation was maintained within the permissible limit. This further affirms the importance of considering inertia in the planning model.

Table 4.9: Frequency nadir values during contingency for the different case studies

Case study	Frequency nadir (Hz) during loss of 500 MW generation (Gen. 3)	Minimum acceptable frequency nadir (Hz) at a RoCoF limit of 1 Hz/s	Corresponding system inertia constant (s)	Corresponding inertia energy (MWs)
Case 1	48.5318	49	5.133	14 165.000
Case 2	48.8318	49	5.671	14 965.000
Case 3	49.0568	49	6.812	15 565.000

4.5 CONCLUSION

This chapter addressed two key issues in the modern power grid with a high share of REG, namely (1) declining grid inertia that leads to frequency instability, and (2) emission concerns related to thermal generators. To address these challenges, a new GTEP model was developed, which was formulated as an MIQCP problem and solved using CPLEX solver in GAMS. To combat the declining inertia and mitigate frequency instability in the modern grid, appropriate inertia constraint was introduced in the planning model, while an ERI was introduced in the GTEP model in which power operators are incentivised if they are able to maintain a preset emission limit.

Three different case studies were used to analyse the effectiveness of the model by implementing it on an IEEE 9-bus test system. The key findings of the analyses are summarised as follows:

- By considering inertia in the planning model (Case 3), the overall system inertia improved from 5.133s in the base case (Case 1) to 6.812s in Case 3 (24% increase). This shows the importance of considering inertia in the planning model.
- The introduction of an ERI constraint into the planning model reduced the CO_2 emissions from 10.542 million tonnes in the base case (Case 1) to 9.5258 million tonnes in Case 3, which led to a cost saving of $77.476 million. This shows the effectiveness of an ERI constraint in meeting the goal of emission reduction in a power system.
- Achieving higher system inertia at a reduced emission level in power system planning comes at a cost, as seen in Case 3. The overall cost increased from $486 million in the base case to $859 million in Case 3. This finding supports Hypothesis 2 (H_2) of the study.
- Considering cost, emission, and inertia in power system planning models is important in order to ensure that one objective is not sacrificed for another, as seen in Cases 1 and 2. Case 1 had the lowest overall cost; however, the frequency limit was violated during system contingency, and the amount of CO_2 emission was also the highest. In Case 2, although the CO_2 emission was the lowest, the frequency limit was violated during system contingency. The proposed model, which considered all three objectives, is deemed the best to guide investors and power operators in their planning.

- Investment in BESS is preferred to PHES, as the former provides higher inertia during times of system contingency.
- Considering inertia in the planning model influenced investment decisions on new REGs, ESUs, and transmission lines, which are responsible for the increased cost of investment.
- VI provided by the REGs with ESS was key to the enhanced overall inertia of the grid, as seen in Case 3. The overall system inertia of the grid can thus be enhanced through proper power system planning and the correct selection of new REG units and ESS designed to provide VI.
- The minimum inertia energy required for grid stability can be set based on the specifications of the system model under consideration as no one rule applies to all power systems.

CHAPTER 5: SENSITIVITY ANALYSIS OF FEED-IN TARIFFS (FiTs) IN JOINT GTEP CONSIDERING THE INERTIA REQUIREMENT OF THE GRID

5.1 INTRODUCTION

To achieve the high renewable energy target, different types of economic incentives schemes, such as FiT, Renewable Portfolio Standards, Renewable Energy Certificates, Renewable Electricity Production Tax Credit, Investment Tax Credit, Residential Energy Credit, Tradable Green Certificates, etc., have been adopted globally to facilitate renewable energy development [125]. Figure 5.1 provides a detailed classification of the different types of FiT schemes, which are classified based on their operational technique and electricity market structure. These economic incentive programmes have already been successfully implemented in countries such as China, Japan, the USA, the UK, Italy, Thailand, Iran, Malaysia, Germany, etc.

FiT is one of the most effective production-based economic incentive schemes for promoting renewable energy development. It offers a guaranteed long-term price per kWh for electricity produced from RESs, which reduces investors' burden and facilitates sustainable renewable energy development [126]. Appropriate FiT rates offer a good return on investment that is sufficient to boost investors' interest in renewable energy technology development [127]. The most commonly used FiT model is the market-independent fixed price type, which is independent of external market influence, and its price can be set based on the cost of the construction of the renewable energy technology under consideration, as well as the available government budget.

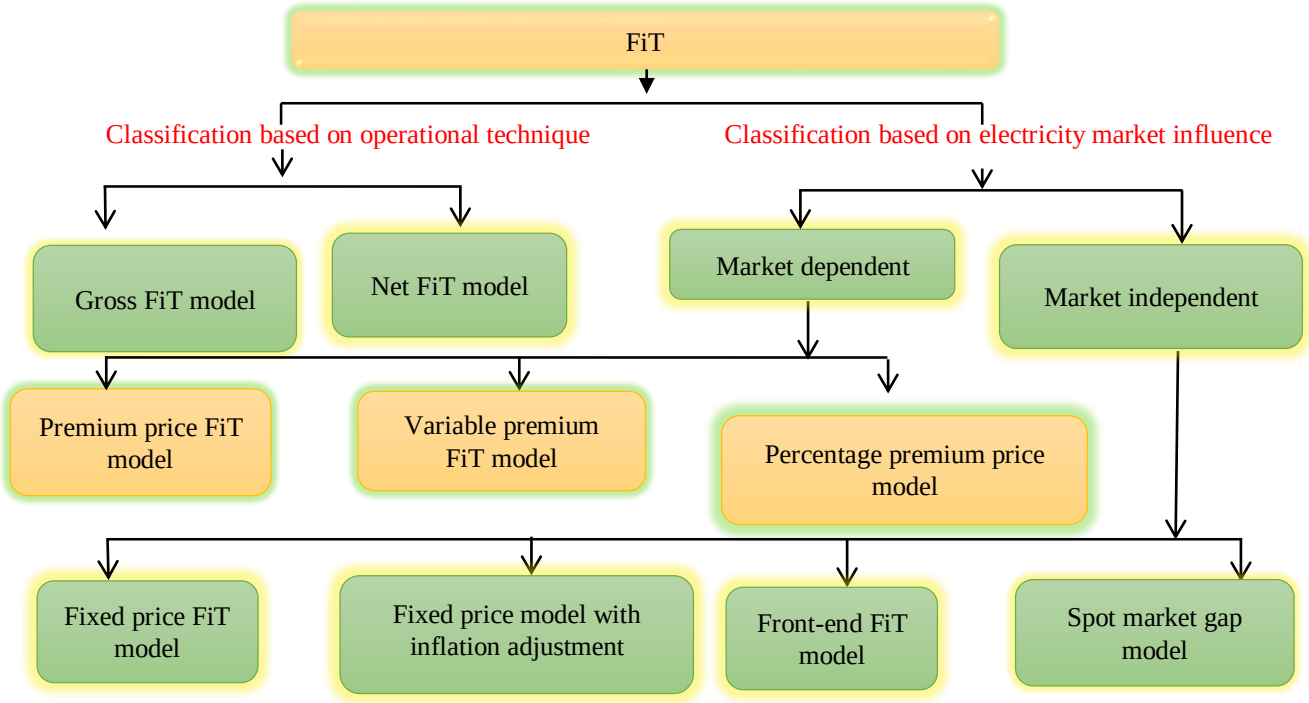

Figure 5.1: Classification of FiT models

The authors in [128] outlined measures to be implemented to address frequency stability challenges in a low-inertia grid such as revised grid code, limit on REG penetration into the grid, VI provision using fast-responding ESS, hybrid ESS, and REGs with a suitable converter control strategy. In developed countries such as Australia, Ireland, the UK, and Nordic countries, minimum inertia, RoCoF, and RES penetration limits have already been set to ensure that the stability of the grid is maintained [91], [129]. In light of this, there is still a need to foster the development of renewable energy technologies by incentivising renewable energy investors, while ensuring that adequate system inertia is maintained in the grid.

Several studies have been conducted on GEP, TEP, as well as the joint GTEP. These power system planning models attempt to make provision for increasing electricity demand by expanding the power system network, while addressing relevant technical challenges in the grid. However, only a few studies have considered system inertia in GTEP modelling. The authors in [92] developed a low-carbon GEP model that considered the inertia requirement of the grid and CO_2 emissions. The key findings of their work indicated that disregarding inertia and CO_2 emissions in the planning model will lead to infeasible and inaccurate planning results. However, the model was not extended to consider TEP as more generators are integrated into the grid. Furthermore, the influence of incentive schemes on model planning decisions was not

considered. The authors in [94] carried out GTEP on an integrated power and natural gas system using simplified system frequency constraints. The key findings of their work revealed that considering inertia in the expansion planning of power systems will require an investment in more power system equipment. Their study, however, did not consider the influence of economic incentive schemes on the planning decisions.

Furthermore, the authors in [130] developed a GTEP model using REGs and BESS units. The model was formulated as an MILP model and solved using Benders dual decomposition technique. The key findings of the model revealed that the incorporation of REGs and BESS into the model reduced the total CO_2 emissions of the model. However, the study did not consider the inertia requirement of the grid and the influence of economic incentive schemes on the planning model. The authors in [61] developed a GTEP model to assess the impact of ESS on total system cost and CO_2 emissions. The key findings of their study were that the introduction of ESS into the planning model reduced the total cost of the model. Furthermore, the authors argued that the introduction of ESS into planning models might not necessarily lead to reduced CO_2 emission because the storage units are not always operational. The model did not consider the influence of inertia and economic incentive schemes on the planning decisions.

Few studies have considered the impact of economic incentives on operational and expansion planning models. Existing studies seem to focus more on the influence of economic incentives on renewable energy development and not on the expansion planning of the power system. The authors in [125] investigated the impact of FiT on the development of PV power generation in China. Their research findings revealed that an FiT scheme helps to promote PV investment. However, the model did not consider the influence of inertia and emission on an expanded planning model. Also, the authors in [131] developed a GTEP model aimed at minimising the total system cost and CO_2 emission, while maximising the overall FiT. The key findings of their study revealed that the integration of a FiT scheme into the model formulation helped to promote the utilisation of energy from REGs, which consequently reduced the total CO_2 emissions in the model. However, this model did not consider the inertia requirement of the grid in the model formulation while maximising the overall FiT.

In this chapter, the model developed in Chapter 4 is extended to consider the role of economic incentives (FiT) in promoting and facilitating REG integration into the grid, while also considering the cost, emissions, and the inertia requirement of the grid. This study therefore proposed a novel FiT and inertia-integrated GTEP model to boost renewable energy development, as well as to improve the frequency stability of the modern grid. The unique

incorporation of system inertia and FiT into GTEP differentiates this model from previous studies, as shown in Table 5.1.

Table 5.1: Comparison of the proposed model relative to the reviewed expansion planning models

Reference	System inertia	FiT	CO_2 emission	TEP model	GEP model	GTEP model
[125]	×	✓	×	×	×	×
[92]	✓	×	✓	✓	✓	✓
[94]	✓	×	×	✓	✓	✓
[130]	×	×	✓	✓	✓	✓
[61]	×	×	✓	✓	✓	✓
[131]	×	✓	✓	✓	✓	✓
[132]	×	×	✓	✓	✓	✓
[62]	×	×	×	✓	×	×
This study	✓	✓	✓	✓	✓	✓

✓: Considered ×: Not considered

Regarding the identified research gap, the main contributions of this study are outlined as follows:

- To formulate a novel FiT- and inertia-integrated GTEP optimisation model.
- To investigate the impact (economic and environmental) of FiT and system inertia integration on GTEP decisions, and to compare its results in a case study without FiT and inertia considerations.
- To conduct a sensitivity analysis of the effect of FiT incentives on the proposed integrated GTEP model under different REG penetration levels.
- To investigate the impact of increasing the RES penetration level on the overall system inertia.

The remainder of this chapter is organised as follows: Section 5.2 presents the mathematical formulation of the integrated FiT and inertia GTEP model, Section 5.3 presents the model simulation and implementation on an IEEE standard test system, Section 5.4 provides the simulation results of the proposed integrated GTEP model, Section 5.5 provides the dynamic frequency response analysis of the model, Section 5.6 presents the sensitivity analysis and discusses the obtained results, and Section 5.7 concludes the chapter.

5.2 FiT AND INERTIA-INTEGRATED GTEP MODEL FORMULATION

A novel FiT- and inertia-integrated GTEP model was developed as an MIQCP model and solved using CPLEX solver in GAMS. The model sought to minimise the total system cost (economic objective) and CO_2 emission levels (environmental objective), while maximising the FiT (economic incentives for renewable energy facilitation) and system inertia (technical objective). The integrated model formulation is described in this section, while Figure 5.2 presents the flowchart of the proposed GTEP model.

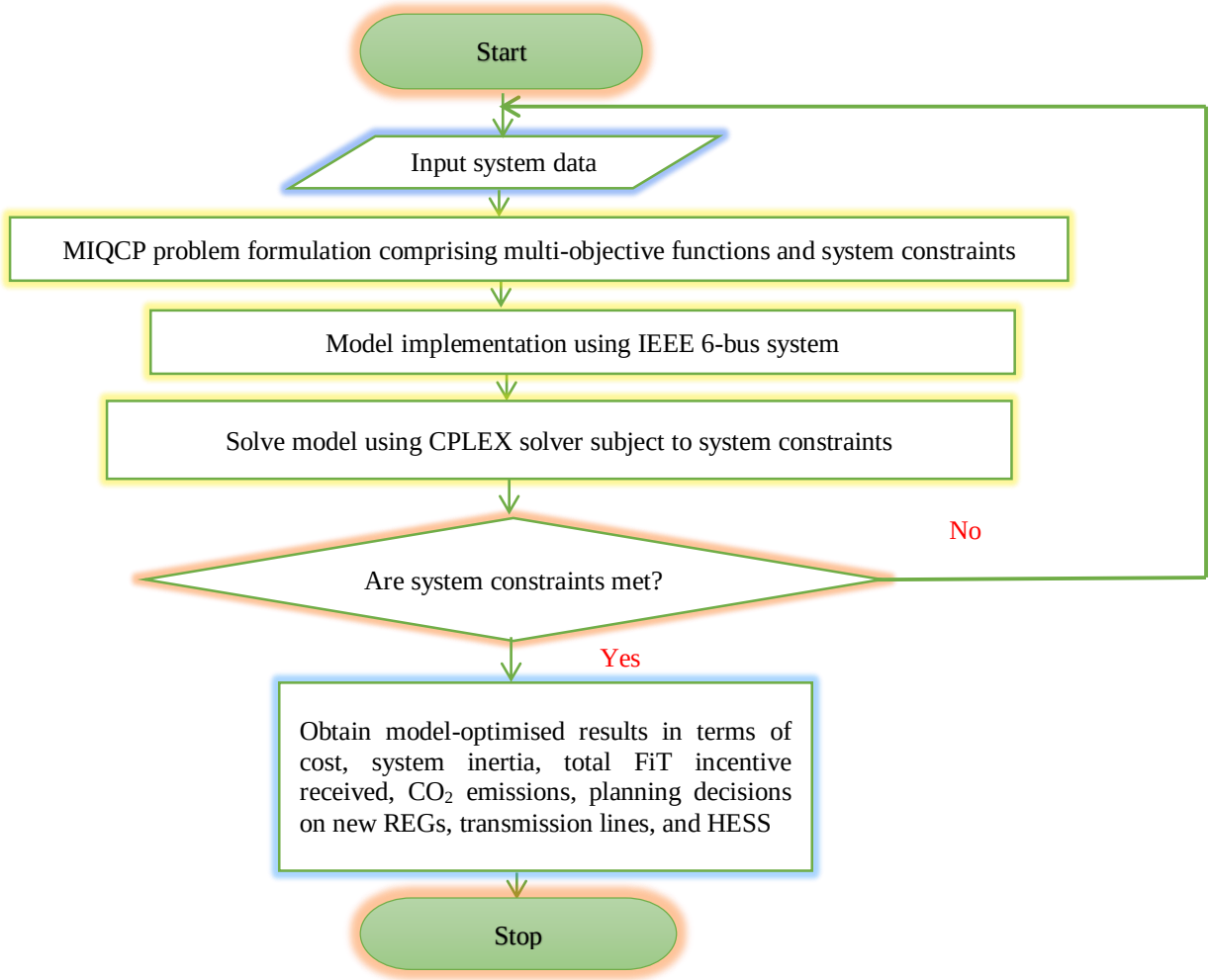

Figure 5.2: Flowchart of proposed FiT and inertia-integrated GTEP model

5.2.1 System inertia objective formulation

System inertia is an important security factor that determines the stability and resilience of the power grid. It can be defined as the amount of rotational energy in the rotor of synchronous generators, which tends to resist changes in the system frequency, particularly during times of contingencies [37]. Hence, in this sub-section, the maximisation of system

inertia is given as one of the problem objectives. The objective function is expressed as in Equation (5.1) [41]:

$$\text{Obj1=Max(system inertia } H) = \max \underbrace{\left[\frac{\sum_{g=1}^{n} H_g \cdot S_g + \sum_{hes=1}^{nhes} H_{hes} \cdot S_{hes} \cdot \mu 1_{hes} + \sum_{w=1}^{nw} H_w \cdot S_w \cdot \mu 2_w + \sum_{s=1}^{ns} H_s \cdot S_s \cdot \mu 3_s}{\sum_{g=1}^{n} S_g + \sum_{hes=1}^{nhes} S_{hes} \cdot \mu 1_{hes} + \sum_{w=1}^{nw} S_w \cdot \mu 2_w + \sum_{s=1}^{ns} S_s \cdot \mu 3_s} \right]}_{\text{system inertia}} \quad (5.1)$$

H_g, H_{hes}, H_w, and H_s are the inertia constant of the thermal generators, HES, wind turbines, and solar PV farms respectively. Similarly, S_g, S_{hes}, S_w, and S_s are the rated apparent power of the thermal generators, HES, wind turbines, and solar PV farms respectively. n, $nhes$, nw, and ns are the number of available thermal generators, candidate HES, candidate solar PV plants, and candidate wind turbines respectively. $\mu 1_{hes}$, $\mu 2_w$, and $\mu 3_s$ are the binary decision variables that determine the selection of prospective HES, wind turbines, and solar PV farms respectively. The variable is 1 if a particular generator technology is selected, and 0 if otherwise.

5.2.2 Cost objective formulation

The proposed model also sought to minimise the total system cost. The total system cost comprises the operational, investment, and economic incentive costs. The operational cost comprises the fuel cost of the thermal generators, the operation and maintenance (O&M) cost of the wind turbines, and the emissions cost of the thermal generators. The investment cost comprises the cost of the purchase and installation of new wind turbines, solar PV plants, HES, and transmission lines, while the economic incentive cost is the total FiT cost expended by the government on power delivered by REGs. The fixed FiT scheme was adopted as the economic incentive scheme in this model, which formed the incentive part of the integrated model formulation. The minimisation of the total system cost of the model is given as one of the problem objectives, as expressed in Equation (5.2), which also implies the maximisation of the total FiT incentive.

$$\text{Obj 2=Min(cost)= } \min \left[\begin{array}{l} \underbrace{\alpha \left[\sum_{g=1}^{n} \left[a_g (P_g)^2 + b_g (P_g) + c_g \right] + \left[\sum_{g}^{n} \lambda_g^{CO_2} \cdot e_g^{CO_2} (P_g) \right] + \sum_{w}^{nw} CO_w^{om} (P_w) \cdot \mu 2_w \right]}_{\text{operational cost}} \\ \underbrace{+ \sum_{hes}^{nhes} CO_{hes}^{inv} \cdot \mu 1_{hes} + \sum_{w}^{nw} CO_w^{inv} \cdot \mu 2_w + \sum_{s}^{ns} CO_s^{inv} \cdot \mu 3_s + \sum_{cl}^{nc} CO_{cl}^{inv} \cdot \mu 4_{cl}}_{\text{investment cost}} \\ + \max \left\{ \underbrace{\sum_{t=1}^{t=\alpha} \left[\sum_{w=1}^{w=nw} P_w^{\max} \cdot CF_w \cdot FiT_w \cdot \mu 2_w + \sum_{s=1}^{s=ns} P_s^{\max} \cdot CF_s \cdot FiT_s \cdot \mu 3_s \right]}_{\text{Economic incentive}} \right\} \end{array} \right] \quad (5.2)$$

a_g, b_g, and c_g are the coefficients used to express the fuel cost ($/hr) of the thermal generators as a quadratic function of the thermal generator's output power P_g [80]. The emission cost is defined as a function of the carbon tax $\lambda_g^{CO_2}$ ($/tCO$_2$), emission factor $e_g^{CO_2}$ (tCO$_2$/kWh), and generating power of the thermal generators in kWh. The total O&M cost in $ of the wind turbines is given in terms of its maintenance cost CO_w^{om} ($/kWh), and the real power delivery P_w of the wind turbines. $CO_{hes}^{inv}, CO_w^{inv}, CO_s^{inv}$, and CO_{cl}^{inv} are the annualised investment cost of candidate HES, wind turbines, solar PV plants, and transmission lines respectively. $\mu 1_{hes}$, $\mu 2_w$, $\mu 3_s$, and $\mu 4_{cl}$ are the binary decision variables that determine investment decisions on HES, wind turbines, solar PV plants, and transmission lines respectively. The decision variable is 1 if a specific technology is selected for installation, and 0 if otherwise. P_g and P_w are decision variables that represent the power output of the thermal generators and wind turbines respectively. nc is the maximum number of candidate transmission lines available for construction during the planning horizon. FiT_w and FiT_s are the fixed FiT incentives rates, in $/kWh, for electricity generated from wind turbine and solar PV plants respectively. $P_w^{\max}$ and $P_s^{\max}$ are the maximum capacity of the installed wind turbines and solar PV plants respectively. CF_w and CF_s are the capacity factors of the wind turbines and solar PV plants respectively. α is the total annual operating time in hours of the generating units. FiT rates of 0.0024 $/kWh and 0.0075 $/kWh were used in the study for wind turbines and solar PV systems respectively.

5.2.3 Environmental (CO_2) objective formulation

The environmental objective of the proposed model was to minimise the total CO_2 emissions. The objective formulation is given in Equation (5.3).

$$\text{Obj3=Min}(CO_2)= \min\overbrace{\left(\left\{\alpha \sum_{g=1}^{n} e_g^{CO_2}(P_g)\right\}\right)}^{CO_2\ emissions} \qquad \forall g \in G \tag{5.3}$$

In this objective function formulation, the decision variable is the power output of the thermal generators P_g, which determines the amount of CO_2 emissions released by the generators.

5.3 MULTI-OBJECTIVE MODEL FORMULATION

In this sub-section, the integration of inertia and FiT into the GTEP model yields a multi-objective optimisation problem, as seen in Equations (5.1) to (5.3). The resulting multi-objective problem minimises the total system cost (economic objective) and CO_2 emissions (environmental objective), while maximising system inertia (technical objective). The multi-objective problem is then converted into a single objective function in Equation (5.4), using the weighted sum approach, in which each objective is multiplied by equal weighting factors and then summed. A detailed description of the weighted sum approach in solving the multi-objective problem is provided in [16]. Weighting factors are used to give preference levels to objective functions. Equal weighting factors were used in this study so that each objective function was given equal preference; that is, a higher priority was not given to one objective at the expense of another. In this research, since there were three objective functions, 0.33 was used as the weighting factor for each objective function, as in Equation (5.5) [133]. The proposed model approach is classical.

$$\text{Obj=min}+\sigma\left[\underbrace{\alpha\left[\sum_{g=1}^{n}\left[a_g(P_g)^2+b_g(P_g)+c_g\right]+\left[\sum_{g}^{n}\lambda_g^{CO_2}\cdot e_g^{CO_2}(P_g)\right]+\sum_{w}^{nw}CO_w^{om}(P_w)\cdot\mu 2_w\right]}_{\text{operational cost}}+\underbrace{\sum_{hes}^{nhes}CO_{hes}^{inv}\cdot\mu 1_{hes}+\sum_{w}^{nw}CO_w^{inv}\cdot\mu 2_w+\sum_{s}^{ns}CO_s^{inv}\cdot\mu 3_s+\sum_{cl}^{nc}CO_{cl}^{inv}\cdot\mu 4_{cl}}_{\text{investment cost}}-\left\{\underbrace{\alpha\left[\sum_{w=1}^{w=nw}P_w^{\max}\cdot CF_w\cdot FiT_w\cdot\mu 2_w+\sum_{s=1}^{s=ns}P_s^{\max}\cdot CF_s\cdot FiT_s\cdot\mu 3_s\right]}_{\text{Economic incentive}}\right\}\right]+\underbrace{\chi\left\{\alpha\sum_{g=1}^{n}e_g^{CO_2}(P_g)\right\}}_{CO2\ \text{emission}}-\beta\underbrace{\left[\frac{\sum_{g=1}^{n}H_g\cdot S_g+\sum_{hes=1}^{nhes}H_{hes}\cdot S_{hes}\cdot\mu 1_{hes}+\sum_{w=1}^{nw}H_w\cdot S_w\cdot\mu 2_w+\sum_{s=1}^{ns}H_s\cdot S_s\cdot\mu 3_s}{\sum_{g=1}^{n}S_g+\sum_{hes=1}^{nhes}S_{hes}\cdot\mu 1_{hes}+\sum_{w=1}^{nw}S_w\cdot\mu 2_w+\sum_{s=1}^{ns}S_s\cdot\mu 3_s}\right]}_{\text{system inertia}} \tag{5.4}$$

$$\sigma+\beta+\chi=1 \tag{5.5}$$

5.3.1 Model constraints

The proposed model was subjected to system equality and inequality constraints. The constraints imposed on the model are described in this sub-section.

5.3.1.1 FiT constraints

It is desirable that FiT rates are attractive, with a good return on investment while not exerting an excessive financial burden on the government. Equations (5.6) and (5.7) define the FiT constraints used in the model [134]. Equation (5.6) defines the total annual FiT payments received for the production of electricity from REGs, which is a function of the FiT rate per technology ($/kWh), the installed capacity per technology (kW), and the capacity factor of the REGs. Equation (5.7) states that the total annual FiT incentive payment disbursed to renewable energy investors must be less than or equal to the renewable energy budget limit. BU_{res} is the maximum monetary budget set for the purchase of new REGs.

$$TFiT=\sum_{t=1}^{t=\alpha}\left[\sum_{w=1}^{nw}P_w^{\max}\cdot CF_w\cdot FiT_w\cdot\mu 2_w+\sum_{s=1}^{s=ns}P_s^{\max}\cdot CF_s\cdot FiT_s\cdot\mu 3_s\right] \tag{5.6}$$

$$TFiT\le BU_{res} \tag{5.7}$$

5.3.1.2 Power balance constraints

Equation (5.8) provides the power balance constraint for the model based on Kirchhoff's current law. It states that at any node, the total power generated by the existing thermal generator *g*, prospective HES, wind turbines, and solar PV plants, plus the sum of net power flowing in the existing and prospective transmission lines, must be greater than or equal to the total load demand [79]. PF_{ij}^{ext+} and PF_{ij}^{ext-} are the active power flow into and out of the existing transmission line respectively. PF_{ij}^{cl+} and PF_{ij}^{cl-} are the active power flow into and out of the candidate transmission lines respectively. LOD_i is the total load demand at bus.

$$\sum_{g}^{n} P_g + \sum_{hes}^{nhes} P_{hes} \cdot \mu 1_{hes} + \sum_{w}^{nw} P_w \cdot \mu 2_w + \sum_{s}^{ns} P_s \cdot \mu 3_s + \sum_{l \in rl} PF_{ij}^{ext+} - \sum_{l \in sl} PF_{ij}^{ext-} + \sum_{l \in rl} PF_{ij}^{cl+} \cdot \mu 4_{cl} - \sum_{l \in sl} PF_{ij}^{cl-} \cdot \mu 4_{cl} \geq \sum_{i} LOD_i \quad (5.8)$$
$$\forall g \in G, \forall s \in S, \forall w \in W, \forall hes \in HES, \forall cl \in CL, \forall ext \in EXT, \forall rl \in RL, \forall i \in I$$

5.3.1.3 Power flow constraints

Equations (5.9) to (5.15) define the power flow constraints formulated based on the DC approximation of Kirchhoff's voltage law to regulate power transmission in existing and prospective transmission lines [121]. $PF_{\max}^{ext}$ and $PF_{ij,\max}^{cl}$ are the maximum power flow in existing and candidate transmission lines respectively. B_{ij}^{ext} and B_{ij}^{cl} are the susceptance of existing and candidate transmission lines connecting bus i to j respectively. θ_i^{rl}, θ_i^{sl}, θ_i^{rcl}, and θ_i^{scl} are the voltage angle at the receiving and sending ends of the existing and candidate transmission lines respectively. θ_i is the voltage angle at bus.

$$-PF_{\max}^{ext} \leq PF_{ij}^{ext} \leq PF_{\max}^{ext} \qquad \forall ext \in EXT \quad (5.9)$$

$$-\mu 4_{cl} \cdot PF_{ij,\max}^{cl} \leq PF_{ij}^{cl} \leq \mu 4_{cl} \cdot PF_{ij,\max}^{cl} \quad \forall cl \in CL \quad (5.10)$$

$$PF_{ij}^{ext} = B_{ij}^{ext}(\theta_i^{sl} - \theta_j^{rl}) \qquad \forall ext \in EXT \quad (5.11)$$

$$-(1-\mu 4_{cl})M \leq PF_{ij}^{cl} - B_{ij}^{cl}(\theta_i^{scl} - \theta_j^{rcl}) \leq M(1-\mu 4_{cl}) \quad \forall i \in I, \forall cl \in CL \quad (5.12)$$

$$-\frac{\pi}{4} \leq \theta_i \leq \frac{\pi}{4} \qquad \forall i \in I \quad (5.13)$$

$$\mu 4_{cl} \in [0,1] \qquad \forall cl \in CL \quad (5.14)$$

$$\sum_{cl} \mu 4_{cl} \leq nc \qquad \forall cl \in CL \quad (5.15)$$

Equations (5.9) and (5.10) define the power flow limit in existing and candidate transmission lines. Equation (5.11) provides the DC power flow equation for existing transmission lines, which is a function of the existing line susceptance, and the bus voltage angle at the receiving and sending ends of the transmission lines. Equation (5.12) defines the DC power flow equations for newly constructed transmission lines using the Big-M parameter. M is a very large number that accommodates all possible values of $\mu 4_{cl}$. Equation (5.13) specifies the acceptable voltage angle limit at bus, which must not be violated. Equation (5.14) defines the binary decision variable that determines that if a new transmission line is to be constructed, the variable is 1, and 0 if otherwise. Equation (5.15) limits the maximum number of candidate transmission lines that can be constructed in the planning horizon.

5.3.1.4 Power generating constraints

Equations (5.16) to (5.22) govern the operation of all existing and prospective REGs [62]. Equation (5.16) specifies the generating power limit for existing thermal generators. Equations (5.17) and (5.18) provide the generating capacity limit for prospective wind turbines and solar PV plants respectively, which is a function of their maximum power rating and capacity factor. Capacity factor was introduced due to the intermittency of RESs. Equation (5.19) provides the binary decision variable for selecting candidate wind turbines and solar PV plants for installation. Equation (5.20) provides the binary investment decision that chooses between wind turbines and solar PV plants for installation at a bus; thus preventing investment in both renewable energy technologies at the same time. Equations (5.21) and (5.22) limit the maximum number of wind turbines and solar PV plants that can be installed during the planning horizon respectively.

$$P_g^{\min} \le P_g \le P_g^{\max} \qquad \forall g \in G \tag{5.16}$$

$$0 \le P_w \le P_w^{\max} \cdot CF_w \qquad \forall w \in W \tag{5.17}$$

$$0 \le P_s \le P_s^{\max} \cdot CF_s \qquad \forall s \in S \tag{5.18}$$

$$\mu 2_w, \mu 3_s \in [0,1] \qquad \forall w, s \tag{5.19}$$

$$\mu 3_w + \mu 4_s \le 1 \qquad \forall w, s \tag{5.20}$$

$$\sum_w \mu 2_w \le nw \qquad \forall w \in W \tag{5.21}$$

$$\sum_s \mu 3_s \le ns \qquad \forall s \in S \tag{5.22}$$

5.3.1.5 Hybrid energy storage (HES) constraints

A conventional power system depends solely on the kinetic energy released from the rotor of synchronous generators to provide an inertia response. However, in modern power systems, HES can also provide an inertia response, as well as a primary frequency response by using suitable VI controllers. Careful selection and appropriate sizing of HES are, however, required for the modern power grid to remain stable [135], [136]. A hybrid combination of high-energy BESS and high-power SCES was selected to provide the needed primary frequency response and inertial response respectively. The operation of the HES is defined by Equations (5.23) to (5.31) [137]:

$$PR_{\min} \geq k \cdot \sum_{i} LOD_i \tag{5.23}$$

$$\sum_{hes}^{nhes} P_{hes} \geq PR_{\min} \tag{5.24}$$

$$P_{hes}^{\min} \leq P_{hes} \leq P_{hes}^{\max} \tag{5.25}$$

$$P_{hes} = \eta_v \cdot P_v + \eta_{sces} \cdot P_{sces} \tag{5.26}$$

$$P_v \geq z \cdot P_{hes} \tag{5.27}$$

$$\sum_{hes}^{nhes} z \cdot P_{hes} \geq [K_{hes} \cdot f_o] \times [\Delta POF] \tag{5.28}$$

$$\sum_{hes}^{nhes} z \cdot P_{hes} \leq q \cdot [K_{hes} \cdot f_o] \times [\Delta POF] \tag{5.29}$$

$$SC_{hes}^{\min} \leq SC_{hes} \leq SC_{hes}^{\max} \tag{5.30}$$

$$\mu 1_{hes} \in [0,1] \qquad \forall hes \in HES \tag{5.31}$$

Equation (5.23) defines the minimum reserve capacity set required to provide a primary frequency response in the power system, which should be greater than or equal to a fraction (5%) of the total load demand at bus. Equation (5.24) states that the sum of the power capacity of all selected candidate HES to be installed must be greater than or equal to the minimum primary reserve set. Equation (5.25) limits the power delivery of HES within upper and lower bounds. Equation (5.26) states that the total power delivered by the HES is equal to the sum of power delivered by the BESS and SCES sources respectively. Equation (5.27) states that the capacity of BESS in the HES mix must be greater than or equal to a certain fraction (80%) of the total capacity of the HES. Equation (5.28) defines the minimum estimated capacity of the BESS in the HES composite required based on the power frequency characteristics of the model to prevent undersizing of storage. Equation (5.29) defines the maximum estimated

capacity of the BESS in the HES composite required based on the power frequency characteristics of the model to prevent oversizing of storage. Equation (5.30) limits the SoC of candidate HES units within upper and lower bounds. Equation (5.31) defines the binary decision variable that determines if a new HES is to be selected for installation at bus. The variable is 1 if HES is selected, and 0 if otherwise.

5.3.1.6 Renewable energy flexibility constraints

Equations (5.32) to (5.34) constrain RES penetration into the grid within a specified limit in line with the renewable energy target of the proposed model [92]. RES penetration target levels are set to 25%, 50%, 75%, and 100%, using a flexible parameter, *f*. Equation (5.32) constrains the total power generation from RES using a flexible parameter, *f*, which is given as a fraction of the total load demand. Equation (5.33) limits the total power generation from thermal generators to at most *(1- f)* percent of total load demand; thus enforcing *f* percent of renewable energy generation [92], [103]. Equation (5.34) defines the range of values of the flexible parameter, *f*, which is used to confine the RES penetration level to between 25% and 100% of the total load demand.

$$\left[\sum_{s=1}^{ns} P_s \cdot \mu 3_s + \sum_{w=1}^{nw} P_w \cdot \mu 2_w\right] \leq f \cdot \left[\sum_i LOD_i\right] \tag{5.32}$$

$$\left[\sum_{g=1}^{n} P_g\right] \leq (1-f) \cdot \left[\sum_i LOD_i\right] \tag{5.33}$$

$$f \in [0.25, 0.5, 0.75, 1] \tag{5.34}$$

5.3.1.7 Inertia constraints

Inertia helps to maintain the balance of the power system after a transient event. To this end, as VI-providing storage units and REGs are used to replace existing synchronous generators, it is important to ensure that the equivalent kinetic energy of the decommissioned synchronous generators can be provided by the VI energy of REGs and storage units [91]. Equations (5.35) to (5.41) provide the inertia constraint formulation that enforces frequency stability in the proposed model [5]. Equation (5.35) defines the acceptable bound for the overall system inertia constant [37]. Equation (5.36) constrains the system's frequency within an acceptable bound based on South Africa's grid code [138]. Equation (5.37) constrains the system's RoCoF within an acceptable range. Equation (5.38) defines the minimum inertia energy set to maintain grid stability following system contingency, calculated in terms of the

nominal system frequency, f_o, magnitude of lost generation during contingency, ΔP, inertia constant of lost generator, H_{gl}, and maximum permissible RoCoF limit, $RoCoF_{\max}$ [89]. Equation (5.39) defines the total inertia energy provided by all online wind turbines, solar PV plants, and HES. Equation (5.40) states that the sum of the inertia energy provided by all online REG sources and HES must be greater than or equal to the minimum inertia energy limit set. Equation (5.41) states that the sum of the inertia energy from the HES must be greater than or equal to the lost rotational energy from the thermal generator(s) during a contingency to compensate for the deficit kinetic energy. The minimum acceptable frequency in the model is taken as 49 Hz [139].

$$H^{\min} \le H \le H^{\max} \qquad \forall g \in G, \forall s \in S, \forall p \in P, \forall w \in W, \forall v \in V \tag{5.35}$$

$$f_r^{\min} \le f_r \le f_r^{\max} \qquad \forall g \in G, \forall s \in S, \forall p \in P, \forall w \in W, \forall v \in V \tag{5.36}$$

$$-RoCoF^{\max} \le RoCoF \le RoCoF^{\max} \tag{5.37}$$

$$IE_{\min} = \frac{\Delta P \cdot f_o}{2 \cdot RoCoF^{\max}} + \Delta P \cdot H_{gl} \tag{5.38}$$

$$IE_{hes,w,s} = \sum_{s=1}^{ns} H_s \cdot S_s + \sum_{w=1}^{nw} H_w \cdot S_w + \sum_{hes=1}^{nhes} H_{hes} \cdot S_{hes} \tag{5.39}$$

$$IE_{hes,w,s} \ge IE_{\min} \tag{5.40}$$

$$\sum_{hes} H_{hes} \cdot S_{hes} \ge \Delta P \cdot H_{gl} \tag{5.41}$$

5.3.2 Model simulation and implementation

In this sub-section, the proposed model is implemented on an IEEE 6-bus system to test the effectiveness of the model. Furthermore, model validation is carried out using various case studies.

Two classes of solar PV plants and wind turbines were considered as candidates for installation. Class II PV plant and Class II wind turbines were assumed to be equipped with VI-provision capability, while Class I PV plants and Class I wind turbines do not have VI capability. In addition, in order to make provision for increased electricity demand and allow for investment in new transmission lines and REG units, the load demand at each bus was assumed to increase by 50%, while the maximum capacity of each transmission line was reduced to half of its initial capacity.

5.3.3 IEEE 6-bus implementation

The IEEE 6-bus test system used for model validation consists of four load points, six existing transmission lines, 10 candidate transmission lines, four candidate HES, four candidate wind turbines, and four candidate solar PV plants, as shown in Figure 5.3. The maximum number of transmission lines permissible per corridor is two. The value of the Big-M parameter used was 10^3. 100-MW REGs were considered as candidate units for installation at buses 2 and 5 (buses with the highest load demand), while prospective 50-MW HES units were considered as candidate units for installation at buses 2 and 5, because of the intermittency of the RESs. System parameters used for the study were obtained from [19], [106], [123], [124], [140], and [141]. The average load demand was given as 1 140 MW [142], while the total thermal generating capacity was 1 400 MW. Bus 1 was taken as the slack bus.

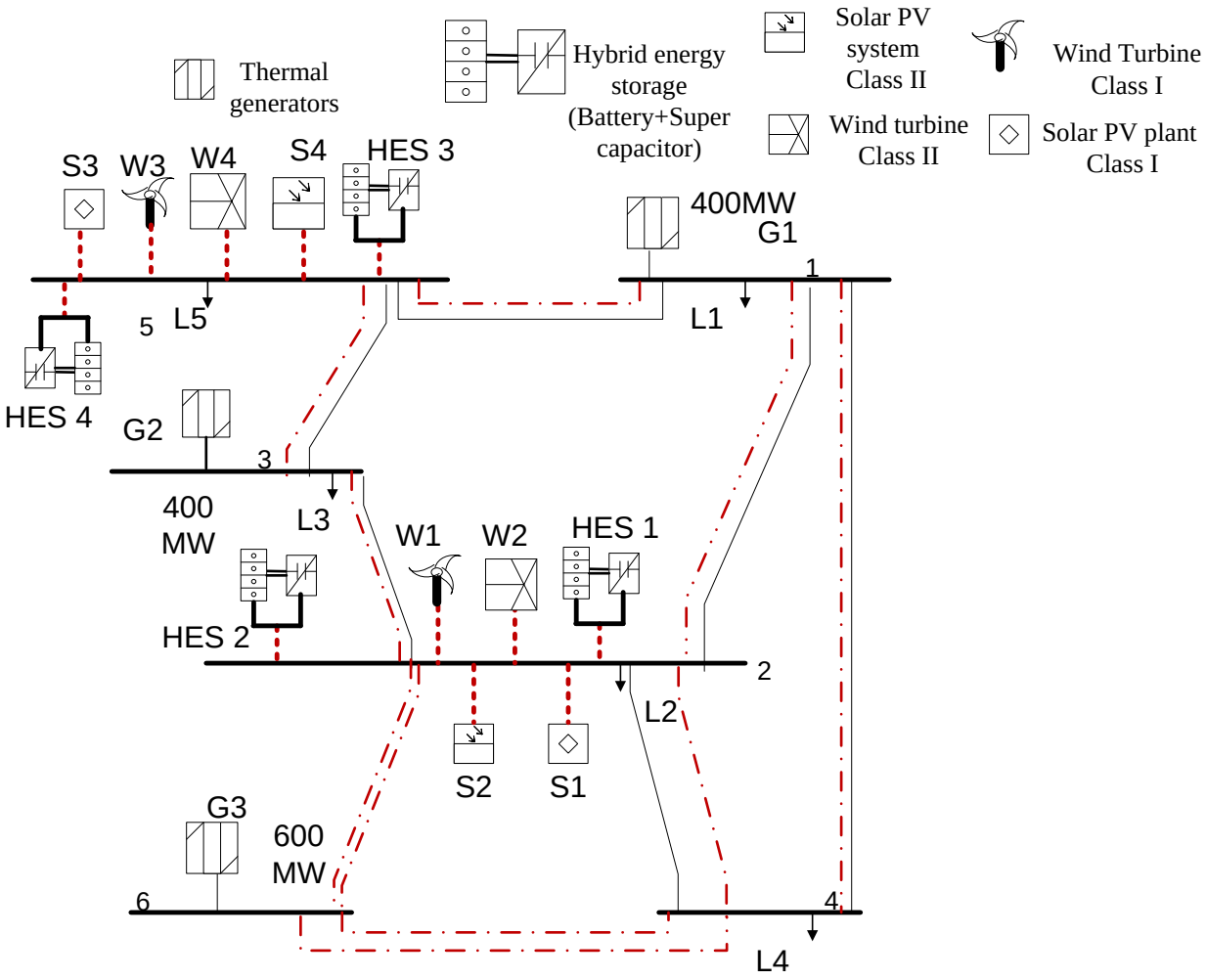

Red dash lines represent candidate REGs, HES, and transmission lines, while solid black lines represent existing thermal generators and transmission lines.

Figure 5.3: IEEE 6-bus test system

5.3.4 Case studies

The performance of the proposed model was evaluated using three case studies, which are outlined as follows:

- Case 1: The model was simulated to minimise CO_2 emissions, without considering system inertia and cost (no FiT). Case 1 represents the base case.
- Case 2: The model was simulated to minimise cost, without considering CO_2 emissions and system inertia.
- Case 3: The model was simulated to minimise all three objectives (CO_2 emissions, cost, and system inertia). In this analysis, minimising cost implies the maximisation of FiT as in Cases 2 and 3, while FiT was not incorporated into the total system cost in Case 1.

5.4 SIMULATION RESULTS AND DISCUSSION

In this section, the results obtained from the model simulation are discussed and analysed.

5.4.1 Simulation results

The simulation results are presented in terms of the overall system inertia, total system cost, investment decisions, total CO_2 emissions, and generation capacity mix.

5.4.1.1 Overall system inertia

The overall system inertia for the different case studies is shown in Table 5.2. It can be observed that the overall inertia constant was the highest in Case 3, with an overall inertia constant of 6.139s, which corresponds to inertia energy of 10 700 MWs. Conversely, the overall system inertia was the lowest in Case 2, with an overall inertia constant of 5.565s, which corresponds to inertia energy of 9 700 MWs. The inertia energy in Case 3 was the highest due to the incorporation of inertia in the model formulation, which influenced the investment decisions. The inertia energy was lower in Cases 1 and 2, where inertia was not considered in the planning decisions.

Table 5.2: Overall inertia for the various case studies

Case study	Overall system inertia constant (s)	Total inertia energy (MWs)		
		Synchronous inertia	VI	Total inertia
Case 1	5.680	8 500	1 400	9 900
Case 2	5.565	8 500	1 200	9 700
Case 3	6.139	8 500	2 200	10 700

5.4.1.2 System cost and investment decisions

Table 5.3 presents the detailed cost analysis and expansion planning decisions on new transmission lines, HES, and REGs for the different case studies. It can be observed that the investment cost and total system cost were the highest in Case 1 and the lowest in Case 3. The disparity in cost is due to the difference in investment decisions made in both cases. The total system cost decreased by 11.94% and 8.86% in Case 3, relative to Cases 1 and 2, while the total investment cost decreased by 44.9% and 38% in Case 3, relative to Cases 1 and 2. On the other hand, the total annual FiT payments received was the highest in Case 2 due to the decision to invest in solar PV plants that offer higher FiT rates compared to investment in wind turbines, as in Cases 1 and 3. This shows that FiT can efficiently influence planning decisions. In addition, the total system cost was the lowest in Case 3 because of the FiT incentives received and the optimal decision to invest in a lower number of transmission lines (three transmission lines) compared to Case 1 (six transmission lines) and Case 2 (five transmission lines).

Table 5.3: Detailed cost analysis and investment decisions under different case studies

Metrics	Case study		
	Case 1	Case 2	Case 3
Fuel Cost ($)	1.7131E + 08	1.7739E + 08	1.7747E + 08
O&M cost on wind turbine ($)	9.3206E + 06	-	9.3206E + 06
Emission cost ($)	2.4342E + 08	2.4342E + 08	2.4432E + 08
Total operational cost ($)	4.24E + 08	4.21E + 08	4.31E + 08
Total investment cost ($)	1.75E + 08	1.58E + 08	9.64E + 07
Total FiT received (PV and wind turbine) ($)	-	3.29E + 06	1.5978E + 6
Total cost ($)	5.99E + 08	5.76E + 08	5.26E + 0 8
Total number of investments in wind turbines	2 (W_1, W_3)	-	2 (W_2,W_4)
Total number of solar PV investments	-	2 (S3, S4)	-
Total number of investments in HES	2	2	2
Transmission lines investment	(2-6) (x2) (3-5) (x2) (4-6) (x2)	(4-6)(x2) (2-6) (x2) (3-5)	(4-6) (3-5) (2-6)

5.4.1.3 CO_2 emissions and generation capacity mix

The total CO_2 emissions and overall capacity mix for the different generating technologies after planning decisions have been implemented are provided in this sub-section. The total CO_2 emissions from the thermal generators and the capacity mix for the different case studies are provided in Table 5.4. It can be observed from Table 5.4 that the total CO_2 emissions were 2.2% less in Case 3 than Case 2. The integrated model that considered FiT (cost), emissions, and system inertia thus had a significant impact on the total CO_2 emissions as the emissions decreased by 0.226 million tonnes. It can also be observed that the total generating capacity mix was the highest in Case 3, because of the choice of wind turbines with a higher capacity factor than solar PV plants. Figure 5.4 illustrates the generating output power for all thermal generators. It can be observed that the total CO_2 emissions from the thermal generators were the highest in Case 2 (where emission minimisation was not considered in the objective function), compared to Cases 1 and 3.

Table 5.4: CO_2 emissions and generation capacity mix for the different case studies

Metrics	Case study		
	Case 1	**Case 2**	**Case 3**
Total CO_2 emissions (tCO_2)	9.7367E + 6	0.9999E + 7	9.7729E + 6
Total generated power from thermal generators (MW)	963.9	989.9	967.5
Total generated power from wind turbines (MW)	76	-	76
Total generated power from solar PV systems (MW)	-	50	-
Total power generation (MW)	1 039.9	1 039.9	1 043.5

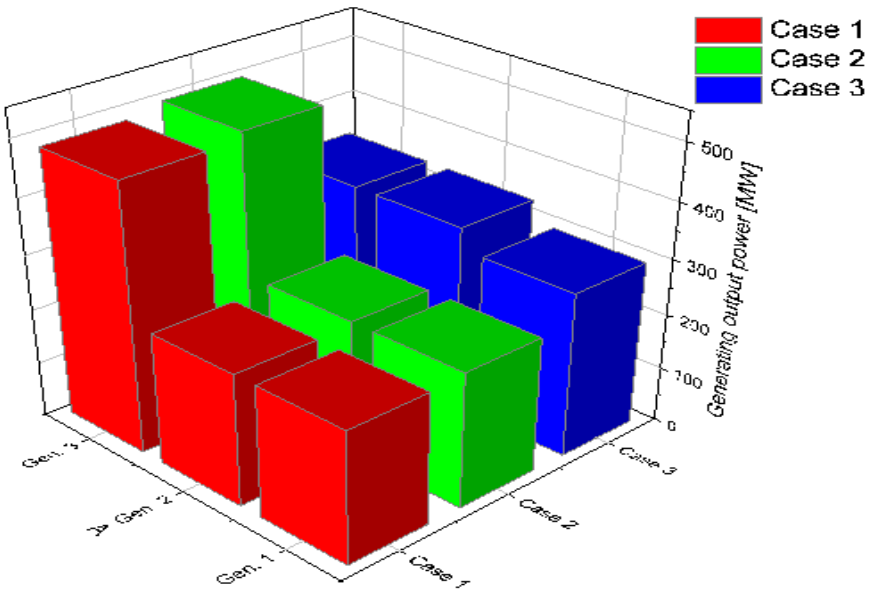

Figure 5.4: Generating output power of thermal generators for the different case studies

5.5 DYNAMIC FREQUENCY RESPONSE ANALYSIS OF THE MODEL

In this section, the dynamic frequency response of the model is evaluated for the different case studies. The analysis was conducted following the loss of the largest synchronous generator with an installed capacity of 600 MW. A variation in system frequency in response to the disturbance was observed for all case studies, as presented in Table 5.5. It can be observed that in Cases 1 and 2, where system inertia was not considered in the model formulation, frequency nadirs of 48.9396 Hz and 48.9523 Hz were observed respectively. These frequency nadir values were below the acceptable frequency limit set for the study. On the other hand, in Case 3, where system inertia was considered in the model, the frequency nadir was observed to be 49.002 Hz, which was within the accepted frequency limit. The proposed model thus improved the overall resilience of the modern grid and supports Hypothesis 1 (H_1) of the study.

Table 5.5: Dynamic frequency response during contingency for the different case studies

Case study	System inertia (s)	Frequency drop	Frequency nadir
Case 1	5.680	1.0477	48.9523
Case 2	5.565	1.0604	48.9396
Case 3	6.139	0.998	49.002

5.6 SENSITIVITY ANALYSIS AND DISCUSSION OF RESULTS

The sensitivity analysis of the model parameters (FiT and system inertia) was conducted by subjecting the model to different RES penetration levels. The corresponding changes in the total FiT received and overall system inertia were then observed.

5.6.1 Sensitivity analysis of the FiT

To investigate the sensitivity of the FiT incentives received under varying RES penetration levels, four different scenarios were assumed; as follows:

- Scenario 1: Model with 25% RES penetration level (base scenario).
- Scenario 2: Model with 50% RES penetration level.
- Scenario 3: Model with 75% RES penetration level.
- Scenario 4: Model with 100% RES penetration level.

Table 5.6 presents the generation mix for the different RES penetration levels. It also provides the total investment cost and FiT payments received for the different RES penetration scenarios. It can be observed that the FiT payments received had a significant impact on the total investment cost. Furthermore, Figure 5.5 shows the fraction of the investment cost covered by the FiT payments received. As shown in Table 5.6 and Figure 5.5, the sensitivity analysis revealed that the higher the penetration of RESs, the higher the total system cost and total FiT received; however, the fraction of FiT payments received relative to the total investment cost decreased after 50% RES penetration for the same FiT rates.

Table 5.6: Capacity mix for different RES penetration levels

Generator installed capacity per technology (MW)	**RES penetration level (%)**			
	25 (%)	**50 (%)**	**75 (%)**	**100 (%)**
Thermal (MW)	1 400	800	400	0
Wind (MW)	400	400	800	1 200
Solar (MW)	-	600	600	600
Investment cost on new REGs ($)	3.2000E + 07	8.76E + 07	1.17E + 08	1.46E + 08
Total FiT received ($)	3.1956E + 06	1.31E + 07	1.62E + 07	1.94E + 07

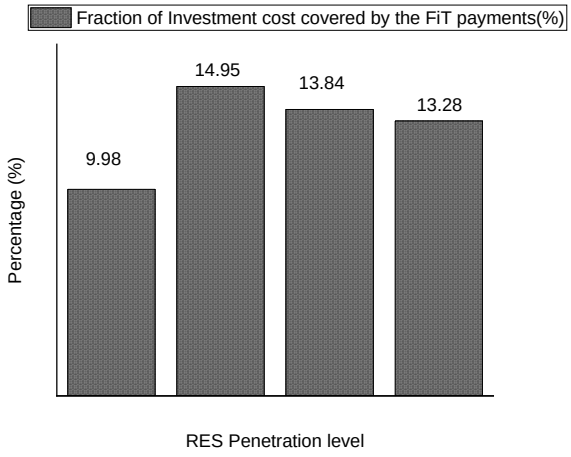

Figure 5.5: Fraction of investment cost covered by the total FiT payments

5.6.2 Sensitivity analysis of system inertia

A sensitivity analysis was conducted to investigate the effect of increasing RES share on the overall system inertia of the integrated GTEP model. The sensitivity analysis was conducted for different RES penetration levels using two scenarios: in Scenario 1, REGs and HES were not equipped with VI capability, while in Scenario 2, REGs and HES were equipped with VI capability.

The results of the sensitivity analysis are presented in Table 5.7, Figure 5.6, and Figure 5.7. It can be observed from Table 5.7 and Figure 5.6 that the higher the RES penetration level, the lower the overall system inertia for both scenarios; however, the rate of decline of system inertia was higher in Scenario 1, where the VI capability of the REGs and HES was ignored, than in Scenario 2, where the VI capability of REGs and HES was considered. Furthermore, Table 5.7 and Figure 5.7 show that the overall inertia constant declined from 5.333s to 1.4860s (72.1%) in Scenario 1, and from 6.827s to 4.2105s in Scenario 2 (38.3%). In addition, based on the preset inertia constant limit for the model in Equation (5.35), the maximum permissible RES penetration limit should be less than 50% in Scenario 1, while in Scenario 2, the RES penetration limit can reach up to 100% without violating the preset inertia constant limit. However, it is noteworthy that although the RES penetration in Scenario 2 can reach up to RES 100% without violating the inertia limit set, the stability of the grid at such a high level might not be assured because of the obvious decline in the overall inertia constant. The stability of the grid at 100% RES penetration level will be investigated in the future.

Table 5.7: Inertia values for various RES penetration levels

RES penetration (%)	Scenario 1			Scenario 2		
	Inertia constant (s)	Total inertia energy (MWs)	Corresponding frequency nadir values (Hz)	Inertia constant (s)	Total inertia energy (MWs)	Corresponding frequency nadir values (Hz)
25	5.333	9 600	48.85	6.827	11 900	49.35
50	2.6890	4 800	47.96	4.8179	8 600	48.68
75	2.1176	3 600	47.77	4.5938	8 200	48.60
100	1.4860	2 400	47.56	4.2105	6 800	48.47

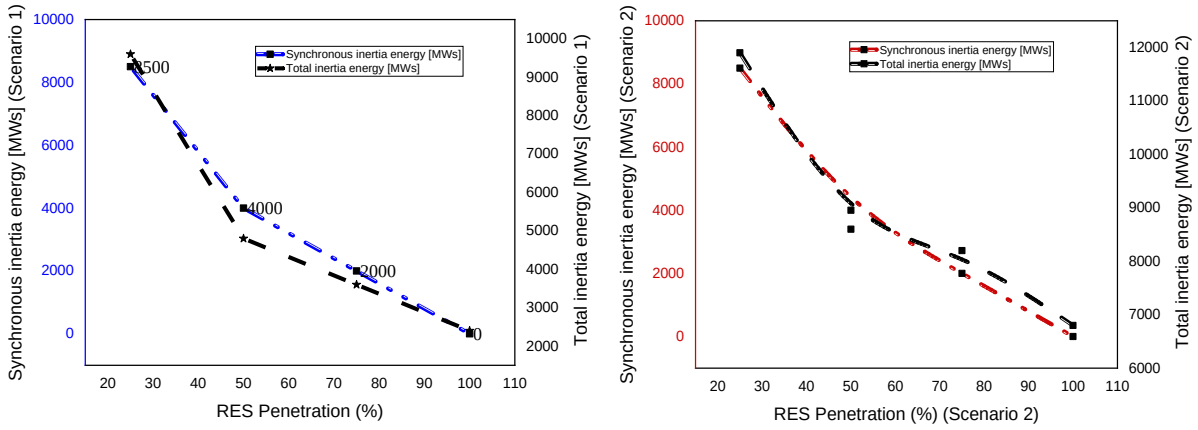

(a) Scenario 1 (b) Scenario 2

Figure 5.6: Variation of synchronous inertia and total inertia energy with increasing RES penetration for the different scenarios

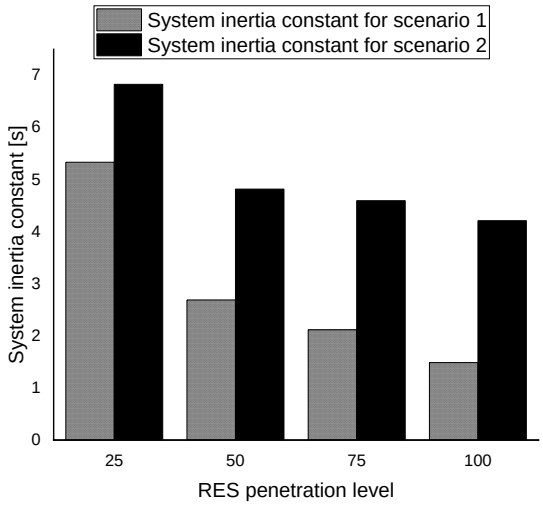

Figure 5.7: Variation of system inertia constant for the different RES penetration levels

5.6.3 Discussion of results

The simulation results show that considering inertia, emissions, and FiT in the developed GTEP model (Case 3) had a significant influence on the model, particularly in terms of cost, system inertia, and CO_2 emissions. It can be observed that when inertia, emissions, and FiT were considered in the model design (Case 3), the total system cost decreased by 8.86%, while the total CO_2 emissions reduced by 2.2%, and the overall system inertia constant increased by 10.3% (5.565s to 6.139s), relative to Case 2. In addition, optimal planning decisions for the installation of new transmission lines were made in Case 3, compared to Cases 1 and 2. In Case 3, three additional transmission lines were selected for installation, while six and five additional transmission lines were selected for installation in Cases 1 and 2 respectively, which resulted in increased investment cost for the transmission lines in both cases. Two wind turbines (W_2 and W_4) with VI capabilities were selected for installation in Case 3; thus striking a balance between cost reduction and meeting the inertia requirement of the model. This was unlike the inappropriate planning decision made in Case 1, which favoured the installation of two wind turbine units without VI capabilities (W_1 and W_3).

Furthermore, it is noteworthy that the total FiT received ($3.29 million) was the highest in Case 2 because of the decision to invest in solar PV plants with higher FiT rates, but with a lower inertia constant than wind turbines. On the other hand, although the total FiT received ($1.5978 million) in Case 3 was slightly less than in Case 2, the planning decisions were made considering the need for adequate inertia in the grid. The developed model that considered inertia, emissions, and FiT in GTEP (Case 3) improved the overall system performance using

the highlighted metrics and will guide power system planners in making appropriate expansion planning decisions.

Table 5.8 compares the proposed model using mathematical programming techniques relative to other equivalent models using soft-computing optimisation techniques in terms of computation time. Furthermore, Figure 5.8a shows the convergence curve of the proposed optimisation approach relative to other optimisation techniques. According to the no free lunch theorem, the proposed mathematical optimisation model has the potential to perform well in terms of computational time and convergence speed considering the objective function and constraints considered in this model. In addition, Figure 5.8b provides the Pareto optimal chart, which shows the trade-off between total system cost, CO_2 emissions, and system inertia.

Table 5.8: Comparison of the proposed mathematical approach relative to other soft-computing optimisation techniques in terms of computing time

Solution method	Computation time (s)
Proposed mathematical (MILP) method	14.359
NSGA-II [143]	18.61
GA [144]	33.76
Multi-objective Harris hawks optimisation [84]	253.8
Ant lion optimiser [83]	353.1225
Salp swarm algorithm [83]	384.7674
Improved binary PSO algorithm [81]	3 096

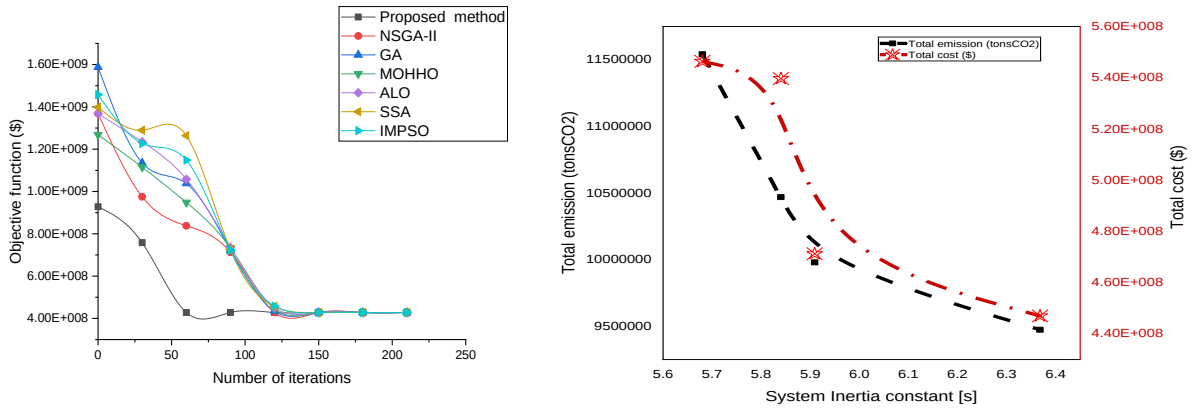

(a) (b)

Figure 5.8: (a) Convergence curve of proposed mathematical model relative to other optimisation techniques; (b) Pareto chart of total system cost and total emission versus system inertia

5.7 CONCLUSION

This chapter proposed a FiT and inertia-integrated GTEP optimisation model. The model was developed as an MIQCP model to minimise the total system cost and CO_2 emissions, while maximising the overall system inertia and FiT incentives. The developed model was implemented on an IEEE 6-bus test system and solved using CPLEX solver in GAMS. Three case studies were used to validate the efficiency of the proposed model, while a sensitivity analysis of FiT and system inertia was conducted under varying RES penetration levels. The key findings of the chapter are outlined as follows:

- Due to the high investment cost of solar PV systems relative to wind turbines, the FiT rate for solar PV systems should be higher than 0.24 $/Wh to stimulate investment by renewable energy investors.
- Due to the consideration of FiT, emissions, and system inertia in the GTEP model (Case 3), the model achieved lower total system cost (11.94% decrease relative to Case 1), higher system inertia (8% increase relative to Case 1), and lower CO_2 emission (2.2% decrease relative to Case 2), with a shorter processing time relative to other soft-computing optimisation techniques.
- The developed integrated model achieved better frequency stability following system contingency due to its higher inertia constant value.
- The sensitivity analysis revealed that the overall system inertia declined by 72.1% when the RES penetration level increased from 25% to 100% with REGs and HES incapable of providing VI. However, the overall system inertia declined by 38.3% when the RES penetration level increased from 25% to 100% with REGs and HES capable of providing VI. This shows the importance of power system planning with RES and HES capable of providing VI.
- The sensitivity analysis also revealed that the higher the penetration of RES, the higher the total system cost and the total FiT received; however, the fraction of FiT payments received relative to the total investment cost decreased after 50% RES penetration for the same FiT rate.
- Based on the preset inertia constant limit for the model in Equation 35, investment in RES technology and HES incapable of providing VI above the 50% RES penetration level violated the minimum inertia limit set, while the inertia limit was not violated in RES penetration levels up to 100% with investment in VI-providing REGs and HES.

- The model analysis was limited to an IEEE 6-bus test system; hence, in the future, the model will be extended to a larger test system, while the stability of the grid at 100% RES penetration will be investigated. In addition, other multi-objective optimisation techniques will be used for the model analysis.

CHAPTER 6: SHORT-TERM RENEWABLE ENERGY UNCERTAINTIES AND INERTIA CONSIDERATIONS IN POWER SYSTEM GEP

6.1 INTRODUCTION

The power output of REGs is influenced by weather factors such as solar irradiance, wind speed, air temperature, air density, snow mass, cloud cover, snowfall, precipitation, etc. [70], [145]. For example, wind turbine power generation is influenced by factors such as changing wind speed and wind orientation, while the active power of solar PV systems is influenced by factors such as varying solar irradiance and temperature [75], [146]. These factors influence the stable operation of the power system.

Several approaches and techniques have been used by researchers to solve optimisation problems with uncertain variables. These approaches are the stochastic optimisation method, probabilistic or statistical methods, robust optimisation, neural network, heuristic optimisation, interval optimisation, possibility method or fuzzy optimisation, information gap decision-making theory, dynamic programming, Lagrangian relaxation, MILP, hybrid optimisation methods, etc. [147], [148], [149], [77]. However, stochastic programming and robust optimisation are the most widely studied approaches [54], [76]. A detailed description and classification of the different types of uncertainty optimisation techniques and solution methods are provided in [150], [151].

Interval optimisation and the possibility method are used when the input parameters can be determined using interval numbers, while robust optimisation is used when the model parameters are known within certain bounds. The robust optimisation method can be divided into the engineering game model, two-stage robust optimisation model, and distributed robust optimisation model. Probabilistic approach and stochastic programming models use historical data to define the PDF of uncertain parameters. In stochastic programming, the PDF of the input parameters can also be determined using scenario-based approaches such as the Monte Carlo sampling technique, Latin hypercube sampling technique, and roulette wheel mechanism [76]. The generated scenarios can then be solved using optimisation methods such as MILP, the branch-and-bound algorithm, Benders decomposition, Lagrangian decomposition, etc. [72], [152].

The authors in [143] highlighted the challenges posed by RES uncertainties in modern power system planning while using non-dominated sorting GA II to solve the associated uncertainty problem. The key findings of the study revealed a 0.21% reduction in cost and a 0.51% reduction in CO_2 emissions using the proposed model. However, the authors did not consider the inertia requirement of the grid in their model formulation. The authors in [74] proposed an optimal model for the dispatch of REG units while minimising the levelised CoE of the system. This work, however, did not consider the need to reduce CO_2 emissions in the model formulation. Furthermore, the authors in [152] proposed an optimal planning model for REGs that considered the stochastic behaviour of RERs. This model was solved using the PSO algorithm. However, the model did not consider the inertia requirement of the grid in planning and the need to minimise CO_2 emissions. The authors in [143] developed a GEP model to minimise the cost of electricity generation and CO_2 emissions. The model, however, did not consider the inertia requirement of the grid in planning, nor uncertainties in RERs. A summarised comparison of reviewed literature is provided in Table 6.1, while Figure 6.1 illustrates the different types of system uncertainties [70], [151].

Table 6.1: Comparison of the proposed model relative to the reviewed literature

Reference	System inertia	CO_2 emission	Renewable energy uncertainties	GEP modelling
[70]	×	✓	✓	×
[150]	×	×	✓	×
[152]	×	×	✓	✓
[74]	✓	✓	✓	✓
[153]	×	×	✓	✓
[56]	✓	×	×	×
[154]	✓	✓	×	✓
[155]	×	×	✓	×
This study	✓	✓	✓	✓

✓: Considered x: Not considered

This chapter extends the model developed in Chapter 5 to consider the uncertainties (solar irradiances and wind speed variabilities) associated with RERs, while also considering the cost, emissions, and inertia requirement of the grid. This chapter proposes a scenario-based MILP model for the optimal planning of power generators considering both RER uncertainties and the inertia requirement of the grid. This will help power operators make the right investment decision based on the RER availability at the installation site. For this research, the chosen study site was the Mangaung Metropolitan Municipality, Bloemfontein, Free State province, South Africa.

Different from the approaches deployed in the reviewed literature, the proposed model was formulated using a classical approach because it guarantees convergence to the optimal solution in a finite number of steps while providing a flexible and accurate modelling framework [156], unlike stochastic and robust programming that involve a large number of random variables that increase the complexity of the model and may result in suboptimal solutions.

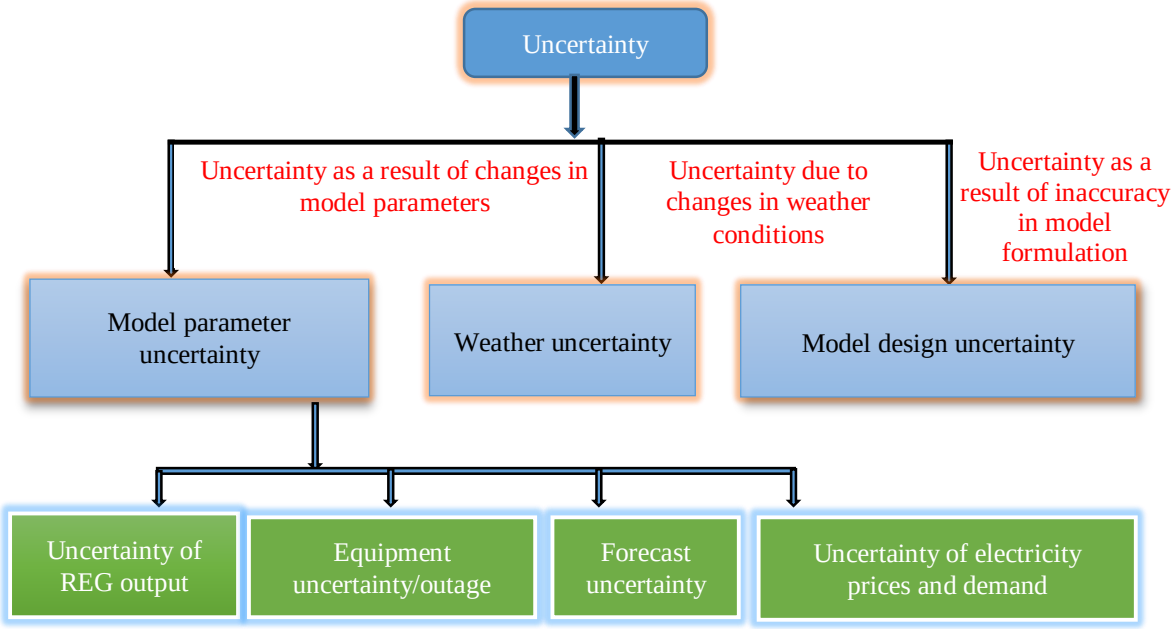

Figure 6.1: Types of system uncertainties

The main contributions of this study are outlined as follows:

- Developing a new deterministic MILP model that considers system inertia and RER uncertainties in GEP.
- Investigating the impact of RES uncertainties considerations on GEP results and the CoE of the power system.
- Developing a deterministic model that ensures appropriate selection of REGs based on RER availability at the installation site.

Furthermore, the novelty of this study is seen in the following:

- The consideration of system inertia and RES uncertainty in GEP.
- The introduction of two types of CO_2 emission penalty cost: CO_2 emission penalty cost on humans and CO_2 emission penalty cost on the ecosystem.
- Inertia constraints introduced in the model formulation.

The remainder of the chapter is organised as follows: Section 6.2 describes the mathematical formulation of the proposed deterministic planning model, model implementation and validation using different case studies are discussed in Section 6.3, while Section 6.4 presents the simulation results and a discussion of the results obtained from the model design. Finally, the conclusion of the chapter is presented in Section 6.5.

6.2 PROPOSED METHODOLOGY

In this section, a scenario-based deterministic planning model is proposed that considers uncertainties associated with REGs and the inertia requirement of the grid. The proposed model was formulated as an MILP model and solved using CPLEX solver in GAMS. The approach was deterministic to ensure accurate results and speedy convergence and to avoid model complexities. Additionally, two types of CO_2 emission penalty costs were introduced to reflect the negative effect of GHGs on humans and the ecosystem.

The uncertainties of wind speed and solar irradiance were characterised using a number of scenarios throughout the 24-hour planning horizon. Scenarios with specified occurrence probability were chosen based on historical data for each uncertain variable in Bloemfontein, South Africa. Each scenario represented hourly values of wind speed and solar irradiance. The time horizon was divided into 24-hour periods with one-hour intervals.

Three different hourly scenarios with their respective approximate probability of occurrence were used to represent each uncertain variable per time. The scenarios are indicated as high, medium, and low, with probabilities of 0.5, 0.3, and 0.2 respectively. A total of 144 hourly scenarios (72 wind scenarios and 72 solar scenarios) were selected for a typical day during the four seasons (i.e., spring, summer, autumn, and winter) experienced in South Africa. The load demand was assumed as constant for all seasons. The developed model was solved using a Toshiba Satellite Pro C660 (64-bit, Core i3 CPU @2.10GHz, 4GB RAM) computer.

6.2.1 Formulation of the multi-objective model

A new GEP model was formulated to minimise CO_2 emissions and CoE, while maximising system inertia in the presence of renewable energy uncertainties. The multi-objective model was developed subject to system constraints. A flowchart of the proposed model is provided in Figure 6.2.

6.2.2 Cost of energy (CoE) objective formulation

The proposed model also sought to minimise the CoE in $/MWh, which was one of the model objectives, as expressed in Equation (6.1). The CoE comprises the total cost of the system ($) and the total energy generation (MWh). The total system cost comprises the operational and investment costs of the system. The operational cost comprises the fuel cost of the thermal generators, the O&M cost of the wind turbines, and the emissions cost of thermal generators. Two types of CO_2 emission penalty costs were introduced in this study: CO_2 penalty tax on humans $\lambda_{man}^{CO_2}$ and CO_2 penalty tax on the ecosystem $\lambda_{eco}^{CO_2}$ due to the negative effect of GHGs on both humans and the environment. The investment cost comprised the cost of construction and installation of new wind turbines, solar PV plants, and BESS units.

$$\text{ObjF1=Min(CoE)}= \min \left[\frac{\left[\underbrace{\sum_{t=1}^{t=24}\left[\sum_{th=1}^{nth}\left[a_{th}(P_{th})^2+b_{th}(P_{th})+c_{th}\right]+\sum_{th}^{nth}\left(\lambda_{man}^{CO_2}+\lambda_{eco}^{CO_2}\right)\cdot em_{th}^{CO_2}\cdot(P_{th})+\sum_{wi}^{nwi}CS_{wi}^{om}\cdot(P_{wi})\cdot\mu_{wi}\right]}_{\text{Operational Cost}} + \underbrace{\sum_{bes}^{nbes}CS_{bes}^{inv}\cdot\mu_{bes}+\sum_{wi}^{nwi}CS_{wi}^{inv}\cdot\mu_{wi}+\sum_{so}^{nso}CS_{so}^{inv}\cdot\mu_{so}}_{\text{investment cost}} \right]}{\left[\sum_{t=1}^{t=24}\sum_{th=1}^{nth}(P_{th})+\sum_{t=1}^{t=24}\sum_{ss=1}^{72}\mu_{so}\cdot\left(\Pr_{ss}^{so}\cdot Va_{ss}^{so}\cdot P_{so}^{\max}\right)+\sum_{t=1}^{t=24}\sum_{sw=1}^{72}\mu_{wi}\cdot\left(\Pr_{sw}^{wi}\cdot Va_{sw}^{wi}\cdot P_{wi}^{\max}\right)\right]} \right] \quad (6.1)$$

a_{th}, b_{th}, c_{th} are the fuel cost ($/hr) coefficients of the thermal generators expressed as a quadratic function of the generating power of the thermal generators, P_{th}. The emission cost is defined as a function of the emission factor $em_{th}^{CO_2}$ (tCO_2/kWh), generating power of the thermal generators in kWh, carbon penalty tax on humans $\lambda_{man}^{CO_2}$ ($/tCO_2$), and carbon penalty tax on the ecosystem $\lambda_{eco}^{CO_2}$ ($/tCO_2$). The total O&M cost in $ of the candidate wind turbines is given in terms of its maintenance cost CS_{wi}^{om} ($/kWh), and the real power delivery P_{wi}, of the wind turbine. The real power delivery of the wind turbine is expressed in terms of probability of occurrence per time $\Pr_{sw}^{wi}$, wind variability constant per time Va_{sw}^{wi}, and the installed capacity of the wind turbine $P_{wi}^{\max}$. Similarly, the real power delivery of the solar PV plants is expressed in terms of its probability of occurrence per time $\Pr_{ss}^{so}$, solar variability constant per time Va_{ss}^{so}, and the installed capacity of the solar PV plant $P_{so}^{\max}$. $CS_{bes}^{inv}, CS_{wi}^{inv}$, and CS_{so}^{inv} are the investment cost of candidate BESS, wind turbines, and solar PV plants respectively. $\mu_{bes}, \mu_{wi}, \mu_{so}$ are the binary decision variables that determine investment decisions on BESS, wind turbines, and

solar PV plants respectively. The decision variable is 1 if a specific technology is selected for installation, and 0 if otherwise. $nth, nbes, nwi,$ and nso are the maximum number of thermal generators, candidate BESS, candidate wind turbines, and candidate solar PV plants respectively. t is the 24-hour time period in a day.

6.2.3 Environmental objective formulation

One of the model objectives (environmental) was to minimise the total CO_2 emissions. The objective formulation is provided in Equation (6.2).

$$\text{ObjF2=Min}(CO_2)= \min\overbrace{\left(\left\{\sum_{t=1}^{t=24}\sum_{th=1}^{nth} em_{th}^{CO_2}(P_{th})\right\}\right)}^{CO_2\ emissions} \qquad \forall \text{th} \in \text{TH} \tag{6.2}$$

6.2.4 System inertia objective formulation

System inertia can be defined as the amount of rotational energy available in the rotational part of synchronous generators that provides resistance to the frequency instability in the grid during times of contingency [41]. Adequate system inertia is essential to ensure the security and resilience of the modern grid. The maximisation of system inertia was one of the model objectives, as expressed in Equation (6.3):

$$\text{ObjF3=Max(system inertia } H) = \max\underbrace{\left(\left[\frac{\sum_{th=1}^{nth} H_{th}\cdot S_{th}^{\max} + \sum_{bes=1}^{nbes} H_{bes}\cdot S_{bes}\cdot \mu_{bes} + \sum_{wi=1}^{nwi} H_{wi}\cdot S_{wi}^{\max}\cdot \mu_{wi} + \sum_{so=1}^{nso} H_{so}\cdot S_{so}^{\max}\cdot \mu_{so}}{\sum_{th=1}^{nth} S_{th}^{\max} + \sum_{bes=1}^{nbes} S_{bes}\cdot \mu_{bes} + \sum_{wi=1}^{nwi} S_{wi}^{\max}\cdot \mu_{wi} + \sum_{so=1}^{nso} S_{so}^{\max}\cdot \mu_{so}}\right]\right)}_{\text{system inertia}} \tag{6.3}$$

H_{th}, H_{bes}, H_{wi}, and H_{so} are the inertia constant of the thermal generators, BESS, wind turbines, and solar PV farms respectively. Similarly, $S_{th}^{\max}, S_{bes}, S_{wi}^{\max}$ and, $S_{so}^{\max}$ are the rated apparent power of the thermal generators, BESS, wind turbines, and solar PV farms respectively. $\mu_{bes}, \mu_{wi}, and\ \mu_{so}$ are the binary decision variables that determine the selection of prospective BESS, wind turbines, and solar PV farms respectively. The variable is 1 if a particular generator technology is selected, and 0 if otherwise.

6.2.5 Multi-objective model formulation

The integration of all three objectives into the proposed GEP model yielded a multi-objective optimisation problem. The resulting multi-objective problem minimised the CoE

(economic objective) and CO_2 emissions (environmental objective) while maximising the system inertia (technical objective). The multi-objective problem was then converted into a single objective function using the weighted sum approach, in which each objective was multiplied by equal weighting factors and summed, as seen in Equation (6.4). Equal weighting factors were used in this study such that the sum of the absolute values of the weights of each objective must be equal to 1, as expressed in Equation (6.5).

$$\begin{aligned}\text{ObjF=min}\;\; & we_1\left\{\frac{\underbrace{\left[\sum_{t=1}^{t=24}\left[\sum_{th=1}^{n}\left[a_{th}(P_{th})^2+b_{th}(P_{th})+c_{th}\right]+\sum_{th}^{nth}\left(\lambda_{man}^{CO_2}+\lambda_{eco}^{CO_2}\right)\cdot em_{th}^{CO_2}\cdot(P_{th})+\sum_{wi}^{nwi}CS_{wi}^{om}(P_{wi})\cdot\mu_{wi}\right]\right]}_{\text{operational cost}}}{\left[\sum_{t=1}^{nth}\sum_{th=1}^{nth}(P_{th})+\sum_{t=1}^{t=24}\sum_{so=1}^{nso}\mu_{so}\cdot\left(\text{Pr}_{ss}^{so}\cdot Va_{ss}^{so}\cdot P_{so}^{\max}\right)+\sum_{t=1}^{t=24}\sum_{wi=1}^{nwi}\mu_{wi}\cdot\left(\text{Pr}_{sw}^{wi}\cdot Va_{sw}^{wi}\cdot P_{wi}^{\max}\right)\right]}\right. \\ & \left.\frac{+\underbrace{\sum_{bes}^{nbes}CS_{bes}^{inv}\cdot\mu_{bes}+\sum_{wi}^{nwi}CS_{wi}^{inv}\cdot\mu_{wi}+\sum_{so}^{nso}CS_{so}^{inv}\cdot\mu_{so}}_{\text{investment cost}}}{}\right\} \\ & +\underbrace{we_2\left\{\sum_{t=1}^{24}\sum_{th=1}^{nth}e_{th}^{CO_2}(P_{th})\right\}}_{CO_2\ \text{emission}} \\ & -we_3\underbrace{\left[\frac{\sum_{th=1}^{nth}H_{th}\cdot S_{th}^{\max}+\sum_{hes=1}^{nhes}H_{hes}\cdot S_{hes}\cdot\mu 1_{hes}+\sum_{w=1}^{nwi}H_{wi}\cdot S_{wi}^{\max}\cdot\mu 2_{wi}+\sum_{s=1}^{ns}H_{so}\cdot S_{so}^{\max}\cdot\mu 3_{so}}{\sum_{th=1}^{n}S_{th}^{\max}+\sum_{bes=1}^{nbes}S_{bes}\cdot\mu 1_{bes}+\sum_{wi=1}^{nwi}S_{wi}^{\max}\cdot\mu 2_{wi}+\sum_{s=1}^{ns}S_{so}^{\max}\cdot\mu 3_{so}}\right]}_{\text{system inertia}}\end{aligned} \tag{6.4}$$

$$we_1+we_2+we_3=1 \tag{6.5}$$

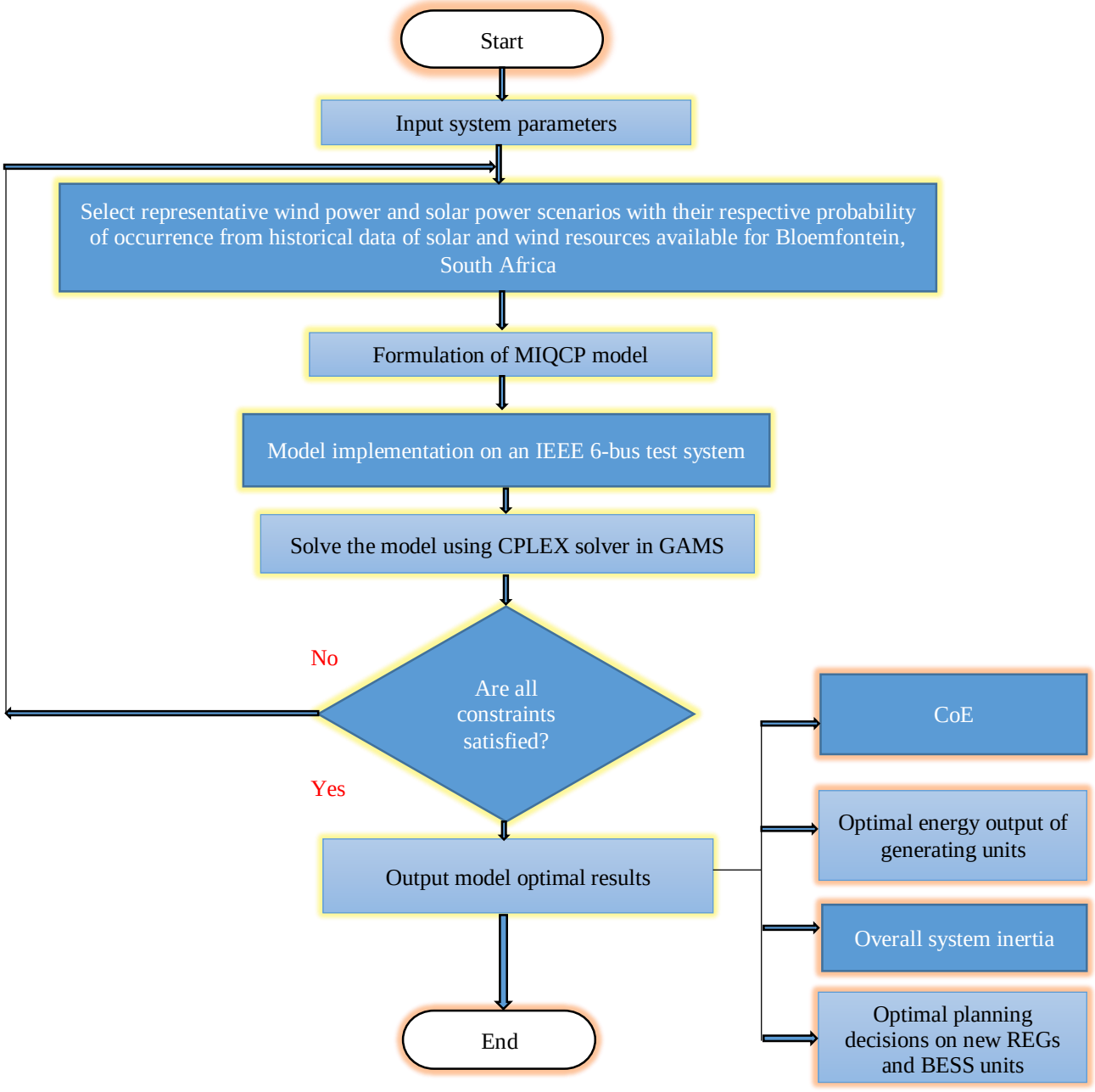

Figure 6.2: Flowchart of the proposed model

6.2.6 System constraints

The planning model was formulated subject to operational, security, and investment constraints.

6.2.6.1 Power balance constraints

The power balance constraint of the model was formulated based on the DC power flow equation as defined in Equation (6.6).

$$\sum_{n=1}^{nth} P_{th} + \sum_{so=1}^{nso} P_{so} + \sum_{wi=1}^{nwi} P_{wi} + \sum_{i} PXF_{i,j}^{+} - \sum_{i} PXF_{i,j}^{-} \geq \sum_{i} LOD_{i} \quad (6.6)$$

Where

PXF^{+} is the power flow into bus through transmission lines,

PXF^{-} is the power flow out of bus through transmission lines, and

LOD_i is the load demand at bus.

Equation (6.6) provides the power balance constraint, which states that the total active power supplied by all online thermal generators, solar PV plants, and wind turbines, plus the active power flowing into and out of bus through transmission lines, must be greater than or equal to the total load demand at bus.

6.2.6.2 Generation capacity limit constraints

Equations (6.7) to (6.13) define the capacity limit of the power system generators.

$$0 \leq P_{so} \leq \mu_{so} \cdot P_{so}^{\max} \quad \forall so \quad (6.7)$$

$$0 \leq P_{wi} \leq \mu_{wi} \cdot P_{wi}^{\max} \quad \forall wi \quad (6.8)$$

$$P_{th}^{\min} \leq P_{th} \leq P_{th}^{\max} \quad \forall th \quad (6.9)$$

$$P_{wi} = \Pr_{sw}^{wi} \cdot Va_{sw}^{wi} \cdot P_{wi}^{\max} \quad \forall wi \quad (6.10)$$

$$P_{so} = \Pr_{ss}^{so} \cdot Va_{ss}^{so} \cdot P_{so}^{\max} \quad \forall so \quad (6.11)$$

$$\sum_{sw=1}^{3} \Pr_{sw}^{wi} = 1 \quad \forall wi \quad (6.12)$$

$$\sum_{ss=1}^{3} \Pr_{ss}^{so} = 1 \quad \forall so \quad (6.13)$$

Equations (6.7) to (6.9) specify the minimum and maximum active power limits of the solar PV plants, wind turbines, and thermal generators respectively. Equation (6.10) provides the active power delivery of the wind turbines for all seasons and scenarios expressed in terms of probability of occurrence (wind power) per time $\Pr_{sw}^{wi}$, wind variability constant per time Va_{sw}^{wi}, and the installed capacity of the wind turbines $P_{wi}^{\max}$. Similarly, Equation (6.11) provides the active power delivery of the solar PV plants for all seasons and scenarios expressed in terms of probability of occurrence (solar power) per time for all scenarios $\Pr_{ss}^{so}$, solar variability constant per time Va_{ss}^{so}, and the installed capacity of the solar PV plants $P_{\max}^{so}$. Equation (6.12) states that the summation of all probabilities of the occurrence of wind power per time over all

scenarios must be equal to 1. Equation (6.13) states that the summation of all probabilities of the occurrence of solar power per hour over all scenarios must be equal to 1.

6.2.6.3 Transmission line constraints

Equation (6.14) defines the power flow limit of the transmission lines. Equation (6.15) provides the DC power flow equations for existing transmission lines, which is a function of the bus voltage angle at the sending θ_i^{se} and receiving θ_j^{re} ends of the transmission line, and the line susceptance $B_{i,j}^{l}$.

$$-PXF_{i,j}^{\max} \le PXF_{i,j} \le PXF_{i,j}^{\max} \tag{6.14}$$

$$PXF_{i,j} = B_{i,j}^{l}\left(\theta_i^{se} - \theta_j^{re}\right) \tag{6.15}$$

6.2.6.4 Phase angle constraints

$$\theta_{p,i}^{\min} \le \theta_{p,i} \le \theta_{p,i}^{\max} \tag{6.16}$$

$\theta_{p,i}^{\min}$ and $\theta_{p,i}^{\max}$ are the minimum and maximum permissible phase angles at bus respectively, and $\theta_{p,i}$ is the phase angle at bus. Equation (6.16) states that the voltage phase angle at bus must be maintained within specified upper and lower limits.

6.2.6.5 Inertia energy constraints

The inertia constraints are formulated as in Equations (6.17) to (6.20) to ensure the security of the modern grid [74], [157].

$$H_{\min} \le H_{eqv} \le H_{\max} \tag{6.17}$$

$$TEK = \sum S_{th}^{\max} \cdot H_{th} + \sum \mu_{wi} \cdot S_{wi}^{\max} \cdot H_{wi} + \sum \mu_{so} \cdot S_{so}^{\max} \cdot H_{so} + \sum \mu_{bes} \cdot S_{bes} \cdot H_{bes} \tag{6.18}$$

$$TEK_{\min} \ge S_o + S_1 \cdot f_{nadir}^{\max} + S_2 \cdot RoCoF^{\max} + S_3 \cdot \Delta P^{\max} \tag{6.19}$$

$$\sum S_{th}^{\max} \cdot H_{th} \ge y \cdot H_{\min}\left(\sum S_{th}^{\max} + \sum \mu_{wi} \cdot S_{wi}^{\max} + \sum \mu_{so} \cdot S_{so}^{\max} + \sum \mu_{bes} \cdot S_{bes}\right) \tag{6.20}$$

Equation (6.17) states that the overall system inertia constant of the power system should be within specified minimum and maximum values. Equation (6.18) provides the total inertia energy available from all online thermal generators, candidate wind turbines, solar PV plants, and BESS units. Equation (6.19) specifies the minimum inertia energy $TEK_{\min}$ in MWs required from all online generators and ESUs defined according to the maximum RoCoF

permissible $RoCoF^{\max}$ in Hz/s, maximum frequency nadir permissible in Hz $f_{nadir}^{\max}$, and maximum contingency level expected in the system $\Delta P^{\max}$ in MW. S_0, S_1, S_2 are constants with $S_0 = -106292.97, S_1 = 2222.9, S_2 = -46.82$, and $S_3 = 6.53$ as obtained from reference [157]. Equation (6.20) specifies the minimum proportion of synchronous inertia that should be available from the total inertia energy of the power system, which is defined using the minimum inertia limit set $H_{\min}$ and flexible constant y. The constant *y* was set at 0.3 for this study. All REGs and BESS used for this system were assumed to be capable of providing VI.

6.2.6.6 N-1 security constraints

In order to ensure the reliable operation of the power system during system contingency, security constraints were formulated as specified in Equations (6.21) to (6.23):

$$f_{\min} \le f \le f_{\max} \tag{6.21}$$

$$RoCoF^{\min} \ge RoCoF \le RoCoF^{\max} \tag{6.22}$$

$$\sum P_{th} + \sum \mu_{wi} \cdot P_{wi} + \sum \mu_{so} \cdot P_{so} + \sum \mu_{bes} \cdot P_{bes} - \Delta P^{\max} \ge \sum_i LOD_i \tag{6.23}$$

Equation (6.21) defines the maximum and minimum permissible frequency of the model. Equation (6.22) states that the RoCoF of the system should be maintained within the permissible RoCoF limit even during the loss of the largest generator $\Delta P^{\max}$, which is the most severe contingency case. Equation (6.23) states that the sum of active power from all online thermal generators, wind turbines, and solar PV plants must be greater than the total load demand at bus even during the loss of a thermal generator.

6.2.6.7 Reserve constraints

Power system operators must ensure that an adequate amount of reserve is available in the grid at all times for the reliable operation of the power system. In this model, reserve constraints were formulated as seen in Equations (6.24) to (6.27) to address the variability of load demand and REG power output. Additionally, the curtailed energy from wind turbines and solar PV plants also served as a reserve to provide frequency support to the grid during times of contingency.

$$\sum P_{th}^{res} + \sum \mu_{so} \cdot P_{so}^{res} + \sum \mu_{wi} \cdot P_{wi}^{res} + \sum \mu_{bes} \cdot P_{bes} \ge z \cdot \sum_i LOD_i^{peak} \tag{6.24}$$

$$P_{so}^{res} = P_{so}^{\max} - \left(Va_{ss}^{so} \cdot P_{so}^{\max}\right) \tag{6.25}$$

$$P_{wi}^{res} = P_{wi}^{\max} - \left(Va_{sw}^{wi} \cdot P_{wi}^{\max}\right) \tag{6.26}$$

$$P_{th}^{res} = P_{th}^{\max} - P_{th} \tag{6.27}$$

Equation (6.24) states that the sum of reserve energy from all connected thermal generators, solar PV plants, and wind turbines, plus the power delivery from BESS units, must be greater than or equal to a pre-specified fraction of the peak load demand at bus. A flexible parameter z is used to set the model reserve fraction at 5%. Equation (6.25) specifies the reserve constraint for solar PV plants defined in terms of its maximum capacity $P_{so}^{\max}$ and the time variability constant of the solar PV plant Va_{ss}^{so}. Similarly, Equation (6.26) specifies the reserve constraint for wind turbines defined in terms of maximum capacity $P_{wi}^{\max}$ and the time variability constant of the wind turbine Va_{wi}^{so}. Equation (6.27) defines the reserve constraint of the thermal generator given in terms of its maximum generator capacity $P_{th}^{\max}$ and operating capacity P_{th}.

6.2.6.8 Battery energy storage system (BESS) constraints

In order to mitigate the effects of renewable energy uncertainties, the use of BESS is desired [67], [158]. The operation of the BESS units used in this study was regulated according to Equations (6.28) to (6.31):

$$SoC_{bes}^{\min} \le SoC_{bes} \le SoC_{bes}^{\max} \tag{6.28}$$

$$\mu_b^{ch}, \mu_b^{dis} \in \{0,1\} \tag{6.29}$$

$$\mu_b^{ch} + \mu_b^{dis} \le 1 \tag{6.30}$$

$$\overline{SA_{bes}^{\max}} \le \left[\frac{H_{\min}(\sum S_{th} + \sum S_{wi} + \sum S_{so}) - \sum S_{wi} \cdot H_{wi} - \sum S_{so} \cdot H_{so}}{H_{bes} - H_{\min}}\right] \tag{6.31}$$

Equation (6.28) specifies the minimum and maximum SoC of the BESS. Equation (6.29) defines the binary variable used to regulate the charging and discharging of the BESS. Equation (6.30) prevents simultaneous charging and discharging of the BESS. Equation (6.31) provides the maximum sizing of the BESS that should be installed during the planning horizon. It is formulated based on the minimum inertia constant limit $H_{\min}$ set for the model.

6.2.6.9 Investment constraints

The investment constraints that regulate expansion decisions in the planning model are defined as in Equations (6.32) to (6.40).

$$\sum_{s=1}^{nso} \mu_{so} \cdot S_{so}^{\max} \leq \overline{SA_{so}^{\max}} \tag{6.32}$$

$$\sum_{w=1}^{nwi} \mu_{wi} \cdot S_{wi}^{\max} \leq \overline{SA_{wi}^{\max}} \tag{6.33}$$

$$\sum_{bes=1}^{nbes} \mu_{bes} \cdot S_{bes} \leq \overline{SA_{bes}^{\max}} \tag{6.34}$$

$$\sum_{s=1}^{nso} CS_{so} \cdot \mu_{so} + \sum_{w=1}^{nwi} CS_{wi} \cdot \mu_{wi} + \sum_{bes=1}^{nbes} CS_{bes} \cdot \mu_{bes} \leq \overline{MB} \tag{6.35}$$

$$\mu_{so} + \mu_{wi} \leq 1 \tag{6.36}$$

$$\sum \mu_{so} \leq nso \tag{6.37}$$

$$\sum \mu_{wi} \leq nwi \tag{6.38}$$

$$\sum \mu_{bes} \leq nbes \tag{6.39}$$

$$\mu_{so}, \mu_{wi}, \mu_{bes} \in \{0,1\} \tag{6.40}$$

Equations (6.32) to (6.34) specify the maximum capacity limit for candidate wind turbines, solar PV plants, and BESS to be built respectively. Equation (6.35) states that the total investment cost of candidate solar PV plants, wind turbines, and BESS must be less than the maximum monetary budget allocated $\overline{MB}$. Equation (6.36) prevents simulation installation of solar PV plants and wind turbines at bus. Equations (6.37) to (6.39) specify the maximum number of candidate solar PV plants, wind turbines, and BESS that can be selected for investment during the planning horizon. Equation (6.40) specifies the binary variables used to indicate investment decisions on candidate solar PV plants, wind turbines, and BESS respectively. The variable is 1 if a particular generation technology is selected for investment, and 0 if otherwise.

6.3 MODEL VALIDATION AND IMPLEMENTATION

In this section, the efficiency of the proposed model is validated on an IEEE 6-bus test system. The test system comprised three thermal generators, three candidate solar PV plants, three candidate wind turbines, three candidate BESS units, five load points, and seven existing transmission lines, as presented in Figure 6.3. The average and peak load demands of the test system were 760 MW and 800 MW respectively. However, in order to expand the power network based on anticipated increase in future load demand, the load at each bus was raised by half.

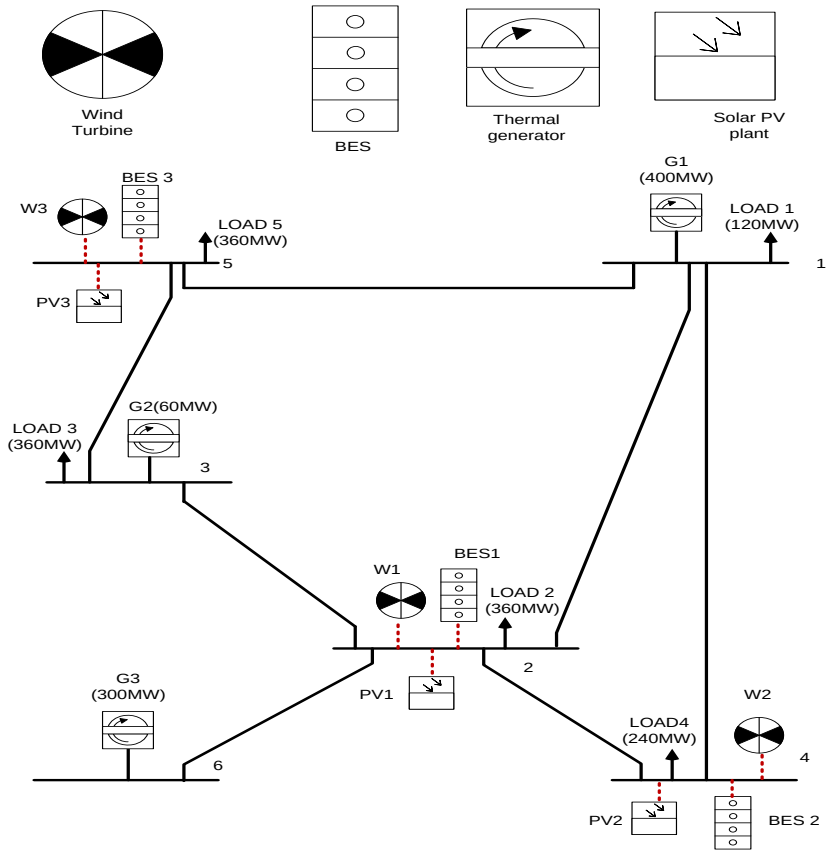

Red dash lines indicate candidate REGs and ESUs, while solid black lines indicate existing transmission lines and generating units.

Figure 6.3: IEEE 6-bus network with existing thermal generators and candidate REGs and ESUs

6.3.1 Model parameters

The model utilised meteorological data of the Mangaung Metropolitan Municipality in the Free State province of South Africa, which is located at latitude -29.095177◦N, longitude 26.176987◦E, and elevated 1 395 m (4 577 feet) above sea level. The 2019 historical data of wind speed and wind power used were obtained from Renewables.ninja, while the solar irradiance and solar power data used are available from the online Geographic Information System tool PVGIS. Figure 6.4 shows the solar resource map of the various provinces in South Africa, while the hourly scenarios with their respective probability of occurrence used for the study are presented in Table 6.2. The hourly scenarios were estimated from the RERs available at the study site. Tables 6.3 and 6.4 provide the modelling specifications of solar plants, wind turbines, BESS, and thermal generators used for the study, while Tables 6.5 and 6.6 indicate the transmission line parameters and modelling parameters used for the study.

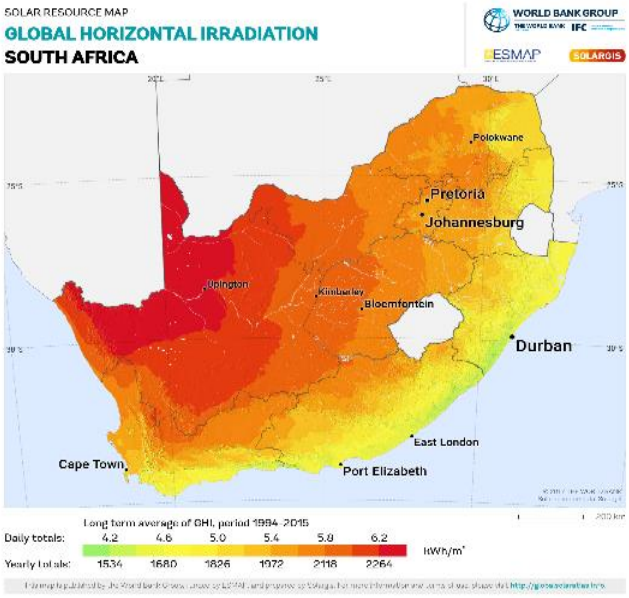

Figure 6.4: Solar resource map in South Africa [82]

Table 6.2: Occurrence probabilities of hourly scenarios of wind and solar power

Time	Occurrence probabilities of hourly scenarios for solar			Summer occurrence probabilities of hourly scenarios for wind speed		
	Low probability scenario	Medium probability scenario	High probability scenario	Low probability scenario	Medium probability scenario	High probability scenario
0:00	0.0000	0.0000	0.0000	0.59225	0.04798	0.32012
1:00	0.0000	0.0000	0.0000	0.60371	0.05891	0.33131
2:00	0.0000	0.0000	0.0000	0.61025	0.06474	0.33749
3:00	0.0000	0.0000	0.0000	0.60067	0.07072	0.33569
4:00	0.0261	0.0013	0.0137	0.57480	0.07971	0.32725
5:00	0.1164	0.0613	0.0888	0.51626	0.08668	0.30147
6:00	0.3615	0.1858	0.2737	0.34363	0.02723	0.18543
7:00	0.5955	0.3444	0.4700	0.31230	0.04252	0.13489
8:00	0.7644	0.4321	0.5983	0.40122	0.02278	0.18922
9:00	0.8661	0.4769	0.6715	0.49142	0.00770	0.24956
10:00	0.9117	0.4884	0.7001	0.54277	0.02439	0.28358
11:00	0.8751	0.4551	0.6651	0.58035	0.03336	0.30685
12:00	0.7829	0.3922	0.5875	0.59943	0.03482	0.31713
13:00	0.6661	0.3120	0.4890	0.59070	0.02669	0.30869
14:00	0.4700	0.1758	0.3229	0.53318	0.01158	0.27238
15:00	0.2454	0.1078	0.1766	0.51909	0.00687	0.25611
16:00	0.0505	0.0228	0.0367	0.53229	0.01961	0.25634
17:00	0.0000	0.0000	0.0000	0.56071	0.02173	0.26949
18:00	0.0000	0.0000	0.0000	0.58803	0.01864	0.28470
19:00	0.0000	0.0000	0.0000	0.59670	0.00697	0.29487
20:00	0.0000	0.0000	0.0000	0.59747	0.00949	0.30348
21:00	0.0000	0.0000	0.0000	0.58870	0.02600	0.30735
22:00	0.0000	0.0000	0.0000	0.58054	0.03919	0.30986
23:00	0.0000	0.0000	0.0000	0.58254	0.04785	0.31520

Table 6.3: Specification of candidate wind turbine, solar plant, and storage units

Bus	Generating technology	Average capacity factor (%)	Model	Capacity (MW)	Investment cost ($/yr)	Max. no. of units	Inertia constant	O&M cost ($/MWh)
2, 4, 5	Solar PV plant	22.9	Generic PV	100	8 446 720	3	2	-
2, 4, 5	Wind turbine	29.3	Vestas V90 2000	100	8 000 000	3	4	500
2, 4, 5	BESS	-	Lithium-ion	100	191 050	3	10	-

Table 6.4: Thermal generator parameters

Generator	Bus	Apparent power (MVA)	a_{th}	b_{th}	c_{th}	Carbon emission factor (tCO_2/MWh)	Capacity factor	Inertia constant
Gen. 1	1	500	0.12	14.80	89	1.135	0.8	8
Gen. 2	3	75	0.17	16.57	83	1.135	0.8	6
Gen. 3	6	375	0.15	15.55	100	1.135	0.8	7

Table 6.5: Transmission line parameters for IEEE 6-bus system

From bus	To bus	Resistance (p.u.)	Reactance (p.u.)	Susceptance (p.u.)	Max. line rating (MVA)
1	2	0.0026	0.0139	0.4611	175
1	5	0.0546	0.2112	0.0572	175
1	4	0.0218	0.0845	0.0229	175
2	4	0.0328	0.1267	0.0343	175
2	6	0.0497	0.1920	0.0520	175
2	3	0.0308	0.1190	0.0322	175
3	5	0.0023	0.0839	0.0281	175

Table 6.6: System modelling parameters

Parameters	Values
CO_2 penalty tax (human) ($/tCO_2$)	10
CO_2 penalty tax (ecosystem)	15
Maximum permissible frequency (Hz)	51
Minimum permissible frequency (Hz)	49
Nominal frequency (Hz)	50
System base power (MVA)	100
Minimum kinetic energy (MWs)	2 612
Minimum permissible overall inertia constant (s)	4
Maximum permissible overall inertia constant (s)	10
Minimum SoC of BESS	20%
Maximum SoC of BESS	80%
BESS efficiency (%)	95
Budget on new REGs and ESS ($10^6$$)	800
Minimum reserve limit set (%)	5

6.3.2 Model case study

The proposed model that considers system uncertainties and system inertia in GEP was validated using three different case studies:

- Case 1: Model formulation considering only cost, while REG uncertainties and system inertia were neglected.
- Case 2: Model formulation considering inertia, while REG uncertainties were neglected.
- Case 3 (optimal case): Model formulation considering both REG uncertainties and the inertia requirement of the grid.

6.4 RESULTS

This section presents the simulation results of the developed model in terms of renewable energy variability analysis and planning results.

6.4.1 Renewable energy resource (RER) variability analysis

The variability analysis of RERs at the study site is provided for the different seasons. South Africa has four distinct seasons: spring (September to November), summer (December to February), autumn (March to May), and winter (June to August).

Figure 6.5 shows the monthly wind power and solar irradiance variability. It is shown that January is the best-performing month for wind resources, while October is the best-performing month for solar resources. Figure 6.6 illustrates the seasonal variability of wind power, wind speed, solar irradiance, and solar power in Bloemfontein, South Africa. Figure 6.6 shows that both wind turbines and solar plants performed the best (highest RERs available) in spring relative to other seasons in 2019. The wind speed varied from 3.5 to 8.4 m/s, while the diffuse solar irradiance varied between 0 and 822.4 W/m^2 throughout the year.

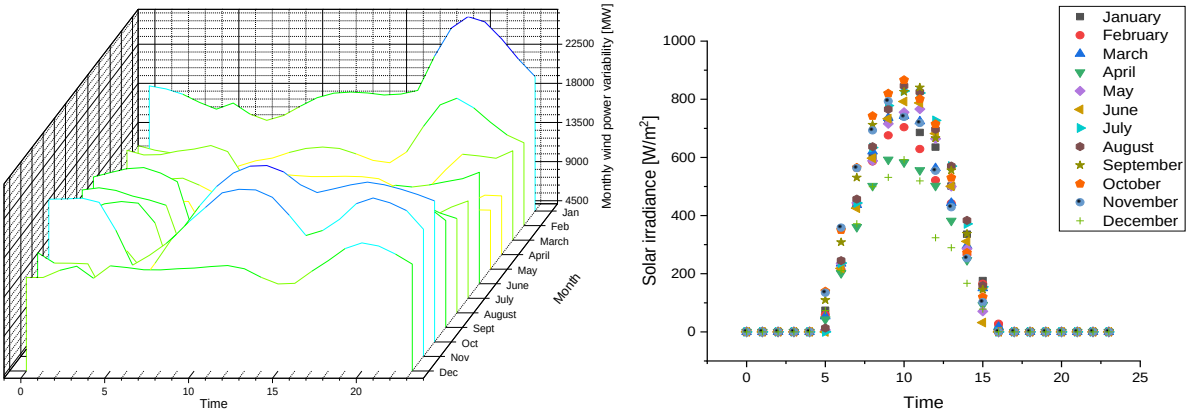

Figure 6.5: Monthly wind power and solar irradiance variability

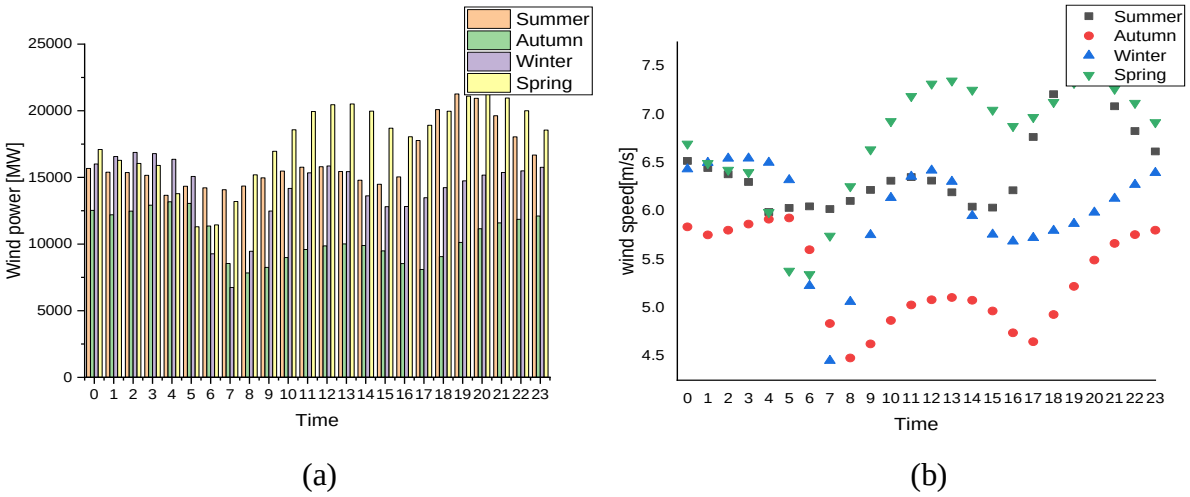

(a) (b)

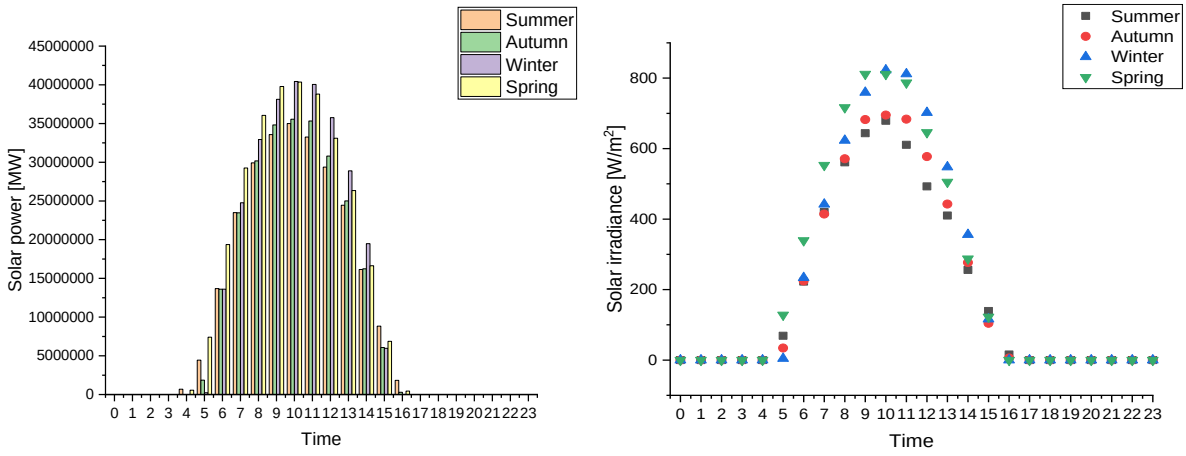

(c) (d)

Figure 6.6: Seasonal variability of (a) wind power, (b) wind speed, (c) solar power, and (d) solar irradiance

6.4.2 Model planning results

This sub-section presents and analyses the planning results in terms of total system cost, CoE, power generated from generators, and overall system inertia for the different case studies. The planning results for the different case studies are presented in Tables 6.7 to 6.9. Table 6.7 provides the detailed cost analysis of the different case studies, while Table 6.8 shows the total generated energy from all operating generators during the planning horizon. Table 6.9 lists the overall system inertia and CoE for the different case studies.

In Case 1, where only cost was considered, planning decisions favoured investment in three new solar PV plants and three BESS units. This case had the highest investment cost (2.5913E + 7$) due to inappropriate planning decisions made. On the other hand, in Cases 2 and 3, planning decisions favoured investment in three new wind turbine plants and three BESS units. Overall, the optimal planning decisions favoured the installation of new wind turbines over solar PV plants based on the RERs available in Bloemfontein, South Africa.

Furthermore, Tables 6.7 and 6.9 show that the total system cost (2.62E + 7$) and CoE (1614.50 $/MWh) were the lowest in Case 3 (optimal case), where the stochastic characteristics of REGs and system inertia were considered in the planning model, while the total system cost and CoE were the highest in Case 2, where renewable energy uncertainty was not considered. This shows that not considering renewable energy uncertainties in planning will give an inaccurate calculation of the system CoE, which can misguide power system operators.

In terms of overall system inertia, Table 6.9 shows that the overall system inertia in Cases 2 and 3 were higher (6.304s) than in Case 1 (5.875s) because of the consideration of system inertia in the planning model.

Furthermore, in terms of the total energy generated from all generators, it is seen that in Case 2, where renewable energy uncertainty was not considered, the total energy generated deviated by 1.49% from the true value obtained in Case 3, where renewable energy uncertainties were considered. Consequently, the CoE values in Case 2 deviated by 8.57% from the optimal case (Case 3). It can therefore be inferred that not considering renewable energy uncertainties can misinform system operators, which will lead to inappropriate generator scheduling.

Table 6.7: Cost analysis of the different case studies

Case study	Operational cost					
	Fuel cost ($)	Emission cost			O&M cost of wind turbine ($)	Total operational cost ($)
		Human emission cost ($)	Ecosystem emission cost ($)	Total emission cost ($)		
Case 1	1.5667E + 5	2.0348E + 5	3.0522E + 5	5.0871E + 5	-	6.65E + 0 5
Case 2	1.5667E + 5	2.0348E + 5	3.0522E + 5	5.0871E + 5	3.6000E + 6	4.27E + 06
Case 3	1.5667E + 5	2.0348E + 5	3.0522E + 5	5.0871E + 5	9.3429E + 5	1.60E + 06

Table 6.8: Total energy generated from all generators for all cases

Case study	Total energy from wind turbine (MWh)	Total energy from solar plant	Total energy from thermal generators	Total energy generated (MWh)
Case 1	-	1 648.800	14 342.400	15 991.2
Case 2	2 109.600	-	14 342.400	16 452
Case 3	1 868.580	-	143 42.400	16 210.98

Table 6.9: Overall inertia constant and CoE results

Case study	Overall inertia constant (s)	CoE ($/MWh)
Case 1	5.875	1 662.06
Case 2	6.304	1 752.88
Case 3	6.304	1 614.50

6.4.3 Discussion of results

The simulation results show the significant effects of considering renewable energy uncertainties on the model performance, as seen in Case 3. It is observed that the overall system cost decreased by 9%, while the CoE decreased by 7.8% relative to Case 2. On the other hand, considering system inertia in the model helped to improve the overall system inertia by 7.3% (from 5.875s to 6.304s). It is also observed that the optimal case (Case 3) was when both the system inertia and the RER uncertainties were considered in the planning model. This case (Case 3) achieved higher system inertia and obtained more accurate CoE values.

In addition, the renewable energy variability analysis revealed that wind turbines performed better than solar PV plants throughout the study year (2019). Also, based on the available renewable energy data used for the study, the REGs performed the best during spring (highest RERs available). Furthermore, the model analysis revealed that January was the best-performing month for wind resources, while October was the best-performing month for solar resources relative to other months. The wind speed of the study location varied from 3.5 to 8.4 m/s, while the diffuse solar irradiance varied between 0 and 822.4 W/m^2 throughout the year.

6.5 CONCLUSION

This chapter presented a novel GEP model that considered renewable energy uncertainties and the inertia requirement of the grid. Renewable energy uncertainties in the Mangaung Metropolitan Municipality, Free State province, South Africa, were used for the model analysis. The model was developed as an MILP model to minimise system CoE while maximising system inertia. The model was solved using CPLEX solver in GAMS while the intermittencies in wind speed and solar irradiance were addressed using a scenario-based approach. To validate the presented approach, the model was implemented on an IEEE 6-bus system and solved for the three different case studies. The key findings revealed the following:

- Considering both system inertia and renewable energy uncertainties (Case 3) gives appropriate planning results with a notable reduction in the total system cost (from 2.88E + 7$ to 2.62E + 7$) and CoE (from 1 752.88 $/MWh to 1 614.50 $/MWh), while the overall system inertia was enhanced (from 5.875s to 6.304s).
- Neglecting renewable energy uncertainties in power system planning may lead to suboptimal investment decisions, as seen in Cases 1 and 2.
- Ignoring renewable energy uncertainties in model design will give an inaccurate estimation of system parameters such as CoE, which will misdirect system operators and lead to inappropriate scheduling of power generators.
- Investment in REGs capable of providing VI to the grid is recommended in order to improve the overall inertia of the power grid.
- The renewable energy variability analysis revealed that wind turbines performed better than solar PV plants throughout the year (2019), while RERs were the highest during the spring season at the study location.
- January was revealed as the best-performing month for wind resources, while October was the best-performing month for solar resources at the study location.
- The developed model thus serves as an effective method for considering renewable energy uncertainties and system inertia in modern power planning, which will provide guidance to power system operators regarding the most feasible REG technologies to build and to help with the appropriate scheduling of REGs. In the future, the model will be expanded to consider seasonal variations in load demand, as well as system component failures.

CHAPTER 7: CONCLUSION AND FUTURE STUDIES

7.1 SUMMARY

The gradual shift towards a renewable energy-dominant grid is in line with the net zero goal by 2050. However, the resulting grid is associated with frequency challenges because of the lack of sufficient inertia from PV plants and modern (Type III and IV) wind turbines. This work thus focused on the development of a multi-objective optimisation model to mitigate frequency instability in a renewable energy-sourced power system. This was achieved by considering system inertia in the operational and planning optimisation model while integrating new REGs into the grid.

Chapter 2 presented a comprehensive literature review on the system inertia requirement in power systems. It further reviewed the various types of VI control strategies and topology in power systems. The review revealed that adequate system inertia is required in the modern renewable energy-dominant grid to ensure stability; it should thus be considered in power system operational and planning optimisation models.

Chapter 3 aimed to develop a new deterministic optimisation model to minimise cost and emissions while maximising system inertia in a renewable energy-sourced grid. This was achieved by developing an optimal planning model of REGs in modern power grids for enhanced system inertia. In this chapter, a new mathematical model for planning of new generators in the power system considering the inertia requirement of the grid was formulated. The model was designed to guide investment in REGs and ESS in such a way as to increase the overall system inertia of the grid and, by implication, improve the resilience of the grid, while minimising the system cost and CO_2 emissions. The model was developed as an MILP problem and solved using CPLEX solver in GAMS. The model was validated using a modified IEEE 9-bus test system. The model results revealed that the developed model achieved higher system inertia than the conventional model, which does not consider the inertia requirement of the grid in planning. This was achieved as investment in VI-equipped REGs and ESS is favoured for enhancing the overall inertia constant of the grid. The findings in this chapter support the hypothesis H_2 of the study (see Section 1.6), as higher inertia was achieved however at a higher investment cost and increased levelised CoE.

In Chapter 4, a joint GTEP model for improved modern power system resilience was discussed. The model developed in Chapter 3 was extended to consider transmission line expansion as more REGs are integrated into the grid. A new mathematical model that considers

system inertia in generation and transmission expansion was thus developed. The model was formulated as a mixed-integer quadratic constrained problem and solved using CPLEX solver in GAMS. To combat the declining inertia and mitigate frequency instability in the modern grid, appropriate inertia constraint was introduced into the planning model. An ERI was also introduced in the GTEP model in which power operators were incentivised if they are able to maintain a preset emission limit. The results revealed that the developed model achieved a 24% increase in system inertia and a 9.62% reduction in CO_2 emissions. This shows the effectiveness of ERI constraints in meeting the goal of emission reduction in the power system. The findings in this chapter support the hypotheses H_1 and H_3 of the study, as higher inertia achieved in case 3 improved the overall frequency stability of the grid, while reduced emission levels from the thermal power generators affected the power output of the generators.

Chapter 5 aimed to develop a new deterministic optimisation model considering HES and conducted a sensitivity assessment of the effect of economic incentives on the optimised model under various level of RES penetration into the grid. To achieve this, a sensitivity analysis of FiT in a joint GTEP considering the inertia requirement of the grid was conducted. This model was an extension of the model developed in Chapter 4. A novel FiT and inertia-integrated GTEP optimisation model was developed that considered the influence of economic incentives (FiT) on promoting the integration of REGs into the grid while meeting the inertia requirement of the grid. The model was developed as an MIQCP model to minimise the total system cost and CO_2 emissions, while maximising the overall system inertia and FiT incentives. The developed model was then implemented on an IEEE 6-bus test system and solved using CPLEX solver in GAMS. The model results revealed that the overall system inertia declined by 72.1% when the RES penetration level was increased from 25% to 100% with REGs and HES incapable of providing VI. The sensitivity analysis revealed that the higher the penetration of RES, the higher the total system cost and total FiT received; however, the fraction of FiT payments received relative to the total investment cost decreased after 50% RES penetration for the same FiT rate.

Chapter 6 aimed to develop an optimisation model that accounts for uncertainties parameters arising from renewable energy-sourced generators such as PV plants and wind turbines. To achieve this, a short-term renewable energy uncertainties and inertia consideration in power system generation expansion was carried out. This chapter extended the model developed in Chapter 5 to consider the effect of RER uncertainties and system inertia in the generation planning. The intermittencies of wind speed and solar irradiance were addressed using a scenario-based approach. The variability of RERs (solar irradiance and wind speed) at

Mangaung Metropolitan Municipality in the Free State province of South Africa was considered for the year 2019. The model was developed as an MILP model to minimise system CoE while maximising system inertia. The model was solved using CPLEX solver in GAMS and implemented on an IEEE 6-bus system. The model results revealed that considering both system inertia and renewable energy uncertainties (Case 3) provided appropriate planning results with a notable 9% reduction in the total system cost and a 7.9% reduction in CoE, while the overall system inertia was enhanced by 7.3%. Also, January was revealed as the best-performing month for wind resources, while October was revealed as the best-performing month for solar resources at the study location.

The aforementioned developed models were used in the thesis to achieve the aim of the study, which was to develop a multi-objective optimisation model to mitigate frequency instability in a renewable energy-sourced power system. In addition, the findings of the study support the hypotheses of the study (see Section 1.6), namely that achieving higher system inertia in the modern grid will increase the overall CoE while improving the frequency stability of the grid, and that reduced CO_2 emission levels are achieved at the expense of the power output (reduced) of the thermal generators.

7.2 CONCLUSION

The following are the conclusions of this research:

- Considering system inertia in a power system operational and planning optimisation model will help to achieve higher system inertia (a 24% increase) compared to the case where system inertia is not considered in the optimisation model when implemented on a standard IEEE 9-bus test system.
- Introducing ERI constraints or limits and emission penalty cost in a power system optimisation model can help to achieve a reduction in CO_2 emissions (a 9.62% reduction) compared to the case where ERI constraints or limits are not considered in the optimisation model when implemented on a standard IEEE 9-bus test system.
- The overall system inertia declined by 72.1% when the RES penetration level was increased from 25% to 100% with REGs and HES incapable of providing VI. The sensitivity analysis revealed that the higher the penetration of RES, the higher the total system cost and total FiT received; however, the fraction of FiT payments received relative to the total investment cost decreased after 50% RES penetration for the same FiT rate when implemented on a standard IEEE 6-bus test network.

- Considering both system inertia and renewable energy uncertainties in a power system operational and planning optimisation model provides appropriate planning results with a notable 9% reduction in the total system cost and a 7.9% reduction in CoE, while the overall system inertia is enhanced by 7.3% when implemented on a standard IEEE 6-bus test network.
- Neglecting system inertia in a power system planning and optimisation model could lead to frequency instability in the modern grid.
- Neglecting system inertia in power system planning could lead to inappropriate investment decisions in new REGs, and makes the modern grid vulnerable to frequency stability challenges.

7.3 SCIENTIFIC CONTRIBUTION

This research has extended the frontiers of power system operational and planning optimisation models by incorporating system inertia into power system operational and planning models.

The following are the specific scientific contributions of this study:

- The development of a novel mathematical model for planning of new generators in the power system considering the inertia requirement of the grid.
- The development of a new GTEP model that minimises the system cost and CO_2 emissions while maximising the overall system inertia of the modern grid.
- The development of a novel FiT and inertia-integrated GTEP optimisation model that minimises the total system cost and CO_2 emissions, while maximising the overall system inertia and FiT incentives.
- The development of a novel scenario-based MILP model that considers the variability of RERs while minimising system CoE and maximising the overall system inertia.

7.4 SUGGESTIONS FOR FUTURE RESEARCH

The following are suggestions for future research:

- The developed model can be applied to a real-time power grid such as the South African power grid.
- The developed models can be extended to a large IEEE test system such as the IEEE 118-test system.

- The dynamic response of the developed model can be analysed using an advanced power system simulator such as Dlgsilent PowerFactory or Electrical Transient Analyzer Program (ETAP).
- The model analysis can be conducted using other objective optimisation techniques to further validate the model results.
- The model can also be expanded to consider seasonal variations in load demand, as well as system component failures.

REFERENCES

[1] Ulbig, A., Borsche, T.S. & Andersson, G. 2014. Impact of low rotational inertia on power system stability and operation. *IFAC Proceedings*, 47(3):7290-7297.

[2] Muhssin, M.T., Cipcigan, L.M., Obaid, Z.A. & Al-Ansari, W.F. 2017. A novel adaptive deadbeat-based control for load frequency control of low inertia system in interconnected zones north and south of Scotland. *International Journal of Electrical Power & Energy Systems*, 89:52-61.

[3] Chen, L., Wang, X., Min, Y., Li, G., Wang, L., Qi, J. & Xu, F. 2020. Modelling and investigating the impact of asynchronous inertia of induction motor on power system frequency response. *International Journal of Electrical Power & Energy Systems*, 117:105708.

[4] Johnson, S.C., Rhodes, J.D. & Webber, M.E. 2020. Understanding the impact of non-synchronous wind and solar generation on grid stability and identifying mitigation pathways. *Applied Energy*, 262:114492.

[5] Nycander, E., Söder, L., Olauson, J. & Eriksson, R. 2020. Curtailment analysis for the Nordic power system considering transmission capacity, inertia limits and generation flexibility. *Renewable Energy*, 152:942-960.

[6] Ratnam, K.S., Palanisamy, K. & Yang, G. 2020. Future low-inertia power systems: Requirements, issues, and solutions – A review. *Renewable and Sustainable Energy Reviews*, 124:109773.

[7] Akram, U., Nadarajah, M., Shah, R. & Milano, F. 2020. A review on rapid responsive energy storage technologies for frequency regulation in modern power systems. *Renewable and Sustainable Energy Reviews*, 120:109626.

[8] Ulbig, A., Borsche, T.S. & Andersson, G. 2015. Analyzing rotational inertia, grid topology and their role for power system stability. *IFAC-PapersOnLine*, 48(30):541-547.

[9] Fini, M.H. & Golshan, M.E.H. 2018. Determining optimal virtual inertia and frequency control parameters to preserve the frequency stability in islanded microgrids with high penetration of renewables. *Electric Power Systems Research*, 154:13-22.

[10] Rezkalla, M., Zecchino, A., Martinenas, S., Prostejovsky, A.M. & Marinelli, M. 2018. Comparison between synthetic inertia and fast frequency containment control based on single phase EVs in a microgrid. *Applied Energy*, 210:764-775.

[11] Nikolic, D. & Negnevitsky, M. 2019. Adding inertia to isolated power systems for 100% renewable operation. *Energy Procedia*, 159:460-465.

[12] Fernández-Guillamón, A., Gómez-Lázaro, E., Muljadi, E. & Molina-García, Á. 2019. Power systems with high renewable energy sources: A review of inertia and frequency control strategies over time. *Renewable and Sustainable Energy Reviews*, 115:109369.

[13] Wilson, D., Yu, J., Al-Ashwal, N., Heimisson, B. & Terzija, V. 2019. Measuring effective area inertia to determine fast-acting frequency response requirements. *International Journal of Electrical Power & Energy Systems*, 113:1-8.

[14] Rouse, J.P., Garvey, S.D., Cárdenas, B. & Davenne, T.R. 2018. A series hybrid "real inertia" energy storage system. *Journal of Energy Storage*, 20:1-15.

[15] Karbouj, H., Rather, Z.H., Flynn, D. & Qazi, H.W. 2019. Non-synchronous fast frequency reserves in renewable energy integrated power systems: A critical review. *International Journal of Electrical Power & Energy Systems*, 106:488-501.

[16] Zhang, X., Zhu, Z., Fu, Y. & Li, L. 2020. Optimized virtual inertia of wind turbine for rotor angle stability in interconnected power systems. *Electric Power Systems Research*, 180:106157.

[17] Fichter, T., Soria, R., Szklo, A., Schaeffer, R. & Lucena, A.F. 2017. Assessing the potential role of concentrated solar power (CSP) for the northeast power system of Brazil using a detailed power system model. *Energy*, 121:695-715.

[18] Mahmood, M., Traverso, A., Traverso, A.N., Massardo, A.F., Marsano, D. & Cravero, C. 2018. Thermal energy storage for CSP hybrid gas turbine systems: Dynamic modelling and experimental validation. *Applied Energy*, 212:1240-1251.

[19] Gauché, P., Rudman, J., Mabaso, M., Landman, W.A., Von Backström, T.W. & Brent, A.C. 2017. System value and progress of CSP. *Solar Energy*, 152:106-139.

[20] Samanta, S., Mishra, J.P. & Roy, B.K. 2019. Implementation of a virtual inertia control for inertia enhancement of a DC microgrid under both grid connected and isolated operation. *Computers & Electrical Engineering*, 76:283-298.

[21] Yang, L., Hu, Z., Xie, S., Kong, S. & Lin, W. 2019. Adjustable virtual inertia control of supercapacitors in PV-based AC microgrid cluster. *Electric Power Systems Research*, 173:71-85.

[22] Zhang, Y., Zhang, X., Qian, T. & Hu, R. 2020. Modeling and simulation of a passive variable inertia flywheel for diesel generator. *Energy Reports*, 6:58-68.

[23] Anuta, O.H., Taylor, P., Jones, D., McEntee, T. & Wade, N. 2014. An international review of the implications of regulatory and electricity market structures on the emergence of grid scale electricity storage. *Renewable and Sustainable Energy Reviews*, 38:489-508.

[24] Rehimi, S., Mirzaei, R. & Bevrani, H. 2020. Interconnected microgrids frequency response model: An inertia-based approach. *Energy Reports*, 6:179-186.

[25] Kim, M.J., Kim, T.S., Flores, R.J. & Brouwer, J. 2020. Neural-network-based optimization for economic dispatch of combined heat and power systems. *Applied Energy*, 265:114785.

[26] Faridpak, B., Farrokhifar, M., Murzakhanov, I. & Safari, A. 2020. A series multi-step approach for operation Co-optimization of integrated power and natural gas systems. *Energy*, 204:117897.

[27] Lok, W.J., Ng, L.Y. & Andiappan, V. 2020. Optimal decision-making for combined heat and power operations: A fuzzy optimisation approach considering system flexibility, environmental emissions, start-up and shutdown costs. *Process Safety and Environmental Protection*, 137:312-327.

[28] Jaszczur, M., Hassan, Q., Palej, P. & Abdulateef, J. 2020. Multi-objective optimisation of a micro-grid hybrid power system for household application. *Energy*, 202:117738.

[29] Mohammadi, H. & Mohammadi, M. 2020. Optimization of the micro combined heat and power systems considering objective functions, components and operation strategies by an integrated approach. *Energy Conversion and Management*, 208:112610.

[30] Delgado-Antillón, C.P. & Domínguez-Navarro, J.A. 2018. Probabilistic siting and sizing of energy storage systems in distribution power systems based on the islanding feature. *Electric Power Systems Research*, 155:225-235.

[31] Panda, A., Mishra, U. & Aviso, K.B. 2020. Optimizing hybrid power systems with compressed air energy storage. *Energy*, 205:117962.

[32] Shi, X., Dini, A., Shao, Z., Jabarullah, N.H. & Liu, Z. 2019. Impacts of photovoltaic/wind turbine/microgrid turbine and energy storage system for bidding model in power system. *Journal of Cleaner Production*, 226:845-857.

[33] Ravikumar, S., Vennila, H. & Deepak, R. 2020. Hybrid power generation system with total harmonic distortion minimization using improved rider optimization algorithm: Analysis on converters. *Journal of Power Sources*, 459:228025.

[34] Kusakana, K. 2019. Optimal electricity cost minimization of a grid-interactive Pumped Hydro Storage using ground water in a dynamic electricity pricing environment. *Energy Reports*, 5:159-169.

[35] Koko, S.P., Kusakana, K. & Vermaak, H.J. 2018. Optimal power dispatch of a grid-interactive micro-hydrokinetic-pumped hydro storage system. *Journal of Energy Storage*, 17:63-72.

[36] Giglmayr, S., Brent, A.C., Gauché, P. & Fechner, H. 2015. Utility-scale PV power and energy supply outlook for South Africa in 2015. *Renewable Energy*, 83:779-785.

[37] Ayamolowo, O.J., Manditereza, P. & Kusakana, K. 2022. An overview of inertia requirement in modern renewable energy sourced grid: Challenges and way forward. *Journal of Electrical Systems and Information Technology*, 9(1):11.

[38] Makolo, P., Zamora, R. & Lie, T.T. 2021. The role of inertia for grid flexibility under high penetration of variable renewables: A review of challenges and solutions. *Renewable and Sustainable Energy Reviews*, 147:111223.

[39] Mimica, M., Dominković, D.F., Capuder, T. & Krajačić, G. 2021. On the value and potential of demand response in the smart island archipelago. *Renewable Energy*, 176:153-168.

[40] Ariyaratna, P., Muttaqi, K.M. & Sutanto, D. 2018. A novel control strategy to mitigate slow and fast fluctuations of the voltage profile at common coupling Point of rooftop solar PV unit with an integrated hybrid energy storage system. *Journal of Energy Storage*, 20:409-417.

[41] Ayamolowo, O.J., Manditereza, P.T. & Kusakana, K. 2022. Optimal planning of Renewable energy generators in modern power grid for enhanced system inertia. *Technology and Economics of Smart Grids and Sustainable Energy*, 7(1):33.

[42] Mallemaci, V., Mandrile, F., Rubino, S., Mazza, A., Carpaneto, E. & Bojoi, R. 2021. A comprehensive comparison of Virtual Synchronous Generators with focus on virtual inertia and frequency regulation. *Electric Power Systems Research*, 201:107516.

[43] Tamrakar, U., Shrestha, D., Maharjan, M., Bhattarai, B.P., Hansen, T.M. & Tonkoski, R. 2017. Virtual inertia: Current trends and future directions. *Applied Sciences*, 7(7):654.

[44] Del Giudice, D., Brambilla, A., Grillo, S. & Bizzarri, F. 2021. Effects of inertia, load damping and dead-bands on frequency histograms and frequency control of power systems. *International Journal of Electrical Power & Energy Systems*, 129:106842.

[45] Cheng, Z., Li, Z., Li, S., Gao, J., Si, J., Das, H.S. & Dong, W. 2020. A novel cascaded control to improve stability and inertia of parallel buck-boost converters in DC microgrid. *International Journal of Electrical Power & Energy Systems*, 119:105950.

[46] Daadaa, M., Séguin, S., Demeester, K. & Anjos, M.F. 2021. An optimization model to maximize energy generation in short-term hydropower unit commitment using efficiency points. *International Journal of Electrical Power & Energy Systems*, 125:106419.

[47] Hou, W. & Wei, H. 2021. Data-driven robust day-ahead unit commitment model for hydro/thermal/wind/photovoltaic/nuclear power systems. *International Journal of Electrical Power & Energy Systems*, 125:106427.

[48] Feng, Z.K., Niu, W.J., Wang, W.C., Zhou, J.Z. & Cheng, C.T. 2019. A mixed integer linear programming model for unit commitment of thermal plants with peak shaving operation aspect in regional power grid lack of flexible hydropower energy. *Energy*, 175:618-629.

[49] Moretti, L., Martelli, E. & Manzolini, G. 2020. An efficient robust optimization model for the unit commitment and dispatch of multi-energy systems and microgrids. *Applied Energy*, 261:113859.

[50] Lin, Z., Chen, H., Wu, Q., Huang, J., Li, M. & Ji, T. 2021. A data-adaptive robust unit commitment model considering high penetration of wind power generation and its enhanced uncertainty set. *International Journal of Electrical Power & Energy Systems*, 129:106797.

[51] Resener, M., Haffner, S., Pereira, L.A., Pardalos, P.M. & Ramos, M.J. 2019. A comprehensive MILP model for the expansion planning of power distribution systems – Part I: Problem formulation. *Electric Power Systems Research*, 170:378-384.

[52] Koltsaklis, N.E. & Dagoumas, A.S. 2018. Incorporating unit commitment aspects to the European electricity markets algorithm: An optimization model for the joint clearing of energy and reserve markets. *Applied Energy*, 231:235-258.

[53] Gbadamosi, S.L. & Nwulu, N.I. 2020. A multi-period composite generation and transmission expansion planning model incorporating renewable energy sources and demand response. *Sustainable Energy Technologies and Assessments*, 39:100726.

[54] Eghbali, N., Hakimi, S.M., Hasankhani, A., Derakhshan, G. & Abdi, B. 2022. Stochastic energy management for a renewable energy based microgrid considering battery, hydrogen storage, and demand response. *Sustainable Energy, Grids and Networks*, 30:100652.

[55] Jiang, T., Yuan, C., Zhang, R., Bai, L., Li, X., Chen, H. & Li, G. 2021. Exploiting flexibility of combined-cycle gas turbines in power system unit commitment with natural gas transmission constraints and reserve scheduling. *International Journal of Electrical Power & Energy Systems*, 125:106460.

[56] Đaković, J., Krpan, M., Ilak, P., Baškarad, T. & Kuzle, I. 2020. Impact of wind capacity share, allocation of inertia and grid configuration on transient RoCoF: The case of the Croatian power system. *International Journal of Electrical Power & Energy Systems*, 121:106075.

[57] Yamchi, H.B., Safari, A. & Guerrero, J.M. 2021. A multi-objective mixed integer linear programming model for integrated electricity-gas network expansion planning considering the impact of photovoltaic generation. *Energy*, 222:119933.

[58] Gonzato, S., Bruninx, K. & Delarue, E. 2021. Long term storage in generation expansion planning models with a reduced temporal scope. *Applied Energy*, 298:117168.

[59] Maluenda, B., Negrete-Pincetic, M., Olivares, D.E. & Lorca, Á. 2018. Expansion planning under uncertainty for hydrothermal systems with variable resources. *International Journal of Electrical Power & Energy Systems*, 103:644-651.

[60] Firoozjaee, M.G. & Sheikh-El-Eslami, M.K. 2021. A hybrid resilient static power system expansion planning framework. *International Journal of Electrical Power & Energy Systems*, 133:107234.

[61] Larsen, M. & Sauma, E. 2021. Economic and emission impacts of energy storage systems on power-system long-term expansion planning when considering multi-stage decision processes. *Journal of Energy Storage*, 33:101883.

[62] Qorbani, M. & Amraee, T. 2021. Long term transmission expansion planning to improve power system resilience against cascading outages. *Electric Power Systems Research*, 192:106972.

[63] Pereira, A. & Sauma, E. 2020. Power systems expansion planning with time-varying CO_2 tax. *Energy Policy*, 144:111630.

[64] Iakubovskii, D., Krupenev, D., Komendantova, N. & Boyarkin, D. 2021. A model for power shortage minimization in electric power systems given constraints on controlled sections. *Energy Reports*, 7:4577-4586.

[65] De Lima, T.D., Tabares, A., Arias, N.B. & Franco, J.F. 2021. Investment & generation costs vs CO_2 emissions in the distribution system expansion planning: A multi-objective stochastic programming approach. *International Journal of Electrical Power & Energy Systems*, 131:106925.

[66] Pinto, R.S., Unsihuay-Vila, C. & Tabarro, F.H. 2021. Coordinated operation and expansion planning for multiple microgrids and active distribution networks under uncertainties. *Applied Energy*, 297:117108.

[67] Taghikhani, M.A. 2021. Renewable resources and storage systems stochastic multi-objective optimal energy scheduling considering load and generation uncertainties. *Journal of Energy Storage*, 43:103293.

[68] Abdelmalak, M. & Benidris, M. 2021. A polynomial chaos-based approach to quantify uncertainties of correlated renewable energy sources in voltage regulation. *IEEE Transactions on Industry Applications*, 57(3):2089-2097.

[69] Moarefdoost, M.M., Lamadrid, A.J. & Zuluaga, L.F. 2016. A robust model for the ramp-constrained economic dispatch problem with uncertain renewable energy. *Energy Economics*, 56:310-325.

[70] Liu, Z., Cui, Y., Wang, J., Yue, C., Agbodjan, Y.S. & Yang, Y. 2022. Multi-objective optimization of multi-energy complementary integrated energy systems considering load prediction and renewable energy production uncertainties. *Energy*, 254:124399.

[71] Adefarati, T. & Bansal, R.C. 2017. Reliability and economic assessment of a microgrid power system with the integration of renewable energy resources. *Applied Energy*, 206:911-933.

[72] Yan, R., Wang, J., Wang, J., Tian, L., Tang, S., Wang, Y., Zhang, J., Cheng, Y. & Li, Y. 2022. A two-stage stochastic-robust optimization for a hybrid renewable energy CCHP system considering multiple scenario-interval uncertainties. *Energy*, 247:123498.

[73] Hakimi, S.M., Hasankhani, A., Shafie-khah, M. & Catalão, J.P. 2021. Stochastic planning of a multi-microgrid considering integration of renewable energy resources and real-time electricity market. *Applied Energy*, 298:117215.

[74] Curto, D., Favuzza, S., Franzitta, V., Guercio, A., Navia, M.A.N., Telaretti, E. & Zizzo, G. 2022. Grid stability improvement using synthetic inertia by battery energy storage systems in small islands. *Energy*, 254:124456.

[75] Shang, X., Li, Z., Zheng, J. & Wu, Q.H. 2019. Equivalent modeling of active distribution network considering the spatial uncertainty of renewable energy resources. *International Journal of Electrical Power & Energy Systems*, 112:83-91.

[76] Sreenivasulu, G., Sahoo, N.C. & Balakrishna, P. 2022. A coordinated stochastic dispatch model for hybrid energy markets with renewable energy uncertainties using moth flame optimization. *Energy Systems*, 2022:1-41.

[77] Zaman, F., Elsayed, S.M., Ray, T. & Sarker, R.A. 2016. Evolutionary algorithms for power generation planning with uncertain renewable energy. *Energy*, 112:408-419.

[78] Ayamolowo, O.J., Manditereza, P.T. & Kusakana, K. 2022. South Africa power reforms: The path to a dominant renewable energy-sourced grid. *Energy Reports*, 8:1208-1215.

[79] Kazemi, M. & Ansari, M.R. 2022. An integrated transmission expansion planning and battery storage systems placement: A security and reliability perspective. *International Journal of Electrical Power & Energy Systems*, 134:107329.

[80] Zheng, L., Hu, W., Lu, Q. & Min, Y. 2015. Optimal energy storage system allocation and operation for improving wind power penetration. *IET Generation, Transmission & Distribution*, 9(16):2672-2678.

[81] Li, Y., Feng, B., Wang, B. & Sun, S. 2022. Joint planning of distributed generations and energy storage in active distribution networks: A Bi-Level programming approach. *Energy*, 245:123226.

[82] Soroudi, A. & Afrasiab, M. 2012. Binary PSO-based dynamic multi-objective model for distributed generation planning under uncertainty. *IET Renewable Power Generation*, 6(2):67-78.

[83] Ali, Z.M., Aleem, S.H.A., Omar, A.I. & Mahmoud, B.S. 2022. Economical-environmental-technical operation of power networks with high penetration of renewable energy systems using multi-objective coronavirus herd immunity algorithm. *Mathematics*, 10(7):1201.

[84] Omar, A.I., Ali, Z.M., Al-Gabalawy, M., Abdel Aleem, S.H. & Al-Dhaifallah, M. 2020. Multi-objective environmental economic dispatch of an electricity system considering integrated natural gas units and variable renewable energy sources. *Mathematics*, 8(7):1100.

[85] Evangeline, S.I. & Rathika, P. 2021. A real-time multi-objective optimization framework for wind farm integrated power systems. *Journal of Power Sources*, 498:229914.

[86] El Sehiemy, R.A., Selim, F., Bentouati, B. & Abido, M.A. 2020. A novel multi-objective hybrid particle swarm and salp optimization algorithm for technical-economical-environmental operation in power systems. *Energy*, 193:116817.

[87] Ayamolowo, O.J., Manditereza, P.T. & Kusakana, K. 2020. Exploring the gaps in renewable energy integration to grid. *Energy Reports*, 6:992-999.

[88] Vetoshkin, L. & Müller, Z. 2021. A comparative analysis of a power system stability with virtual inertia. *Energies*, 14(11):3277.

[89] Wu, Y.K., Huang, C.L. & Chen, S.L. 2021. Effect of system inertia on frequency response in power systems with renewable energy integration. In *2021 IEEE International Future Energy Electronics Conference (IFEEC)*. New Jersey: IEEE. pp. 1-6.

[90] Mudaheranwa, E., Sonder, H.B., Cipcigan, L. & Ugalde-Loo, C.E. 2022. Estimation of Rwanda's power system inertia as input for long-term dynamic frequency response regulation planning. *Electric Power Systems Research*, 207:107853.

[91] Mehigan, L., Al Kez, D., Collins, S., Foley, A., Ó'Gallachóir, B. & Deane, P. 2020. Renewables in the European power system and the impact on system rotational inertia. *Energy*, 203:117776.

[92] Wogrin, S., Tejada-Arango, D., Delikaraoglou, S. & Botterud, A. 2020. Assessing the impact of inertia and reactive power constraints in generation expansion planning. *Applied Energy*, 280:115925.

[93] Lee, Y.Y. & Baldick, R. 2013. A frequency-constrained stochastic economic dispatch model. *IEEE Transactions on Power Systems*, 28(3):2301-2312.

[94] Safari, A., Farrokhifar, M., Shahsavari, H. & Hosseinnezhad, V. 2021. Stochastic planning of integrated power and natural gas networks with simplified system frequency constraints. *International Journal of Electrical Power & Energy Systems*, 132:107144.

[95] Ramkumar, A. & Rajesh, K. 2021. Generation expansion planning with wind power plant using DE algorithm. *Materials Today: Proceedings*, 80(3):2109-2114.

[96] Tso, W.W., Demirhan, C.D., Heuberger, C.F., Powell, J.B. & Pistikopoulos, E.N. 2020. A hierarchical clustering decomposition algorithm for optimizing renewable power systems with storage. *Applied Energy*, 270:115190.

[97] Li, G., Chen, Y., Luo, A. & Wang, Y. 2021. An inertia phase locked loop for suppressing sub-synchronous resonance of renewable energy generation system under weak grid. *IEEE Transactions on Power Systems*, 36(5):4621-4631.

[98] Elmetwaly, A.H., ElDesouky, A.A., Omar, A.I. & Saad, M.A. 2022. Operation control, energy management, and power quality enhancement for a cluster of isolated microgrids. *Ain Shams Engineering Journal*, 13(5):101737.

[99] Al-Gabalawy, M., Hosny, N.S., Dawson, J.A. & Omar, A.I. 2021. State of charge estimation of a Li-ion battery based on extended Kalman filtering and sensor bias. *International Journal of Energy Research*, 45(5):6708-6726.

[100] Fitiwi, D.Z., Lynch, M. & Bertsch, V. 2020. Enhanced network effects and stochastic modelling in generation expansion planning: Insights from an insular power system. *Socio-Economic Planning Sciences*, 71:100859.

[101] Scott, I.J., Carvalho, P.M., Botterud, A. & Silva, C.A. 2019. Clustering representative days for power systems generation expansion planning: Capturing the effects of variable renewables and energy storage. *Applied Energy*, 253:113603.

[102] Vatanpour, M. & Yazdankhah, A.S. 2018. The impact of energy storage modeling in coordination with wind farm and thermal units on security and reliability in a stochastic unit commitment. *Energy*, 162:476-490.

[103] Li, Y., Dai, M., Hao, S., Qiu, G., Li, G., Xiao, G. & Liu, D. 2021. Optimal generation expansion planning model of a combined thermal–wind–PV power system considering multiple boundary conditions: A case study in Xinjiang, China. *Energy Reports*, 7:515-522.

[104] Ndiritu, S.W. & Engola, M.K. 2020. The effectiveness of feed-in-tariff policy in promoting power generation from renewable energy in Kenya. *Renewable Energy*, 161:593-605.

[105] Makolo, P., Oladeji, I., Zamora, R. & Lie, T.T. 2021. Data-driven inertia estimation based on frequency gradient for power systems with high penetration of renewable energy sources. *Electric Power Systems Research*, 195:107171.

[106] Rahman, M.M., Oni, A.O., Gemechu, E. & Kumar, A., 2021. The development of techno-economic models for the assessment of utility-scale electro-chemical battery storage systems. *Applied Energy*, 283:116343.

[107] Astriani, Y., Shafiullah, G.M. & Shahnia, F. 2021. Incentive determination of a demand response program for microgrids. *Applied Energy*, 292:116624.

[108] Machlev, R., Chowdhury, N.R., Belikov, J. & Levron, Y. 2022. Distributed storage placement policy for minimizing frequency deviations: A combinatorial optimization approach based on enhanced cross-entropy method. *International Journal of Electrical Power & Energy Systems*, 134:107332.

[109] Ayamolowo, O.J., Manditereza, P.T. & Kusakana, K. 2021. Investigating the potential of solar trackers in renewable energy integration to grid. *Journal of Physics: Conference Series*, 2022(1):012031.

[110] Shair, J., Li, H., Hu, J. & Xie, X. 2021. Power system stability issues, classifications and research prospects in the context of high-penetration of renewables and power electronics. *Renewable and Sustainable Energy Reviews*, 145:111111.

[111] Mandal, R. & Chatterjee, K. 2021. Virtual inertia emulation and RoCoF control of a microgrid with high renewable power penetration. *Electric Power Systems Research*, 194:107093.

[112] Paturet, M., Markovic, U., Delikaraoglou, S., Vrettos, E., Aristidou, P. & Hug, G. 2020. Stochastic unit commitment in low-inertia grids. *IEEE Transactions on Power Systems*, 35(5):3448-3458.

[113] Heylen, E., Teng, F. & Strbac, G. 2021. Challenges and opportunities of inertia estimation and forecasting in low-inertia power systems. *Renewable and Sustainable Energy Reviews*, 147:111176.

[114] Magdy, G., Ali, H. & Xu, D. 2021. A new synthetic inertia system based on electric vehicles to support the frequency stability of low-inertia modern power grids. *Journal of Cleaner Production*, 297:126595.

[115] Markovic, U., Stanojev, O., Vrettos, E., Aristidou, P. & Hug, G. 2019. Understanding stability of low-inertia systems.

[116] Yap, K.Y., Lim, J.M.Y. & Sarimuthu, C.R. 2021. A novel adaptive virtual inertia control strategy under varying irradiance and temperature in grid-connected solar power system. *International Journal of Electrical Power & Energy Systems*, 132:107180.

[117] Vasudevan, K.R., Ramachandaramurthy, V.K., Venugopal, G., Ekanayake, J.B. & Tiong, S.K. 2021. Variable speed pumped hydro storage: A review of converters, controls and energy management strategies. *Renewable and Sustainable Energy Reviews*, 135:110156.

[118] Javed, M.S., Ma, T., Jurasz, J. & Amin, M.Y. 2020. Solar and wind power generation systems with pumped hydro storage: Review and future perspectives. *Renewable Energy*, 148:176-192.

[119] Zhang, Y. & Gole, A.M. 2012. *Consideration of inertia for design of reactive power compensation devices for HVDC transmission systems*. Paper presented at the 10th IET International Conference on AC and DC Power Transmission (ACDC 2012), Birmingham, 4-5 December.

[120] Quiroga, D., Sauma, E. & Pozo, D. 2019. Power system expansion planning under global and local emission mitigation policies. *Applied Energy*, 239:1250-1264.

[121] Emmanuel, M., Doubleday, K., Cakir, B., Marković, M. & Hodge, B.M. 2020. A review of power system planning and operational models for flexibility assessment in high solar energy penetration scenarios. *Solar Energy*, 210:169-180.

[122] Tan, B., Zhao, J., Netto, M., Krishnan, V., Terzija, V. & Zhang, Y. 2022. Power system inertia estimation: Review of methods and the impacts of converter-interfaced generations. *International Journal of Electrical Power & Energy Systems*, 134:107362.

[123] Javed, M.S., Zhong, D., Ma, T., Song, A. & Ahmed, S. 2020. Hybrid pumped hydro and battery storage for renewable energy based power supply system. *Applied Energy*, 257:114026.

[124] Markovic, U., 2020. Towards reliable operation of converter-dominated power systems: Dynamics, optimization and control (Doctoral dissertation). Eidgenössische Technische Hochschule Zürich.

[125] Zhang, L., Chen, C., Wang, Q. & Zhou, D. 2021. The impact of feed-in tariff reduction and renewable portfolio standard on the development of distributed photovoltaic generation in China. *Energy*, 232:120933.

[126] Sagulpongmalee, K., Therdyothin, A. & Nathakaranakule, A. 2019. Analysis of feed-in tariff models for photovoltaic systems in Thailand: An evidence-based approach. *Journal of Renewable and Sustainable Energy*, 11(4):045903.

[127] Li, H.X., Zhang, Y., Li, Y., Huang, J., Costin, G. & Zhang, P. 2021. Exploring payback-year based feed-in tariff mechanisms in Australia. *Energy Policy*, 150:112133.

[128] Bevrani, H., Golpira, H., Messina, A.R., Hatziargyriou, N., Milano, F. & Ise, T. 2021. Power system frequency control: An updated review of current solutions and new challenges. *Electric Power Systems Research*, 194:107114.

[129] Rezkalla, M. & Marinelli, M. 2019. Augmenting system inertia through fast acting reserve – A power system case study with high penetration of wind power. In *Proceedings of the 54th International Universities Power Engineering Conference (UPEC)*. New Jersey: IEEE. pp. 1-6.

[130] Moradi-Sepahvand, M. & Amraee, T. 2021. Integrated expansion planning of electric energy generation, transmission, and storage for handling high shares of wind and solar power generation. *Applied Energy*, 298:117137.

[131] Gbadamosi, S.L., Nwulu, N.I. & Sun, Y. 2018. Multi-objective optimisation for composite generation and transmission expansion planning considering offshore wind power and feed-in tariffs. *IET Renewable Power Generation*, 12(14):1687-1697.

[132] Asgharian, V. & Abdelaziz, M. 2020. A low-carbon market-based multi-area power system expansion planning model. *Electric Power Systems Research*, 187:106500.

[133] Abdi, H. 2021. Profit-based unit commitment problem: A review of models, methods, challenges, and future directions. *Renewable and Sustainable Energy Reviews*, 138:110504.

[134] Yang, D.X., Jing, Y.Q., Wang, C., Nie, P.Y. & Sun, P. 2021. Analysis of renewable energy subsidy in China under uncertainty: Feed-in tariff vs. renewable portfolio standard. *Energy Strategy Reviews*, 34:100628.

[135] Akram, U., Mithulananthan, N., Shah, R. & Pourmousavi, S.A. 2021. Sizing HESS as inertial and primary frequency reserve in low inertia power system. *IET Renewable Power Generation*, 15(1):99-113.

[136] Ayamolowo, O.J., Manditereza P.T. & Kusakana, K. 2023. Combined generation and transmission expansion planning model for improved modern power system resilience. *Electric Power and Components and Systems*, 51(9): 898-914.

[137] Wang, R., Yang, W., Li, X., Zhao, Z. & Zhang, S. 2022. Day-ahead multi-objective optimal operation of Wind–PV–Pumped Storage hybrid system considering carbon emissions. *Energy Reports*, 8:1270-1279.

[138] Sewchurran, S. & Davidson, I.E. 2017. Introduction to the South African Renewable Energy Grid Code version 2.9 requirements (Part I – Introduction). In *2017 IEEE AFRICON*. New Jersey: IEEE. pp. 1220-1224

[139] Gandhi, I., Ravi, L., Vijayakumar, V. & Subramaniyaswamy, V. 2020. Improving security for wind energy systems in smart grid applications using digital protection technique. *Sustainable Cities and Society*, 60:102265.

[140] Alguacil, N., Motto, A.L. & Conejo, A.J. 2003. Transmission expansion planning: A mixed-integer LP approach. *IEEE Transactions on Power Systems*, 18(3):1070-1077.

[141] Naderipour, A., Ramtin, A.R., Abdullah, A., Marzbali, M.H., Nowdeh, S.A. & Kamyab, H. 2022. Hybrid energy system optimization with battery storage for remote area application considering loss of energy probability and economic analysis. *Energy*, 239:122303.

[142] Al-Ghussain, L., Ahmad, A.D., Abubaker, A.M. & Mohamed, M.A. 2021. An integrated photovoltaic/wind/biomass and hybrid energy storage systems towards 100% renewable energy microgrids in university campuses. *Sustainable Energy Technologies and Assessments*, 46:101273.

[143] Jena, C., Guerrero, J.M., Abusorrah, A., Al-Turki, Y. & Khan, B. 2022. Multi-objective generation scheduling of hydro-thermal system incorporating energy storage with demand side management considering renewable energy uncertainties. *IEEE Access*, 10:52343-52357.

[144] Bawazir, R.O. & Cetin, N.S. 2020. Comprehensive overview of optimizing PV-DG allocation in power system and solar energy resource potential assessments. *Energy Reports*, 6:173-208.

[145] Ayamolowo, O.J., Adigun, S.O. & Manditereza, P.T. 2020. Short-term solar irradiance evaluation and modeling of a hybrid distribution generation system for a typical Nigeria university. In *2020 IEEE PES/IAS PowerAfrica*. New Jersey: IEEE. pp. 1-5.

[146] Zhou, B., Lei, Y., Li, C., Fang, B., Wu, Q., Li, L. & Li, Z. 2019. Electrical LeaderRank method for node importance evaluation of power grids considering uncertainties of renewable energy. *International Journal of Electrical Power & Energy Systems*, 106:45-55.

[147] Yan, B., Di Somma, M., Graditi, G. & Luh, P.B. 2020. Markovian-based stochastic operation optimization of multiple distributed energy systems with renewables in a local energy community. *Electric Power Systems Research*, 186:106364.

[148] Kazemzadeh, N., Ryan, S.M. & Hamzeei, M. 2019. Robust optimization vs. stochastic programming incorporating risk measures for unit commitment with uncertain variable renewable generation. *Energy Systems*, 10:517-541.

[149] Seljom, P., Kvalbein, L., Hellemo, L., Kaut, M. & Ortiz, M.M. 2021. Stochastic modelling of variable renewables in long-term energy models: Dataset, scenario generation & quality of results. *Energy*, 236:121415.

[150] Jiang, M., Liu, T., Goh, H.H., Zhang, D., Dai, W., Liu, J. & Wu, T. 2020. Estimation of operation cost of residential multiple energy system considering uncertainty of loads and renewable energies. *IEEE Access*, 9:4874-4885.

[151] Fan, H., Wang, C., Liu, L. & Li, X. 2022. Review of uncertainty modeling for optimal operation of integrated energy system. *Frontiers in Energy Research*, 9:947.

[152] Elkadeem, M.R., Abd Elaziz, M., Ullah, Z., Wang, S. & Sharshir, S.W. 2019. Optimal planning of renewable energy-integrated distribution system considering uncertainties. *IEEE Access*, 7:164887-164907.

[153] Yang, D., Jiang, C., Cai, G., Yang, D. & Liu, X. 2020. Interval method based optimal planning of multi-energy microgrid with uncertain renewable generation and demand. *Applied Energy*, 277:115491.

[154] Irawan, C.A., Hofman, P.S., Chan, H.K. & Paulraj, A. 2022. A stochastic programming model for an energy planning problem: Formulation, solution method and application. *Annals of Operations Research*, 311(2):695-730.

[155] Gao, H., Xu, S., Liu, Y., Wang, L., Xiang, Y. & Liu, J. 2020. Decentralized optimal operation model for cooperative microgrids considering renewable energy uncertainties. *Applied Energy*, 262:114579.

[156] Wang, C., Yuan, P., Liu, B., Li, H., Jiang, Z. & Wang, X. 2022. A research on the limit grid-integrated scale of renewable energy under the minimum inertia constraint. In *2022 5th International Conference on Energy, Electrical and Power Engineering (CEEPE)*. New Jersey: IEEE. pp. 1311-1317

[157] Banik, S., Sakib, M.S. & Chowdhury, S. 2019. Estimation of minimum synchronous inertia in a renewable dominated power system. In *2019 IEEE International Conference on Power, Electrical, and Electronics and Industrial Applications (PEEIACON)*. New Jersey: IEEE. pp. 61-64.

[158] Ayamolowo, O.J., Omo-Irabor, B., Buraimoh, E. & Davidson, I.E. 2020. Short-term wind variability analysis of Afe Babalola University. In *2020 Clemson University Power Systems Conference (PSC)*. New Jersey: IEEE. pp. 1-8.

APPENDICES

APPENDIX A: GENERAL ALGEBRAIC MODELING SYSTEM (GAMS) ON OPTIMAL PLANNING OF RENEWABLE ENERGY GENERATORS (REGs) IN A MODERN POWER GRID FOR ENHANCED SYSTEM INERTIA

```
sets i /g1*g5/,
j /e1*e4/,
w /w1*w4/,
d /d1*d4/,
f /f1*f4/,
t /t1*t24/,
r /1*2/,
bus /1*9/,
slack bus /1/;
*d set of battery storage units
*f set of pumped hydro energy storage units
Table e(d,*)
    Pmax  H    S    inv
d1  100   10   100  16000
d2  100   10   100  16000
d3  100   10   100  16000
d4  100   10   100  16000;
Table h(f,*)
    Pmax  H   S    inv
f1  400   2   400  17500
f2  400   2   400  17500
f3  400   2   400  17500
f4  400   2   400  17500;
Table k(i,*)
    Pmax   Pmin   H    S     e      a         b     c    RU    RD
g1  203.1  81.2   4    250   1.135  0.00043   16.6  900  30.5  30.5
g2  194.4  77.8   6    240   1.135  0.00073   15.5  800  29.2  29.2
```

g3 500 100 4 625 1.135 0.00059 14.8 700 200.0 200.0

g4 400 40 2.5 500 1.135 0.00075 15.9 470 360.0 360.0

g5 441.8 44.2 2.5 550 1.135 0.00079 16.6 200 397.6 397.6;

Table l(j,*)

	Pmax	H	S	inv
e1	200	0	200	84467
e2	200	0	200	84467
e3	200	4	200	84467
e4	200	4	200	84467;

Table o(w,*)

	Pmax	H	S	inv	cul
w1	200	4	200	80000	5
w2	200	4	200	80000	5
w3	200	2	200	72641	2
w4	200	2	200	72641	2;

* e investment in solar

* w investment in wind turbine

Set GB(bus,i) connectivity index of each generating unit to each bus

/1.g1

2.g2

3.g3

4.g4

6.g5/;

Table BD(bus,*) Demands of each bus in MW

	pd
1	512
2	239
3	341
4	683
5	171
6	853
7	273
8	171
9	171;

alias (bus,node);

table br(bus,node,*) Network technical characteristics

	r	x	b	limit
1.6	0.0020	0.0200	0.0360	800
2.3	0.0040	0.0040	0.0540	800
2.6	0.0060	0.040	0.0720	800
3.4	0.0080	0.050	0.0900	800
3.6	0.0070	0.0600	0.1080	800
4.5	0.0050	0.0700	0.1260	800
4.6	0.0030	0.0800	0.1440	800
4.9	0.0010	0.0700	0.1260	800
6.7	0.0030	0.060	0.1080	800
6.8	0.0050	0.050	0.0900	800
7.8	0.0070	0.0400	0.0720	800
8.9	0.0060	0.0300	0.0540	800
1.4	0.0060	0.0300	0.0540	800;

Table WS(t,*)

	w	d	w1	w2	S1	s2
t1	0.0786666666666667	0.684511335492475	0.35	0.35	0.00	0.00
t2	0.0866666666666667	0.644122690036197	0.38	0.38	0.00	0.00
t3	0.117333333333333	0.61306915602972	0.41	0.41	0.00	0.00
t4	0.258666666666667	0.599733282530006	0.47	0.47	0.00	0.00
t5	0.361333333333333	0.588874071251667	0.53	0.53	0.00	0.00
t6	0.568	0.787007048961707	0.59	0.59	0.00	0.00
t7	0.538	0.787007048961707	0.65	0.65	0.00	0.00
t8	0.598	0.687007048961707	0.71	0.71	0.00	0.00
t9	0.528	0.987007048961707	0.77	0.77	0.06	0.06
t10	0.548	0.487007048961707	0.79	0.79	0.13	0.13
t11	0.568	0.587007048961707	0.81	0.81	0.20	0.20
t12	0.248	0.887007048961707	0.84	0.84	0.22	0.22
t13	0.348	0.187007048961707	0.86	0.86	0.22	0.22
t14	0.248	0.587007048961707	0.87	0.87	0.18	0.18
t15	0.248	0.587007048961707	0.89	0.89	0.12	0.12
t16	0.248	0.587007048961707	0.92	0.92	0.05	0.05

t17 0.248 0.587007048961707 0.95 0.95 0.01 0.01

t18 0.248 0.587007048961707 0.96 0.96 0.00 0.00

t19 0.248 0.587007048961707 0.97 0.97 0.00 0.00

t20 0.248 0.587007048961707 0.97 0.97 0.00 0.00

t21 0.248 0.587007048961707 0.96 0.96 0.00 0.00

t22 0.248 0.587007048961707 0.94 0.94 0.00 0.00

t23 0.248 0.587007048961707 0.90 0.90 0.00 0.00

t24 0.248 0.587007048961707 0.84 0.84 0.00 0.00;

```
Parameter Wcap(bus )
/5 200
9 200/;
Parameter Scap(bus )
/6 200
8 200/;
parameter SOCmax(bus)
/5 100
4 100
1 100
6 100/;
parameter socp(bus)
/5 100
4 100
1 100
6 100/;
parameter SOC0(bus);
SOC0(bus)=0.2*SOCmax(bus);
br (bus,node,'x')$(br(bus,node,'x')=0)=br(node,bus,'x');
br (bus,node,'Limit')$(br(bus,node,'Limit')=0)=br(node,bus,'Limit');
br (bus,node,'bij')$br(bus,node,'Limit')=1/br(bus,node,'x') ;
br  (bus,node,'z')$br(bus,node,'Limit')=sqrt(power(br(bus,node,'x'),2)+power(br(bus,node,'r'),2
));
br(node,bus,'z')=br(bus,node,'z');
parameter conex(bus,node);
conex(bus,node)$(br(bus,node,'limit') and br(node,bus,'limit'))=1;
```

```
conex (bus,node)$(conex(node,bus))=1;
* e set of solar plant
* w set of wind farm
* prospective ESS to boost the inertia of the system
Parameter data (r,i,*);
data (r,i,'DP')=(k(i,'Pmax')-k(i,'Pmin'))/card (r);
data(r,i,'Pini')=(ord(r)-1)*data(r,i,'DP')+k(i,'Pmin');
data(r,i,'Pfin')=data(r,i,'Pini')+ data(r,i,'DP');
data(r,i,'Cini')=k(i,'a')*power(data(r,i,'Pini'),2)+k(i,'b')*data(r,i,'Pini')+k(i,'c');
data(r,i,'Cfin')=k(i,'a')*power(data(r,i,'Pfin'),2)+k(i,'b')*data(r,i,'Pfin')+k(i,'c');
data(r,i,'s')=(data(r,i,'Cfin')-data(r,i,'Cini'))/data(r,i,'DP');
scalar dem /3414/,
sbase  /2282.5/,
cem /75/,
omw /5/,
ceb /0.95/ ,
deb /0.95/;
*ceb is the charging efficiency of battery while deb is the discharging efficiency of battery
*omw is the cost of wind curtailment or the cost of operation and maintenance of wind turbine
variable
Heq,P(i),z(j),PG,KP,AG,IG,CE,N(w),MG,BA(d),PP,PU(f),OP,BP,PUG,BG,cov,coe,cee,pk(i,
t,r),OPP,TC,delta(bus,t),Pij(bus,node,t),Pw(bus,t),ePd(t),ePc(t),oppw,SI,TI,SS,SBA,Fu,IN;
binary variable u(j),m(w),v1(d),v2(f);
*u(j) binary variable t=that decides selection of solar system
*there might be a need to decommission some thermal generators so we might introduce a
binary variable to indicate the thermal generators that should be put to service
P.up(i)= k(i,'pmax');
P.lo(i)= k(i,'pmin');
z.up(j)=l(j,'S');
z.lo(j)=0;
N.lo(w)=0;
N.up(w)=o(w,'S');
BA.lo(d)=0;
BA.up(d)=e(d,'S');
```

```
PU.lo(f)=0;
PU.up(f)=h(f,'S');
Pk.up(i,t,r)=data(r,i,'DP');
Pk.lo(i,t,r)=0;
equations
eq1,eq2,eq3,eq4(j),eq5,eq6,eq7,eq8,eq9,eq10(w),eq11,eq12,eq13,eq14,eq15,eq16,eq17,eq18,
eq19,eq20(f),eq21,eq22,eq23,eq24,eq25,eq26,eq27,eq28,eq29,eq30,eq31,eq32,eq33,eq34,eq3
5,eq36,eq37;
eq1..KP+PG+OP+BP+PP=l=(dem*1.5);
eq2..(SI+IG+MG+BG+PUG)/Sbase=e=Heq;
eq3..sum(i,P(i))=e=PG;
eq4(j)..l(j,'s')*u(j)=e=z(j);
* to get the estimated system base, the following variables are needed: KP, OP, BP, PP
eq5..sum(i,k(i,'s')* k(i,'H'))=e=AG;
eq6..sum(j,l(j,'s')*l(j,'H')*u(j))=e=IG;
eq7..sum(j,(u(j)))=l=4;
eq8..sum(j,z(j))=e=KP;
eq9..sum(j,l(j,'cost')*u(j))+sum(w,o(w,'cost')*m(w))=e=CE;
eq10(w)..o(w,'s')*m(w)=e=n(w);
eq11..sum(w,o(w,'s')*o(w,'H')*m(w))=e=MG;
eq12..sum(w,(m(w)))=l=4;
eq13..sum(w,(m(w)))+sum(j,(u(j)))=e=4;
eq14..sum(w,n(w))=e=OP;
eq15(d)..e(d,'s')*v1(d)=e=BA(d);
eq16..sum(d,e(d,'s')*e(d,'H')*v1(d))=e=BG;
eq17..sum(d,(v1(d)))=l=4;
eq18..sum(d,(v1(d)))+sum(f,(v2(f)))=e=4;
eq19..sum(d,BA(d))=e=BP;
eq20(f)..h(f,'s')*v2(f)=e=PU(f);
eq21..sum(f,h(f,'s')*h(f,'H')*v2(f))=e=PUG;
eq22..sum(f,(v2(f)))=l=4;
eq23..sum(f,PU(f))=e=PP;
eq24..sum(f,h(f,'inv')*v2(f))+sum(d,e(d,'inv')*v1(d))+sum(j,l(j,'inv')*u(j))+sum(w,o(w,'inv')*
m(w))=e=cov;
```

```
eq25..cee*8760=e=coe;
eq26..sum(i,p(i)*k(i,'e'))=e=cee;
eq27..cee=l=1000;
eq28..OPP=e=((sum((t,i),k(i,'a')*power(k(i,'Pmin'),2)+k(i,'b')*k(i,'Pmin')+k(i,'c')+sum(r,data(
r,i,'s')*pk(i,t,r))))*8760)+oppw;
eq29..TC=e=OPP+coe+cov;
eq30(bus,node,t)$(conex(bus,node))..Pij(bus,node,t)=e=br(bus,node,'bij')*(delta(bus,t)-
delta(node,t));
eq31.. (sum(w,n(w)*o(w,'cul')*8760))=e=oppw;
eq32..SI=e=sum(i,k(i,'s')*k(i,'H'));
eq33..TI=e=IG+MG+BG+PUG ;
eq34..SS=e=sum(i,k(i,'s'));
eq35..SBA=e=(KP+OP+PP+BP+SS);
eq36..Fu=e=((sum((t,i),k(i,'a')*power(k(i,'Pmin'),2)+k(i,'b')*k(i,'Pmin')+k(i,'c')+sum(r,data(r,i
,'s')*pk(i,t,r))))*8760) ;
eq37..IN=e=SI+IG+MG+BG+PUG  ;
Heq.up=10;
Heq.lo=3.6;
model test1 /all/;
delta.up(bus,t)=pi/6;
delta.lo(bus,t)=-pi/6;
Pij.up(bus,node,t)$((conex(bus,node)))=1*br(bus,node,'Limit')/Sbase ;
Pij.lo(bus,node,t)$((conex(bus,node)))=-1*br(bus,node,'Limit')/Sbase;
solve test1 using miqcp max Heq;
```

APPENDIX B: GAMS CODE ON JOINT GENERATION AND TRANSMISSION EXPANSION PLANNING (GTEP) MODEL FOR IMPROVED MODERN POWER SYSTEM RESILIENCE AGAINST FREQUENCY INSTABILITY

```
Sets bus /1*9/,
slack (bus) /1/,
Gen /g1*g5/,
s /s1*s4/,
w /w1*w6/,
b /b1*b6/,
p /p1*p6/,
k /k1*k2/;
*k is the maximum number of transmission lines that can be installed in a corridor
alias (bus,node);
Scalars
Sbase /800/,
M /1000/,
dem /300/,
ct /20/,
Emax /11541850/,
KEmin /8000/
fmin /49/,
fmax /51/,
nl /100/,
*nl is the maximum no. of candidate transmission lines available for construction
*fmax and fmin are the minimum and maximum values of permissible system frequency
*KEmin is the minimum required emergency energy that should be available at all times from all generators (synchronous, renewable, and energy storage units)
sbase1 /2285/,
BCOX /700000000/,
BCOS /3.8E+7/,
BCOW /3.8E+7/,
```

BCOB /3.8E+7/,

BCOP /3.E+7/,

*let dem be the peak load demand

*BCOX, BCOS, BCOB, and BCOP are the monetary budgets for candidate solar, wind, battery, and pumped hydro energy storage

*BCOX is the maximum budget for a new transmission line

*ct is carbon tax in $/MWh

*emission factor in tCO_2/MWh

T;

T=8760*1;

* T is the planning time, taken as one year in this case

Set conex(bus,node);

*means bus and node can be used interchangeably

Table GenData (Gen,*) Generating units' characteristics

	Pmax	Pmin	H	S	e	a	b	be	c	RU	RD
g1	203.1	81.2	4	250	0.932	0.00043	17.87	16.6	900	30.5	30.5
g2	194.4	77.8	6	240	1.135	0.00073	21.62	15.5	800	29.2	29.2
g3	500	100	4	625	0.411	0.00059	23.9	14.8	700	200.0	200.0
g4	400	40	2.5	500	0.619	0.00075	21.6	15.9	470	360.0	360.0
g5	441.8	44.2	2.5	550	0.880	0.00079	22.54	16.6	200	397.6	397.6;

Table SO(s,*)

	Pmax	H	S	inv	cap
s1	100	0	100	8446720	0.27
s2	100	4	100	9265480	0.27
s3	100	0	100	8446720	0.27
s4	100	4	100	9265480	0.27;

Table WO(w,*)

	Pmax	H	S	inv	op	cap
w1	100	4	100	8000000	5	0.30
w2	100	2	100	7264180	2	0.30
w3	100	4	100	8000000	5	0.30
w4	100	2	100	7264180	2	0.30
w5	100	4	100	8000000	5	0.30
w6	100	2	100	7264180	2	0.30;

Table BO(b,*)

	Pmax	H	S	inv	soc
b1	100	10	100	382100	0.8
b2	100	10	100	382100	0.8
b3	100	10	100	382100	0.8
b4	100	10	100	382100	0.8
b5	100	10	100	382100	0.8
b6	100	10	100	382100	0.8;

Table PO(p,*)

	Pmax	H	S	inv	ef
p1	300	2	300	1247100	0.87
p2	300	2	300	1247100	0.87
p3	300	2	300	1247100	0.87
p4	300	2	300	1247100	0.87
p5	300	2	300	1247100	0.87
p6	300	2	300	1247100	0.87;

Set GBconect (bus,Gen) connectivity index of each generating unit to each bus

/1.g1

2.g2

3.g3

4.g4

6.g5/;

Table BusData (bus,*) Demands of each bus in MW

	Pd
1	512
2	239
3	341
4	683
5	171
6	853
7	273
8	171
9	194;

table branch (bus,node,*) Network technical characteristics

```
        r      x       b       Limit  stat cost
1.6     0.0020 0.0200 0.0360  800    1    112.084000
2.3     0.0040 0.0040 0.0540  800    1    112.084000
2.6     0.0060 0.040  0.0720  800    1    112.084000
3.4     0.0080 0.050  0.0900  800    1    112.084000
4.5     0.0050 0.0700 0.1260  800    0    112.084000
4.6     0.0030 0.0800 0.1440  800    1    112.084000
4.9     0.0010 0.0700 0.1260  800    1    112.084000
6.7     0.0030 0.060  0.1080  800    1    112.084000
6.8     0.0050 0.050  0.0900  800    1    112.084000
7.8     0.0070 0.0400 0.0720  800    1    112.084000
8.9     0.0060 0.0300 0.0540  800    1    112.084000
1.4     0.0060 0.0300 0.0540  800    1    112.084000 ;
conex (bus,node)$(branch (bus,node,'x'))=yes;
conex (bus , node )$conex (node,bus)=yes ;
branch (bus,node,'x')$branch(node,bus ,'x')=branch (node,bus,'x');
*establishing the node is the same as bus so that the susceptance for bus-node is the same as
that from node-bus
branch (bus ,node,'cost')$branch(node, bus,'cost')=branch(node,bus,'cost');
branch (bus,node,'stat')$branch(node,bus,'stat')=branch(node,bus,'stat');
branch (bus,node,'Limit')$(branch(bus,node,'Limit')=0)=branch(node,bus,'Limit') ;
branch (bus,node,'bij')$conex(bus,node)=1/branch(bus,node,'x');
*this means that all said parameters are same for node-bus and bus-node.
M=smax((bus,node)$conex(bus,node),branch (bus,node,'b')*3.14*4/3);
Variables                                   OF,Pij(bus,node,k),Pg(Gen),delta(bus),LS
(bus),SA,TG,WA,TD,PA,BA,OPM,EC,EE,CE,SH,WH,PH,BH,TH,TTH,Heq,COX,FU,LSC,
COS,COW,COB,COP,RC,TAA,WAA,PAA,BAA,SAA;
*EC is the emission cost
binary variable
u1(s),u2(w),u3(p),u4(b),alpha (bus,node,k);
alpha.l(bus,node,k)=1;
alpha.fx(bus,node,k)$(conex(bus,node)and ord (k)=1 and branch (node,bus,'stat'))=1;
Equations
const1A,const1B,const1C,const1D,const1E,const2,const3,eq1,eq2,eq3,eq4,eq5,eq6,eq7,eq8,e
```

```
q9,eq10,eq11,eq12,eq13,eq14,eq15,eq16,eq17,eq18,eq19,eq20,eq21,eq22,eq23,eq24,eq25,eq
26,eq27,eq28,eq29,eq30,eq31,eq32,eq33,eq34,eq35,eq36,eq37,eq38,eq39,eq40,eq41,eq42,eq
43,eq44,eq45,eq46,eq47;
const1A      (bus,node,k)$conex(node,bus)..Pij(bus,node,k)-branch(bus,node,'b')*(delta(bus)-
delta(node))=l=M*(1-alpha(bus,node,k));
const1B(bus,node,k)$conex(node,bus)..Pij(bus,node,k)-branch(bus,node,'b')*(delta(bus)-
delta(node))=g=-M*(1-alpha(bus,node,k));
const1C(bus,node,k)$conex(node,bus)..Pij(bus,node,k)=l=alpha(bus,node,k)*branch(bus,nod
e,'Limit')/Sbase;
const1D(bus,node,k)$conex(node,bus)..Pij(bus,node,k)=g=-
alpha(bus,node,k)*branch(bus,node,'Limit')/Sbase;
const1E(bus,node,k)$conex(node,bus)..alpha(bus,node,k)=e=alpha(node,bus,k);
const2(bus)..(LS(bus)+sum(Gen$GBconect(bus,Gen),Pg(Gen))-
BusData(bus,'pd')/Sbase)=e=+sum((k,node)$conex(node,bus),Pij(bus,node,k));
const3..OF=g=T*(sum(Gen,Pg(Gen)*GenData(Gen,'a')**2+Pg(Gen)*GenData(Gen,'b')+Pg(
Gen)*GenData(Gen,'c'))+1000*sbase*sum(bus,LS(bus)))+OPM-
CE+EC+sum(p,PO(p,'inv')*u3(p))+sum(b,BO(b,'inv')*u4(b))+sum(s,SO(s,'inv')*u1(s))+sum(
w,WO(w,'inv')*u2(w))+1e6*sum((bus,node,k)$conex(node,bus),0.5*branch(bus,node,'cost')*
alpha(bus,node,k)$(ord(k)>1 or branch (node,bus,'stat')=0));
eq1..SA=e=sum(s,SO(s,'S')*SO(s,'cap')*u1(s));
eq2..sum(s,u1(s))=e=2;
eq3..sum(Gen,Pg(Gen))=e=TG;
eq4..TD=e=(TG*sbase)+SA+WA+BA+PA;
eq5..WA=e=sum(w,WO(w,'S')*WO(w,'cap')*u2(w));
eq6..sum(w,u2(w))=l=6;
eq7..PA=e=sum(p,PO(p,'S')*PO(p,'ef')*u3(p));
eq8..sum(p,u3(p))=l=6;
eq9..BA=e=sum(b,BO(b,'S')*BO(b,'soc')*u4(b));
eq10..sum(b,u4(b))=l=6;
eq11..T*(sum(w,WO(w,'op')*u2(w)))=e=OPM;
*note eq11 needs to be multiplied by the power rating of the wind turbine
eq12..sum(b,u4(b))+sum(p,u3(p))=e=6;
eq13..sum(s,u1(s))+sum(w,u2(w))=e=5;
eq14..EC=e=(sum(Gen,Pg(Gen)*GenData(Gen,'e'))*T*ct*sbase);
```

```
eq15..EE=e=(sum(Gen,Pg(Gen)*GenData(Gen,'e'))*T*sbase);
eq16..EC*0.3=e=CE;
eq17..sum(s,SO(s,'S')*SO(s,'H')*u1(s))=e=SH;
eq18..sum(w,WO(w,'S')*WO(w,'H')*u2(w))=e=WH;
eq19..sum(p,PO(p,'S')*PO(p,'H')*u3(p))=e=PH;
eq20..sum(b,BO(b,'S')*BO(b,'H')*u4(b))=e=BH;
eq21..sum(gen,GenData(gen,'S')*GenData(gen,'H'))=e=TH;
eq22..(SH+WH+PH+BH+TH)=e=TTH  ;
eq23..Heq=e=TTH/sbase1;
Heq.up=10;
Heq.lo=4;
eq24..COX=e=1e6*sum((bus,node,k)$conex(node,bus),0.5*branch(bus,node,'cost')*alpha(bu
s,node,k)$(ord(k)>1 or branch (node,bus,'stat')=0));
eq25..COX=l=BCOX;
eq26..FU=E=T*(sum(Gen,Pg(Gen)*GenData(Gen,'a')**2+Pg(Gen)*GenData(Gen,'b')+GenD
ata(Gen,'c')));
eq27..LSC=e=T*(300*sbase*sum(bus,LS(bus))) ;
eq28..COP=e=sum(p,PO(p,'inv')*u3(p)) ;
eq29..COB=e=sum(b,BO(b,'inv')*u4(b)) ;
eq30..COW=e=sum(w,WO(w,'inv')*u2(w)) ;
eq31..COS=e=sum(s,SO(s,'inv')*u1(s));
eq32 ..COS=l=BCOS;
eq33 ..COP=l=BCOP;
eq34..COW=l=BCOW;
eq35 ..COB=l=BCOB;
eq36..TH=g=0.2*TTH;
eq37..EE=l=Emax;
eq38..(TG*sbase)+WA+SA=e=RC;
eq39..RC=g=1.1*dem;
*dem should be the peak load demand
eq40..TD=g=RC;
eq41..TTH=g=1.2*KEmin;
eq42..sum((bus,node,k)$conex(node,bus),alpha(bus,node,k))=l=nl;
eq43..SAA=e=sum(s,SO(s,'S')*u1(s));
```

```
eq44..WAA=e=sum(w,WO(w,'S')*u2(w));
eq45..BAA=e=sum(b,BO(b,'S')*u4(b));
eq46..PAA=e=sum(p,PO(p,'S')*u3(p));
eq47..sum(gen,GenData(Gen,'S'))+SAA+PAA+BAA+WAA=e=TAA;
*nl is the number of candidate transmissions line available for construction
*Emax is the maximum limit on annual emission
*OPM is the maintenance cost of the wind turbine
*EC is the total cost of emission of thermal generators
*CE is the incentive paid when emission limits are not violated
*LSC is the cost of load shedding
*FU is the fuel cost of thermal generators
*BCOX is the maximum budget on new transmission lines
*CE is the incentive paid to maintain a certain emission level
*EE is the annual amount of carbon emitted by thermal generators
*OPM is the operational and maintenance cost of the wind turbine
*This shows that the investment cost of a new transmission line is only when a new transmission line is selected for construction
*1e6 this is to make the cost of investment in a transmission line to be in millions
*PSHij(bus,node,k) phase angle at the bus.
Model loadflow /all/;
option optcr=0;
LS.up(bus)=BusData(bus,'pd')/Sbase;
LS.lo(bus)=0;
Pg.lo(Gen)=GenData(Gen,'Pmin')/sbase;
Pg.up(Gen)=GenData(Gen,'Pmax')/Sbase;
delta.up(bus)=pi/4;
delta.lo(bus)=-pi/4;
delta.fx(slack)=0;
Pij.up(bus,node,k)$((conex(bus,node)))=+1*branch(bus,node,'Limit')/Sbase;
Pij.lo(bus,node,k)$((conex(bus,node)))=-1*branch(bus,node,'Limit')/Sbase;
Solve loadflow min EC us mip;
```

APPENDIX C: GAMS CODE ON SENSITIVITY ANALYSIS OF FEED-IN TARIFF (FiT) IN JOINT GTEP CONSIDERING THE INERTIA REQUIREMENT OF THE GRID

```
Sets bus /1*6/,
slack (bus) /1/,
Gen /g1*g3/,
s /s1*s4/,
w /w1*w4/,
hes /hes1*hes4/,
*s is the set of candidate solar plants, wind turbines, BESS, and BESS-SCES
k /k1*k2/,
counter /c1*c11/;
parameter report(*),rep(counter,*);
*k is the maximum number of transmission lines that can be installed in a corridor
alias (bus,node);
Scalars
ftw /0.0024/,
fts /0.0075/,
*fit for solar is R3.94 and wind is R1.25; the conversion is R16.67 equals $1
ress /0.0036/,
fo /50/,
poft /600/,
pofp /320/,
*ress is constant for calculating the minimum sizing of the power frequency reserve, poft is the target pof, pofp is the pof due to the contingency
*fts and ftw are the FiT for solar plants and wind turbines respectively
Sbase /100/,
M /1000/,
dem /1140/,
ct /25/,
Emax /11541850/,
KEmin /8000/,
```

fmin /49/,

fmax /51/,

nl /20/,

*nl is the maximum no. of candidate transmission lines available for construction

*fmaxand fmin are the minimum and maximum values of permissible system frequency

*KEmin is the minimum required emergency energy that should be available at all times from all generators (synchronous, renewable, and energy storage units)

sbase1 /1743/,

*0.85 is used to multiply the TAA to get the approximate SBASE

BCOX /7000000000/,

BCOS /3.8E+7/,

BCOW /3.8E+7/,

BCOP /3.8E+7/,

BFITT /3.8E+9/,

Elim /90000000000000000/,

*let dem be the peak load demand

*BCOX, BCOS, BCOB, and BCOP are the monetary budgets for candidate solar, wind, battery, and BESS-SCES

*BCOX is the maximum budget for a new transmission line

*ct is carbon tax in $/MWh

*emission factor in tCO_2/MWh

*BFITT is the government budget for FiT

T;

T=8760*1;

*T is the planning time, taken as 1 year in this case

Set conex(bus,node);

*means bus and node can be used interchangeably

Table GenData (Gen,*) Generating units' characteristics

	Pmax	Pmin	H	S	e	a	b	be	c	RU	RD
g1	400	0	4	500	1.153	0.028	12.6	16.6	49	30.5	30.5
g2	400	0	4	500	1.153	0.028	12.6	15.5	49	29.2	29.2
g3	600	0	6	750	1.153	0.012	13.9	14.8	105	200.0	200.0;

Table SO(s,*)

	Pmax	H	S	inv	cap

s1 200 0 200 16893440 0.25

s2 200 2 200 18530960 0.25

s3 200 0 200 16893440 0.25

s4 200 2 200 18530960 0.25;

Table WO(w,*)

	Pmax	H	S	inv	op	cap
w1	200	2	200	14528360	2	0.38
w2	200	6	200	16000000	5	0.38
w3	200	2	200	14528360	2	0.38
w4	200	6	200	16000000	5	0.38;

Table BO(hes,*)

	Pmax	H	S	inv	socmax	socmin	ef
hes1	50	10	50	191050	0.8	0.2	0.95
hes2	50	10	50	191050	0.8	0.2	0.95
hes3	50	10	50	191050	0.8	0.2	0.95
hes4	50	10	50	191050	0.8	0.2	0.95;

Set GBconect (bus,Gen) connectivity index of each generating unit to each bus

/1.g1

3.g2

6.g3/;

Table BusData (bus,*) Demands of each bus in MW

	Pd
1	120
2	360
3	60
4	240
5	360;

*Note here that we used an IEEE 6-bus system

Table branch (bus,node,*) Network technical characteristics

	r	x	b	Limit	stat	cost
1.2	0.0020	0.400	0.0360	50	1	40
1.4	0.0060	0.60	0.0540	40	1	60
1.5	0.0060	0.20	0.0540	50	1	20
2.3	0.0040	0.20	0.0540	50	1	20

```
2.4   0.0060 0.40  0.0720  50   1   40
2.6   0.0080 0.30  0.0900  50   0   30
3.5   0.0050 0.20  0.1260  50   1   20
4.6   0.0030 0.30  0.1440  50   0   30;
conex (bus,node)$(branch (bus,node,'x'))=yes;
conex (bus , node )$conex (node,bus)=yes ;
branch (bus,node,'x')$branch(node,bus ,'x')=branch (node,bus,'x');
*establishing the node is the same as the bus so that the susceptance for bus-node is the same
as that from node-bus
branch (bus,node,'cost')$branch(node, bus,'cost')=branch(node,bus,'cost');
branch (bus,node,'stat')$branch(node,bus,'stat')=branch(node,bus,'stat');
branch (bus,node,'Limit')$(branch(bus,node,'Limit')=0)=branch(node,bus,'Limit') ;
branch (bus,node,'bij')$conex(bus,node)=1/branch(bus,node,'x');
M=smax((bus,node)$conex(bus,node),branch (bus,node,'b')*3.14*4/3);
Variables
OF,Pij(bus,node,k),Pg(Gen),delta(bus),LS(bus),SA,LSD,FITS,FITW,FITT,TG,WA,TD,PA,
OPM,EC,TTD,EE,CE,SH,WH,PH,BH,TH,TTH,Heq,COX,FU,LSC,COS,COW,COB,COP,R
C,TAA,WAA,PAA,SAA,z(s),n(w),ha(hes),PRR,diff,SPF,TRG,BPA,RR,TIE,TOC;
*EC is the emission cost
binary variable
u1(s),u2(w),u3(hes),alpha (bus,node,k);
alpha.l(bus,node,k)=1;
alpha.fx(bus,node,k)$(conex(bus,node)and ord (k)=1 and branch (node,bus,'stat'))=1;
Equations
const1A,const1B,const1C,const1D,const1E,const2,const3,eq1,eq2,eq3,eq4,eq5,eq6,eq7,eq8,e
q9,eq10,eq11,eq12,eq13,eq14,eq15,eq16,eq17,eq18,eq19,eq20(s),eq21,eq22,eq23,eq24,eq25,
eq26,eq27,eq28,eq29(w),eq30,eq31,eq32,eq33,eq34,eq35(hes),eq36,eq37,eq38,eq39,eq40,eq
41,eq42,eq43,eq44,eq45,eq46,eq47,eq48,eq49,eq50,eq51,eq52,eq53,eq54,eq55,eq56,eq57;
const1A      (bus,node,k)$conex(node,bus)..Pij(bus,node,k)-branch(bus,node,'b')*(delta(bus)-
delta(node))=l=M*(1-alpha(bus,node,k));
const1B(bus,node,k)$conex(node,bus)..Pij(bus,node,k)-branch(bus,node,'b')*(delta(bus)-
delta(node))=g=-M*(1-alpha(bus,node,k));
const1C(bus,node,k)$conex(node,bus)..Pij(bus,node,k)=l=alpha(bus,node,k)*branch(bus,nod
e,'Limit')/Sbase;
```

```
const1D(bus,node,k)$conex(node,bus)..Pij(bus,node,k)=g=-
alpha(bus,node,k)*branch(bus,node,'Limit')/Sbase;
const1E(bus,node,k)$conex(node,bus)..alpha(bus,node,k)=e=alpha(node,bus,k);
const2(bus)..(TD-dem/Sbase)=g=+sum((k,node)$conex(node,bus),Pij(bus,node,k));
*Note in equation const2 the power generation was converted to p.u.
*OF is the total cost of the model
const3..OF=g=T*(sum(Gen,GenData(Gen,'a')*Pg(Gen)*Pg(Gen)*10000+Pg(Gen)*GenData(
Gen,'b')*100+Pg(Gen)*GenData(Gen,'c')))+OPM+EC-FITS-
FITW+sum(hes,BO(hes,'inv')*u3(hes))+sum(s,SO(s,'inv')*u1(s))+sum(w,WO(w,'inv')*u2(w)
)+1e6*sum((bus,node,k)$conex(node,bus),0.5*branch(bus,node,'cost')*alpha(bus,node,k)$(or
d(k)>1 or branch (node,bus,'stat')=0));
eq1..SA=e=sum(s,SO(s,'S')*SO(s,'cap')*u1(s));
*SA is the power delivery from solar plants, TG total generation from thermal generators
eq2..sum(s,u1(s))=l=2;
eq3..sum(Gen,Pg(Gen))=e=TG;
eq4..TD=e=(TG*sbase)+SA+WA+PA;
eq5..WA=e=sum(w,WO(w,'S')*WO(w,'cap')*u2(w));
eq6..sum(w,u2(w))=l=2;
eq7..PA=e=sum(hes,BO(hes,'S')*u3(hes));
*PA is the total cost of hes
eq8..sum(hes,u3(hes))=l=2;
eq9..TTD=e=(TG*sbase)+SA+WA+PA+LSD;
eq10..FITS=e=(T*SA*fts*1000);
eq11..T*(sum(w,WO(w,'op')*WA))=e=OPM;
eq12..FITW=e=(T*WA*ftw*1000);
eq13..sum(s,u1(s))+sum(w,u2(w))=e=2;
eq14..EC=e=(sum(Gen,Pg(Gen)*GenData(Gen,'e'))*T*ct*sbase) ;
eq15..EE=e=(sum(Gen,Pg(Gen)*GenData(Gen,'e'))*T*sbase);
eq16..FITT=e=FITS+FITW;
eq17..sum(s,SO(s,'S')*SO(s,'H')*u1(s))=e=SH;
eq18..sum(w,WO(w,'S')*WO(w,'H')*u2(w))=e=WH;
eq19..sum(hes,BO(hes,'S')*BO(hes,'H')*u3(hes))=e=PH;
eq20(s)..SO(s,'s')*u1(s)=e=z(s);
eq21..sum(gen,GenData(gen,'S')*GenData(gen,'H'))=e=TH;
```

eq22..(SH+WH+PH+TH)=e=TTH;

eq23..Heq=e=TTH/sbase1;

Heq.up=10;

Heq.lo=4;

eq24..COX=e=1e6*sum((bus,node,k)$conex(node,bus),0.5*branch(bus,node,'cost')*alpha(bus,node,k)$(ord(k)>1 or branch (node,bus,'stat')=0));

*COS is the total cost of transmission line investment, while BCOX is the budget for COX investment

eq25..COX=l=BCOX;

eq26..FU=e=T*(sum(Gen,GenData(Gen,'a')*Pg(Gen)*Pg(Gen)*10000+Pg(Gen)*GenData(Gen,'b')*100+Pg(Gen)*GenData(Gen,'c')));

eq27..LSC=e=T*(1*sbase*sum(bus,LS(bus)));

eq28..COP=e=sum(hes,BO(hes,'inv')*u3(hes));

eq29(w)..WO(w,'s')*u2(w)=e=n(w);

eq30..COW=e=sum(w,WO(w,'inv')*u2(w));

eq31..COS=e=sum(s,SO(s,'inv')*u1(s));

eq32 ..COS=l=BCOS;

eq33 ..COP=l=BCOP;

eq34..COW=l=BCOW;

eq35(hes)..BO(hes,'s')*u3(hes)=e=ha(hes);

eq36..TH=g=0.2*TTH;

eq37..EE=l=Emax;

eq38..(TG*sbase)+WA+SA=e=RC;

eq39..LSD=e=(sbase*sum(bus,LS(bus)));

eq40..TD=g=dem;

eq41..TTH=g=1.2*KEmin;

eq42..sum((bus,node,k)$conex(node,bus),alpha(bus,node,k))=l=nl;

eq43..SAA=e=sum(s,SO(s,'S')*u1(s));

eq44..WAA=e=sum(w,WO(w,'S')*u2(w));

eq45..PRR=e=0.05*dem;

eq46..PAA=e=sum(hes,BO(hes,'S')*u3(hes));

eq47..sum(gen,GenData(Gen,'S'))+SAA+PAA+WAA=e=TAA;

eq48..PA=g=PRR;

eq49..diff=e=poft-pofp;

eq50..SPF=e=ress*fo*diff;

eq51..TRG=e=SAA+WAA;

eq52..BPA=e=0.8*PA;

eq53..BPA=g=SPF;

eq54..BPA=l=2*SPF;

eq55..RR=e=TRG/dem;

eq56..TIE=e=WH+PH+SH;

eq57..TOC=e=FU+OPM;

*TRG is the total renewable energy generation

*SPF is the minimum sizing of BESSBESS composition of hybrid ESS

*nl is the number of candidate transmission lines available for construction

*Emax is the maximum limit on annual emission

*OPM is the maintenance cost of the wind turbine

*EC is the total cost of emission of thermal generators

*CE is the incentive paid when emission limits are not violated

*LSC is the cost of load shedding

*FU is the fuel cost of thermal generators

*BCOX is the maximum budget for new transmission lines

*CE is the incentive paid to maintain a certain emission level

*EE is the annual amount of carbon emitted by thermal generators

*OPM is the operational and maintenance cost of the wind turbine

*this shows that the investment cost for a new transmission line is only when a new transmission line is selected for construction

*1e6 this is to make the cost of investment in transmission line to be in millions

*PSHij(bus,node,k) phase angle at the bus.

*Note in this session that we conducted the sensitivity analysis under different levels of RES penetration

Model loadflow /all/;

option optcr=0;

LS.up(bus)=BusData(bus,'pd')/Sbase;

LS.lo(bus)=0;

Pg.lo(Gen)=GenData(Gen,'Pmin')/sbase;

Pg.up(Gen)=GenData(Gen,'Pmax')/Sbase;

delta.up(bus)=pi/4;

```
delta.lo(bus)=-pi/4;
delta.fx(slack)=0;
z.up(s)=SO(s,'S');
z.lo(s)=0;
N.lo(w)=0;
N.up(w)=WO(w,'S');
ha.lo(hes)=0;
ha.up(hes)=BO(hes,'S');
Pij.up(bus,node,k)$((conex(bus,node)))=+1*branch(bus,node,'Limit')/Sbase;
Pij.lo(bus,node,k)$((conex(bus,node)))=-1*branch(bus,node,'Limit')/Sbase;
Solve loadflow min OF us miqcp;
report ('maxHeq')=Heq.l;
report ('minOF')=OF.l;
solve loadflow using miqcp min Heq;
*Name of the model is loadflow, kindly note
report ('maxOF')=OF.l;
report ('minHeq')=Heq.l;
loop (counter,
Elim=(report('maxHeq')-report('minHeq'))*((ord(counter)-1)/(card
(counter)-1))+report('minHeq');
solve loadflow min OF us miqcp;
rep(counter,'OF')=OF.l;
rep(counter,'Heq')=Heq.l;
rep(counter,Gen)=Pg.l(Gen);
);
display rep;
```

APPENDIX D: GAMS CODE ON SHORT-TERM RENEWABLE ENERGY UNCERTAINTIES AND INERTIA CONSIDERATION IN POWER SYSTEM GENERATION EXPANSION PLANNING (GEP)

```
sets i /g1*g3/,
j /e1*e3/,
w /w1*w3/,
d /d1*d3/,
t /t1*t24/,
r /1*1/,
bus /1*6/,
slack bus /1/;
*d is set of battery storage units, t is the set of time for a day
*w is set of wind turbines, while e is set of solar plants
Table e(d,*)
    Pmax  H    S   inv
d1  50    10   50  191050
d2  50    10   50  191050
d3  50    10   50  191050;
Table k(i,*)
    Pmax   Pmin  H    S     e      a      b      c   RU    RD
g1  400    0     7    500   1.135  0.12   14.80  89  30.5  30.5
g2  60     0     5    75    1.135  0.17   16.57  83  29.2  29.2
g3  300    0     6    375   1.135  0.15   15.55  100 200.0 200.0;
Table l(j,*)
    Pmax   H   S     inv
e1  100    2   100   8446720
e2  100    2   100   8446720
e3  100    2   100   8446720;
Table o(w,*)
    Pmax   H    S    inv      cul
w1  100    4    100  8000000 500
w2  100    4    100  8000000 500
```

w3 100 4 100 8000000 500;

*e investment in solar

*w investment in wind turbine

Set GB(bus,i) connectivity index of each generating unit to each bus

/1.g1

3.g2

6.g3/;

Table BD(bus,*) Demands of each bus in MW

	pd
1	120
2	360
3	60
4	240
5	360;

alias (bus,node);

table br(bus,node,*) Network technical characteristics

	r	x	b	limit
1.2	0.0026	0.0139	0.4611	175
1.5	0.0546	0.2112	0.0572	175
1.4	0.0218	0.0845	0.0229	175
2.4	0.0328	0.1267	0.0343	175
2.6	0.0497	0.1920	0.0520	175
2.3	0.0308	0.1190	0.0322	175
3.5	0.0322	0.0839	0.0281	175;

TABLE WS(t,) helps the variability of wind turbines and solar plants

Table WS(t,*)

	w1	S1
t1	0.2929	0.00
t2	0.3040	0.00
t3	0.3102	0.00
t4	0.3091	0.00
t5	0.3024	0.0124
t6	0.2799	0.08605
t7	0.1696	0.2648

```
t8      0.1341   0.4574
t9      0.1771   0.5816
t10     0.2253   0.6520
t11     0.2576   0.6789
t12     0.2795   0.6440
t13     0.2888   0.5680
t14     0.2804   0.4713
t15     0.2462   0.3082
t16     0.2325   0.1697
t17     0.2365   0.0353
t18     0.2490   0.00
t19     0.2618   0.00
t20     0.2674   0.00
t21     0.2740   0.00
t22     0.2792   0.00
t23     0.2827   0.00
t24     0.2884   0.00;
Parameter Wcap(bus )
/2 100
4 100
5 100/;
Parameter Scap(bus )
/2 100
4 100
5 100/;
parameter SOCmax(bus)
/2 50
4 50
5 50/;
parameter SOC0(bus);
SOC0(bus)=0.2*SOCmax(bus);
br (bus,node,'x')$(br(bus,node,'x')=0)=br(node,bus,'x');
br (bus,node,'Limit')$(br(bus,node,'Limit')=0)=br(node,bus,'Limit');
br (bus,node,'bij')$br(bus,node,'Limit')=1/br(bus,node,'x') ;
```

```
br  (bus,node,'z')$br(bus,node,'Limit')=sqrt(power(br(bus,node,'x'),2)+power(br(bus,node,'r'),2
));
br(node,bus,'z')=br(bus,node,'z');
parameter conex(bus,node);
conex(bus,node)$(br(bus,node,'limit') and br(node,bus,'limit'))=1;
conex (bus,node)$(conex(node,bus))=1;
*e set of solar plant
*w set of wind farm
*prospective ESS to boost the inertia of the system
Parameter data (r,i,*);
data (r,i,'DP')=(k(i,'Pmax')-k(i,'Pmin'))/card (r);
data(r,i,'Pini')=(ord(r)-1)*data(r,i,'DP')+k(i,'Pmin');
data(r,i,'Pfin')=data(r,i,'Pini')+ data(r,i,'DP');
data(r,i,'Cini')=k(i,'a')*power(data(r,i,'Pini'),2)+k(i,'b')*data(r,i,'Pini')+k(i,'c');
data(r,i,'Cfin')=k(i,'a')*power(data(r,i,'Pfin'),2)+k(i,'b')*data(r,i,'Pfin')+k(i,'c');
data(r,i,'s')=(data(r,i,'Cfin')-data(r,i,'Cini'))/data(r,i,'DP');
*the above equation linearises the fuel cost
scalar dem /1140/,
sbase  /1400/,
Hmin /4/,
omw /500/,
CTM /10/,
CTE /15/,
y /0.3/,
KEmin /2612/,
PLOSS /60/
BUTT /500000000/;
*BUTT is the maximum monetary budget set aside for investment in solar plant, wind turbine,
and BESS
*ceb is the charging efficiency of battery, while deb is the discharging efficiency of battery
*omw is the cost of wind curtailment or the cost of operation and maintenance of the wind
turbine
variable
TCEE,Heq,CTT,TTTT,TKP,TOP,TPG,TSP(j,t),TPT,TSPT,TWPT,TWP(w,t),covr,covb,COE
```

M,COEE,SGA,CG,OPPWN,MO,P(i),z(j),PG,KP,AG,IG,CE,N(w),MG,BA(d),OP,BP,BG,cov ,coe,cee,pk(i,t,r),OPP,TC,delta(bus,t),Pij(bus,node,t),Pw(bus,t),ePd(t),ePc(t),oppw,SI,TI,SS,S BA,Fu,IN,CCOE,SZ,SQ;

binary variable u(j),m(w),v1(d);

*u(j) binary variable t=that decides selection of solar system, m(w) is for wind turbine, v1(d) is for BESS

*there might be need to decommission some thermal generators so we might introduce a binary variable to indicate the thermal generators that should be put to service

*CTT total carbon penalty tax comprising of the carbon penalty due to CO_2 influence on man (ctm) and the ecosystem (cte)

P.up(i)= k(i,'pmax');

P.lo(i)= k(i,'pmin');

z.up(j)=l(j,'S');

z.lo(j)=0;

*Z is the solar plant, which gives the apparent power limit of the solar plant

N.lo(w)=0;

N.up(w)=o(w,'S');

*N is for wind turbine, apparent power limit of the wind turbine

BA.lo(d)=0;

BA.up(d)=e(d,'S');

*BA is for BESS, power limit of BESS

Pk.up(i,t,r)=data(r,i,'DP');

Pk.lo(i,t,r)=0;

equations

eq1,eq2,eq3,eq4(j),eq5,eq6,eq7,eq8,eq9,eq10(w),eq11,eq12,eq13,eq14,eq15,eq16,eq17,eq18, eq19,eq20,eq21,eq22(j,t),eq23,eq24,eq25,eq26,eq27,eq28,eq29,eq30,eq31,eq32,eq33,eq34,eq 35,eq36,eq37,eq38(w,t),eq39,eq40,eq41,eq42,eq43,eq44,eq45,eq46,eq47,eq48,eq49,eq50,eq5 1,eq52,eq53,eq54,eq55,eq56,eq57,eq58;

eq1..KP+PG+OP+BP=g=(dem*1.05);

eq2..(SI+IG+MG+BG)/Sbase=e=Heq;

eq3..sum(i,P(i))=e=PG;

eq4(j)..l(j,'s')*u(j)=e=z(j);

*To get the estimated system base, the following variables are needed: KP, OP, BP, PP

eq5..sum(i,k(i,'s')* k(i,'H'))=e=AG;

eq6..sum(j,l(j,'s')*l(j,'H')*u(j))=e=IG;

eq7..sum(j,(u(j)))=l=3;

eq8..sum(j,z(j))=e=KP;

eq9..sum(j,l(j,'cost')*u(j))+sum(w,o(w,'cost')*m(w))=e=CE;

*CE gives the total investment cost of both the solar plant and wind turbine

eq10(w)..o(w,'s')*m(w)=e=n(w);

*N(W) apparent power capacity of wind turbine

eq11..sum(w,o(w,'s')*o(w,'H')*m(w))=e=MG;

*MG gives the total inertia energy of wind turbines

eq12..sum(w,(m(w)))=l=3;

*states that the maximum no. Of wind turbines in the planning horizon is 3

eq13..sum(w,(m(w)))+sum(j,(u(j)))=e=3;

*states that the maximum no. of all renewable energy generators that can be installed in the planning horizon is 3

eq14..sum(w,n(w))=e=OP;

*total apparent power of wind turbines

eq15(d)..e(d,'s')*v1(d)=e=BA(d);

*total apparent power of all instant BESS

eq16..sum(d,e(d,'s')*e(d,'H')*v1(d))=e=BG;

*total inertia energy of all online BESS

eq17..sum(d,(v1(d)))=l=3;

*max no. of BESS that can be installed in the planning horizon

eq18..cee*24=e=TCEE;

*this gives the total co_2 emissions during the planning horizon

eq19..sum(d,BA(d))=e=BP;

*total apparent power capacity of BESS

eq20..CTT=e=CTM+CTE;

*CTT is the total co_2 penalty cost comprising ctm-CO_2 penalty on man and cte-CO_2 penalty on the ecosystem

eq21..SGA=e=(KP+OP+BP+PG);

*total real power capacity of all connected generators

eq22(j,t)..l(j,'S')*WS(t,'S1')*u(j)=e=TSP(j,t);

eq23..sum((j,t),TSP(j,t))=e=TSPT;

*TSPT gives the sum of the energy generated from the solar plant for 24 hours

eq24..sum(d,e(d,'inv')*v1(d))+sum(j,l(j,'inv')*u(j))+sum(w,o(w,'inv')*m(w))=e=cov;

*COV gives the total investment cost on REGs and BESS

eq25..cee*24*CTT=e=coe;

*COE gives the total emission cost for 24 hours considered total CO_2 penalty cost

eq26..sum(i,p(i)*k(i,'e'))=e=cee;

*total CO_2 emission in tonnes

eq27..cee=l=1000000000;

eq28..OPP=e=((sum((t,i),k(i,'a')*power(k(i,'Pmin'),2)+k(i,'b')*k(i,'Pmin')+k(i,'c')+sum(r,data(r,i,'s')*pk(i,t,r))))*24)+oppw;

*OPP gives the total fuel cost and wind operation and maintenance cost

eq29..TC=e=OPP+coe+cov;

*total cost comprising operation cost and investment cost

eq30(bus,node,t)$(conex(bus,node))..Pij(bus,node,t)=e=br(bus,node,'bij')*(delta(bus,t)-delta(node,t));

eq31..(sum(w,n(w)*o(w,'cul')*24))=e=oppw;

eq32..SI=e=sum(i,k(i,'s')*k(i,'H'));

*total inertia energy from thermal generator

eq33..TI=e=IG+MG+BG;

*TI total inertia from wind turbine, solar plant, and thermal generator

eq34..SS=e=sum(i,k(i,'s'));

*SS is the total capacity of thermal generator

eq35..SBA=e=(KP+OP+BP+SS);

*total installed capacity from BESS, wind turbine, solar plant, and thermal generators

eq36..Fu=e=((sum((t,i),k(i,'a')*power(k(i,'Pmin'),2)+k(i,'b')*k(i,'Pmin')+k(i,'c')+sum(r,data(r,i,'s')*pk(i,t,r))))*24);

*FU is the total fuel cost

eq37..IN=e=SI+IG+MG+BG;

*IN is the total inertia energy from all synchronous generators, REGs, and BESS

eq38(w,t)..o(w,'S')*WS(t,'w1')*m(w)=e=TWP(w,t);

eq39..sum((w,t),TWP(w,t))=e=TWPT;

*TWPT is the total power generated from the wind turbine

eq40..TPT=e=TWPT+TSPT;

eq41..OPPWN=e=TWPT*500;

*TWPT is the total power generated from the solar plant for 24 hours

eq42..cee*24*CTE=e=coee;

*CO_2 emission penalty cost on man

eq43..cee*24*CTM=e=coem;

eq44..IN=g=KEmin;

*Inertia energy in the system must be greater than the calculated minimum inertia energy

eq45..SBA*Hmin*y=e=MO;

eq46..SI=g=MO;

eq47..SBA-PLOSS=e=CG;

eq48..CG=g=dem;

eq49..SZ=e=(KP+OP+SS);

eq50..SQ=e=((SZ*Hmin)-MG-IG)/(10-Hmin);

eq51..BP=l=SQ;

eq52..cov=l=BUTT;

eq53..(PG*24*0.8)=e=TPG;

*0.8 is used as the capacity factor of thermal generators, while 0.229 is used as the capacity factor of solar plants, and 0.293 is the capacity factor of wind turbines

eq54..TKP+TOP=e=TTTT;

eq55..(KP*24*0.229)=e=TKP;

eq56..(OP*24*0.293)=e=TOP;

eq57..sum(j,l(j,'inv')*u(j))+sum(w,o(w,'inv')*m(w))=e=covr;

eq58..sum(d,e(d,'inv')*v1(d))=e=covb;

*the total BESS installed must be installed during the planning horizon

*states that the synchronous inertia in the model must be greater than 0.3 of all available inertia energy

*COEM CO_2 emission penalty cost on ecosystem

Heq.up=10;

Heq.lo=4.0;

model test1 /all/;

delta.up(bus,t)=pi/6;

delta.lo(bus,t)=-pi/6;

Pij.up(bus,node,t)$((conex(bus,node)))=1*br(bus,node,'Limit')/Sbase ;

Pij.lo(bus,node,t)$((conex(bus,node)))=-1*br(bus,node,'Limit')/Sbase;

solve test1 using miqcp min TC;